

**SEMICLASSICAL STUDY OF STATISTICAL MEASURES OF
SPECTRAL FLUCTUATIONS IN SOME
PSEUDOINTEGRABLE BILLIARDS**

BY

HARISHKUMAR DEVRAO PARAB

THEORETICAL PHYSICS DIVISION
Bhabha Atomic Research Centre
Mumbai - 400 085

A THESIS SUBMITTED IN FULFILMENT OF
THE REQUIREMENTS OF THE DEGREE OF
DOCTOR OF PHILOSOPHY IN SCIENCE
IN THE SUBJECT OF
MATHEMATICS

UNIVERSITY OF MUMBAI
MUMBAI
July 1999

Contents

Introduction	3
1 Modern Approaches to Semi-Classical Quantization	9
1.1 Introduction:	9
1.2 Short-wavelength Asymptotics of Schrödinger Equation:	10
1.2.1 Lagrangian Manifold:	12
1.2.2 Solution of H-J and Amplitude Transport Equations: .	16
1.3 Path Integrals and Semi-classical Limit	20
1.3.1 The resolvent operator and its' singularities	21
1.3.2 A Propagator and Path Integral	23
1.3.3 Stationary Phase Approximation:	25
1.4 Density of States for Pseudo-integrable Billiards	29
2 Billiards - Classical Dynamics	33
2.1 Introduction	33
2.1.1 Phase space	33
2.2 Polygonal billiards	35
2.3 Invariant Surface of Polygonal Billiards	40
2.3.1 Construction of the invariant surface	40
2.3.2 Topology of the invariant Surface	41
2.4 Integrability and beyond:	43
2.5 Birkhof-Poincaré Maps and Interval Exchange Maps	45
2.5.1 Interval exchange Map For Rational Billiards	46
3 Periodic Orbits in Some Pseudo-integrable Billiards	51
3.1 Introduction	51
3.2 Periodic orbits of the $\pi/3$ -rhombus billiard	51
3.2.1 Enumeration	52

3.2.2	Polar Construction	57
3.2.3	Classification	60
3.3	The H-M Billiard	67
3.4	The Single Slit Rectangle billiard	70
4	Growth Rate of Periodic Orbits	77
4.1	Introduction	77
4.2	Law of Proliferation of Periodic Orbits in Pseudo-integrable Billiards	79
4.2.1	The $\pi/3$ -Rhombus Billiard	79
4.2.2	The H-M Barrier Billiard:	82
4.2.3	The Single Slit Rectangle Billiard	85
4.3	Proliferation of Periodic Orbits Considering Repetitions	88
4.4	Generalization	89
5	Two-Point Cluster Function and Form Factor: A Diagonal Approximation	93
5.1	Introduction	93
5.2	Spectral Fluctuation Measures	94
5.3	Semi-classical Density of States	97
5.3.1	Symmetry-projected Green's function	99
5.4	Two-Level Cluster Function	102
5.4.1	Density-density correlation function	102
5.4.2	Diagonal approximation	105
5.4.3	Summing over all the periodic orbits	105
5.4.4	Taking spectral average	108
5.5	The Form Factor	113
6	Short and Intermediate Range Spectral Fluctuation Measures	126
6.1	Introduction	126
6.2	Nearest Neighbour Spacing Distribution	126
6.3	The Number Variance	132
6.4	The Spectral Rigidity	137
7	Conclusions	154

Introduction

Study of spectral fluctuations in a quantum dynamical system was initiated by Wigner in 1956 [1]. He provided explanation of observed shortage of close spacing in nuclear energy levels using statistical arguments. For example, one can obtain precise information about levels ranging from number N (of order 10^6) to $N + n$ from neutron-capture experiments in heavy nuclei. Theoretically, it is difficult to analyse levels of this order on the basis of shell structure and collective or individual particle quantum numbers. Wigner successfully shown that the highly excited states can be understood by assuming a working hypothesis that all shell structure is washed out and that no quantum numbers other than spin and parity remains good via statistical theory of energy levels. The aim of statistical theory is not to predict the detailed sequence of levels, but to describe the general appearance and the degree of irregularity of the level structure in the given quantum system.

This view led Wigner to surmise a possible spacing distribution based on the assumption that matrix elements of the Hamiltonian matrix were unknown and unknowable and are randomly distributed. Success of Wigner surmise in explaining the spacing between energy eigenvalues resulted in further development of a one of the tools to study statistical properties of levels, known as Random Matrix Theory(see [2, 3]).

The random matrix theory of Hamiltonian systems is based on the assumption that we know very little about the dynamics of the given system except certain symmetry properties. These symmetry properties impose restrictions on the form of the Hamiltonian matrix. Based on the symmetry properties a normalised probability distribution on the elements of the Hamiltonian matrix can be obtained using a metric in the space of matrix elements

which is invariant under a similarity transformation. The joint probability distribution is chosen to minimize information about the Hamiltonian matrix and subjected to the condition that it is normalized to one and has elements that remain finite.

For real symmetric Hamiltonians (e.g. systems having time reversal symmetry,), the similarity transformation is orthogonal and the probability distribution is said to be described by a Gaussian Orthogonal Ensemble (GOE) of Hamiltonian matrices. For other interesting cases such as Hermitian and real quaternion Hamiltonians, the similarity transformations are unitary and symplectic respectively. The probability distribution of these is said to be described by Gaussian unitary ensemble (GUE) and Gaussian Symplectic Ensembles (GSE).

There are number of statistical properties of eigenvalues of random matrices that are commonly used in the analysis of spectral properties. For, example spacing distribution (or nearest neighbour spacing), the Δ_3 —statistic (or spectral rigidity) of Dyson and Mehta [2, 3].

Random matrix theory (RMT) have been successful in explaining universality in spectral fluctuations (up to second order correlation) for different classes of chaotic systems as above in an appropriate high energy limit. RMT is expected to be applicable only on those time scales where the variables associated with the classical dynamics are random enough, to fully randomize the matrices, associated with the corresponding quantum operators. Moreover, due to underlying assumptions on which framework of RMT is build, it is not expected to shed any light on non-universal behaviour of spectral fluctuations which is the characteristic of a given system.

A new dimension is added to the study of spectral properties of a quantum system after the conjecture of Percival [4] that there exist a *regular* and an *irregular* quantum spectra corresponding to the integrable an non integrable classical dynamics. This indication that the nature of classical dynamics can have its imprints in the behaviour of a corresponding quantum system provided a new direction to study of statistical properties of levels.

Classical Hamiltonian systems can display wide variety of dynamical features from integrability to chaos. Before the works of Poincaré, classical dynamics was viewed as a paradigm of regularity and predictability. The works by Poincaré, and subsequently by Lyapunov, Birkhoff and others opened the complicated world of classical dynamics. Within a few years after these concept of determinism was abandoned from classical mechanics. The concept about classical motion changed radically and led to birth of what is nowadays

called chaos. Broadly now, classical systems can be classified as one showing complete integrability and others showing either complete chaos or mixed behaviour.

For integrable (or regular) systems all constants of motion exist everywhere in the phase space. A typical trajectory resides on a torus like constant energy surface. On other hand one in case of completely chaotic systems no constant of motion exist and a typical trajectory will occupy whole phase space available. Most of the classical systems, however, belong to an intermediate regime between these extremes, showing a mixed behaviour. Typically, some of the trajectories will show regular behaviour winding around tori. These trajectories are separated by the other orbits that explore constant energy surface ergodically.

There are also many Hamiltonian systems that are just step away from the complete integrability, known as pseudo-integrable systems. For these systems constants of motion do not exist on a countable set of singular points. These systems have f -dimensional (f being dimension of the system) sphere with g handles as an invariant surface embedded in $2f$ -dimensional phase space. Typical examples of pseudo-integrable systems are rational of polygonal billiards, where a particle moves freely inside polygonal enclosure whose each angle is of form π/n , reflecting specularly from the walls. Results of some recent studies indicate that generally one can expect coexistence of almost integrable and almost chaotic regions in the mixed phase space. In this work we are concerned with spectral properties of these systems.

The imprints of classical behaviour on a quantum system can best be understood via semiclassical techniques which provides a information regarding quantum dynamics in terms of properties of corresponding classical system. Semiclassical techniques had been developed since the beginning of the quantum mechanics. Due to easiness with classical mechanics the search for connections between classical and quantum mechanics has been naturally sought for. The WKB approximation was the first method built to extract quantum-mechanical properties using information of classical orbits. The recent interest in non-integrable systems further initiated development of semiclassical techniques which are applicable for large class of classical systems.

In this work we will consider dynamical systems as mentioned above known as pseudointegrable billiards. Due to mathematical intractability of these systems, few exact results are known. Numerical studies performed on the energy spectra of these systems led to the belief that the spectral statistic is intermediate between those for the Poisson ensemble and the GOE of

random matrices. However, the results on various measures of the spectral statistics as analysed from the periodic orbit theory have been indicative only and do not bring out a complete or explicit picture of underlying correlations. Moreover, numerical studies have to deal with finite number of levels only. There is thus possibility that numerical results may not represent asymptotic trend.

Our aim here is to extend semiclassical formalism to obtain explicit analytical expressions for various important measures of spectral statistics. This will therefore can bring out dependence of spectral properties on different system dependent parameters.

Plan of the thesis is as follows:

In chapter one we will discuss main issues involved in development of proper semiclassical framework that can be applicable for wide class of systems. The problem with WKB or similar methods developed earlier is that they were applicable only for systems that are separable. Existence caustics prohibits these methods to be useful beyond short time scale. Major improvement in semiclassical methods has been taken place via Path Integrals which ultimately leads to a semiclassical approximation to density of states in terms of summation over periodic orbits of the classical system.

As the periodic orbits and their attributes such as stability, action etc. becomes important in establishing a semiclassical approximation, study of the nature of classical system in question becomes mandatory. In the case of polygonal billiards there exist a large body of knowledge about classical behaviour in the literature. Some of these are very helpful in the study of periodic orbits and their various properties that are relevant to semiclassical methods. These will be discussed in chapter two.

In chapter three we take up the first task [5]: detailed study of periodic orbits in some pseudointegrable billiards. Exploiting geometrical properties of the billiards considered we develop a modified version of interval exchange maps, called as polar maps. From these maps we show how to classify and enumerate all the periodic orbits of these billiards. We will also quantify actions and other parameters required for the semiclassical study.

In chapter four a very important attribute of periodic orbit i.e. growth

rate (with actions, periods or lengths) of periodic orbits is studied [6]. We obtain exact (asymptotic) law for some pseudointegrable billiards. We show that this law is quadratic in length and determine constants associated with it. Some generalization of this law is also suggested.

Using information gathered in chapter 3 and 4 we obtain explicit analytical expression for two point correlation function and its fourier transform in chapter five. Generally semicalssical study ends after establishing a sum over periodic orbits. This does not bring out dependence of spectral fluctuations on the various attributes of periodic orbits explicitly. We here, go further to carry out this summation by converting it into a integration via proper measure, which enables us to obtain analytical forms for spectral fluctuation measures. This also brings out role played by growth rate of periodic orbits explicitly.

In chapter six we use two point correlation function to obtain short and intermediate range spectral measures such as spacing distribution, number variance and spectral rigidity [7]. We will also compare our results with some numerical experiments.

In the concluding chapter we discuss our results and outline some of the future research activities in this field.

Bibliography

- [1] E.P.Wigner SIAM review **9** (1967)1.
- [2] F.J.Dyson J. Math. Phys. **3**, (1962)140, 1191.
- [3] M. L. Mehta, Random Matrices, Academic, New York (1991).
- [4] I.C.Percival, J.Phys. **B6**, (1973)L229.
- [5] S.R.Jain and H.D.Parab, J.Phys A:Math. Gen. **25**, (1992)6669.
- [6] H.D.Parab and S.R. Jain, Phys. Rev. E, **47**, (1993)R776.
- [7] H.D.Parab and S.R.Jain, J.Phys.A:Math. Gen. **29**, (1996)3903.

Chapter 1

Modern Approaches to Semi-Classical Quantization

1.1 Introduction:

Semi-classical methods have been developed since the beginning of quantum mechanics because of the importance of the models based on classical particles and fields. Bohr and Sommerfeld initiated these methods to quantize atomic systems. However their methods implicitly assumed separability between the different internal degrees of freedom and hence were of limited utility since most of the classical systems are not separable[1]. For example even the three-body helium atom problem can not conform to the Bohr-Sommerfeld scheme without further assumptions. There were many attempts to resolve this problem e.g. see [2]. However, major development in this direction had taken place with the advent of Heisenberg's matrix mechanics and of Schrödinger's wave mechanics.

The Schrödinger wave equation of quantum mechanics turns out to be extremely useful in the development of semi-classical theory since it allows a discussion of the relation to classical mechanics along the lines similar to the relation between wave optics and geometric optics, albeit in the multidimensional phase space rather than in the three dimensional physical space. This similarity was developed by Brillouin, Wentzel and Kramers for one degree of freedom (well known as WKB approximation) based of well developed mathematical framework of asymptotic methods of linear mathematical physics[3, 4]. For larger systems that are separable and reducible to several

one-degree of freedom systems variant of this method (EWKB approximation) was developed.

Since semi-classical methods carry out the quantization on the basis of knowledge of the classical motion, they are susceptible to the difficulties caused by the non-linearities of Hamilton's equations of classical mechanics. The inapplicability of standard WKB methods to non-linear systems prompted further development of semi-classical methods[12, 13]. These methods known as the periodic orbit quantization have been applied to a large variety of systems. These methods basically use a semi-classical approximations of the trace of the resolvent of the quantum Hamilton operator. This trace formula, which establishes link between the quantum operator and classical periodic orbits, can be used to obtain approximate values of quantum eigenenergies for wide class of systems. The trace formula which contains different terms depending on the nature and on the stability of the periodic orbits. It not only improves the accuracy of semi-classical methods but also provides a framework for the description of diffraction, non-linear stability effects, bifurcation of periodic orbits etc.

In this thesis we will discuss the imprints of nature of classical Hamiltonian system on the corresponding quantum mechanical system, in particular on the collective properties of quantal eigenenergies. We will use the framework of semi-classical methods for our study. Before coming to the main theme, we will discuss in this chapter some important issues in modern semi-classical methods.

1.2 Short-wavelength Asymptotics of Schrödinger Equation:

Consider the Cauchy problem with rapidly oscillating initial data for the Schrödinger equation [4, 7]

$$i\hbar \frac{\partial \psi(\mathbf{q}, t)}{\partial t} = -\frac{\hbar^2}{2m} \nabla^2 \psi(\mathbf{q}, t) + V(\mathbf{q})\psi(\mathbf{q}, t) \quad (1.1)$$

$$\psi|_{t=0} = A_0(\mathbf{q}) \exp\left(\frac{i}{\hbar} S_0(\mathbf{q})\right) \quad (1.2)$$

where $\mathbf{q} \in R^n$, functions $V(\mathbf{q}), S_0(\mathbf{q})$ are real valued and infinitely differentiable, $A_0(\mathbf{q})$ is infinitely differentiable with compact support. One can seek

an asymptotic solution of the problem as $\hbar \rightarrow 0$ and $\mathbf{q} \in R^n$, $0 \leq t \leq T$. The equation (1.2) can be regarded as the leading term of an asymptotic expansion in \hbar , in which $O(\hbar)$ terms are neglected. It is also assumed that an asymptotic solution of equation (1.1)

$$\psi(\mathbf{q}, t) = A(\mathbf{q}, t) \exp\left(\frac{i}{\hbar} S(\mathbf{q}, t)\right) \quad (1.3)$$

which is valid only for the short elapsed time t , after which it should be replaced by the sum of higher order terms in an asymptotic expansion. The reason for this single term break down is formation of caustic which occur at time of order (\hbar^0) . However for sufficiently longer time above assumption breaks down altogether. We will elaborate these issues in the following paragraphs.

Substituting equation (1.3) in the Schrödinger equation and neglecting terms of order (\hbar) and higher, we get the time-dependent Hamilton-Jacobi(H-J) equation for the action $S(\mathbf{q}, t)$,

$$H\left(\mathbf{q}, \frac{\partial S(\mathbf{q}, t)}{\partial \mathbf{q}}, t\right) + \frac{\partial S(\mathbf{q}, t)}{\partial t} = 0 \quad (1.4)$$

where H is Hamiltonian and the canonical momentum \mathbf{p} of $H(\mathbf{q}, \mathbf{p}, t)$ is replaced by $\mathbf{p} = \partial S / \partial \mathbf{q}$. The order (\hbar) term gives amplitude transport equation for A or the continuity equation for $\rho(\mathbf{q}, t) = |A(\mathbf{q}, t)|^2$ as

$$\frac{\partial \rho(\mathbf{q}, t)}{\partial t} + \frac{\partial}{\partial \mathbf{q}} [\rho(\mathbf{q}, t) v(\mathbf{q}, t)] = 0 \quad (1.5)$$

where the velocity field $v = \partial H(\mathbf{q}, \mathbf{p}, t) / \partial \mathbf{p}$ with $\mathbf{p} = \partial S / \partial \mathbf{q}$. One then solves equation (1.4) for $S(\mathbf{q}, t)$ and use this S to solve equation (1.5).

The H-J equation is typical of non-linear equations, hence has a bewildering variety of solutions. Among them are the complete integrals which gives all the trajectories of the system. As we are concerned with those solutions that have a relationship to a quantum mechanical wave function, it is desirable to find a way of defining S such that it will be a single valued function of its variables. The first step to do this is to use phase space description of trajectories[5, 6]. The concept of *Lagrangian Manifold* becomes important here.

1.2.1 Lagrangian Manifold:

The initial action $S_0(\mathbf{q})$ and momentum field $\mathbf{p}_0 = \partial S_0 / \partial \mathbf{q}$ can be viewed as a vector field on the f -dimensional configuration space. This field represents the initial momenta of the swarm of particles whose initial density is given by $\rho_0(\mathbf{q}) = |A_0(\mathbf{q})|^2$. This swarm of particles and vector field constitute the classical and semi-classical interpretation of the initial action function in configuration space. Since the momentum field imposes f independent constraints on the $2f$ variables (\mathbf{q}, \mathbf{p}) of the phase space, initial swarm of the particles lies on the f -dimensional surface Λ_0 . The surface Λ_0 is graph of the function $\mathbf{p} = \mathbf{p}_0(\mathbf{q})$ i.e. the set of points in phase space of the form $(\mathbf{q}, \mathbf{p}_0(\mathbf{q}))$. This surface satisfy properties of *Lagrangian manifold*, Λ , the formal definition of which is as follows:

Definition 1 *Lagrangian manifold is a f -dimensional surface Λ in $2f$ -dimensional phase space such that $\forall (\mathbf{q}, \mathbf{p}) \in \Lambda$ and for $\forall \delta \bar{z} \equiv (\delta \mathbf{q}, \delta \mathbf{p})$ tangent to Λ at (\mathbf{q}, \mathbf{p}) representing a small displacement, the action of the symplectic form (i.e. differential 2-form) on all $\delta \bar{z}_1, \delta \bar{z}_2 \in \{\delta \bar{z}\}$ defined as*

$$w(\delta \bar{z}_1, \delta \bar{z}_2) \equiv \delta \bar{z}_1 \cdot \underline{\underline{J}}^{-1} \cdot \delta \bar{z}_2 \equiv \delta \mathbf{p}_1 \cdot \delta \mathbf{q}_2 - \delta \mathbf{p}_2 \cdot \delta \mathbf{q}_1 = 0 \quad (1.6)$$

where $\underline{\underline{J}}$ is unit symplectic matrix.

All the curves in the 2-dim. phase space are *Lagrangian manifolds*. The concept is therefore really needed for multidimensional problems. It can be immediately seen that surfaces $\mathbf{q} = \text{const.}$ or $\mathbf{p} = \text{const.}$ are Λ . Since the value of symplectic form of (1.6) is invariant under canonical transformations every Λ is a constant \mathbf{q} or constant \mathbf{p} surface in some set of canonical coordinates. The graph of any curl-free momentum field is surface Λ . The converse is however, not true, since Λ may contain points at which derivatives in the curl-free condition (i.e. $\partial \mathbf{p}_i / \partial \mathbf{q}_j$) are not defined. Such points are generally associated with caustics.

The f -dimensional vectors \mathbf{q} and \mathbf{p} can be regarded as smooth functions of $u = (u_1, u_2, \dots, u_f)$, "co-ordinates" labelling of Λ . The variables $\mathbf{q}(u)$ are locally invertible if Jacobian $|\partial \mathbf{q} / \partial \mathbf{p}|$ do not vanish. Then and only then one can define $\mathbf{p}(\mathbf{q}) = \mathbf{p}(u(\mathbf{q}))$, a function of \mathbf{q} on Λ . If above Jacobian vanishes then

$$\frac{\partial p_i}{\partial q_j} = \sum_k \frac{\partial p_i}{\partial u_k} \cdot \frac{\partial u_k}{\partial q_j}$$

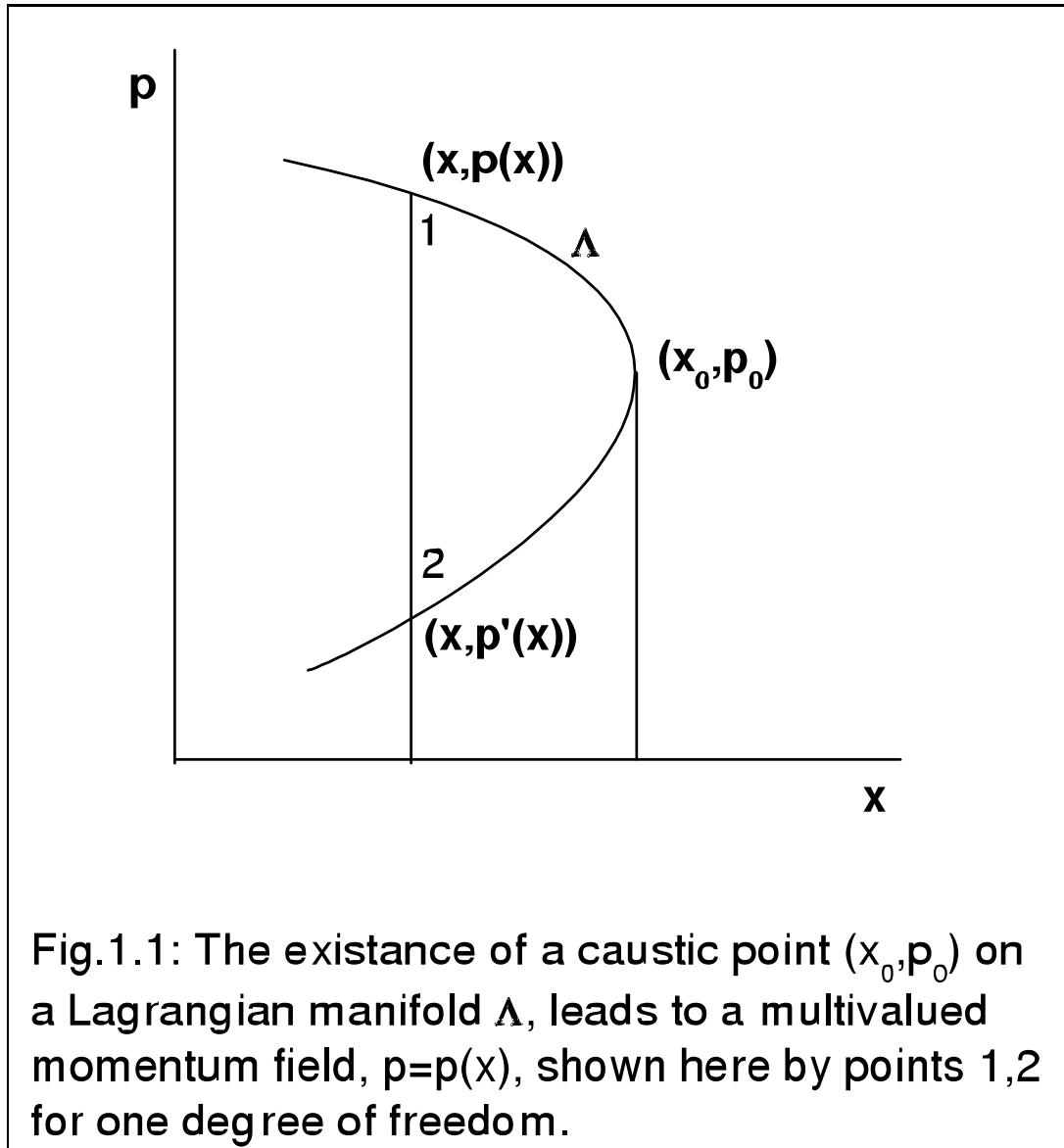
will behave badly. In 1-dimension since $\partial p_i / \partial u_k \neq 0$ it will diverge. In higher dimensions some of the eigenvalues of $[\partial \mathbf{p} / \partial u]$ may vanish at the same place where some of the eigenvalues of $[\partial \mathbf{q} / \partial u]$ also vanish, resulting in the complicated behaviour. A phase space vector δz tangent to Λ can be written in the u -co-ordinates as $\delta z = \left(\frac{\partial \mathbf{q}}{\partial u} \delta u, \frac{\partial \mathbf{p}}{\partial u} \delta u \right)$. If the matrix $[\partial \mathbf{q} / \partial u]$ is singular, then for all $\delta u \neq 0$ and $\delta q = 0$, δz has vanishing components in the q -components resulting in a caustic in the configuration space. The order of caustic or the number of null eigenvectors δu , is given by co-rank of the matrix $[\partial \mathbf{q} / \partial u]$. The order of caustic as well as set of points for which $\partial q / \partial u = 0$ are independent of the choice of u on Λ . The important theorem about Λ is

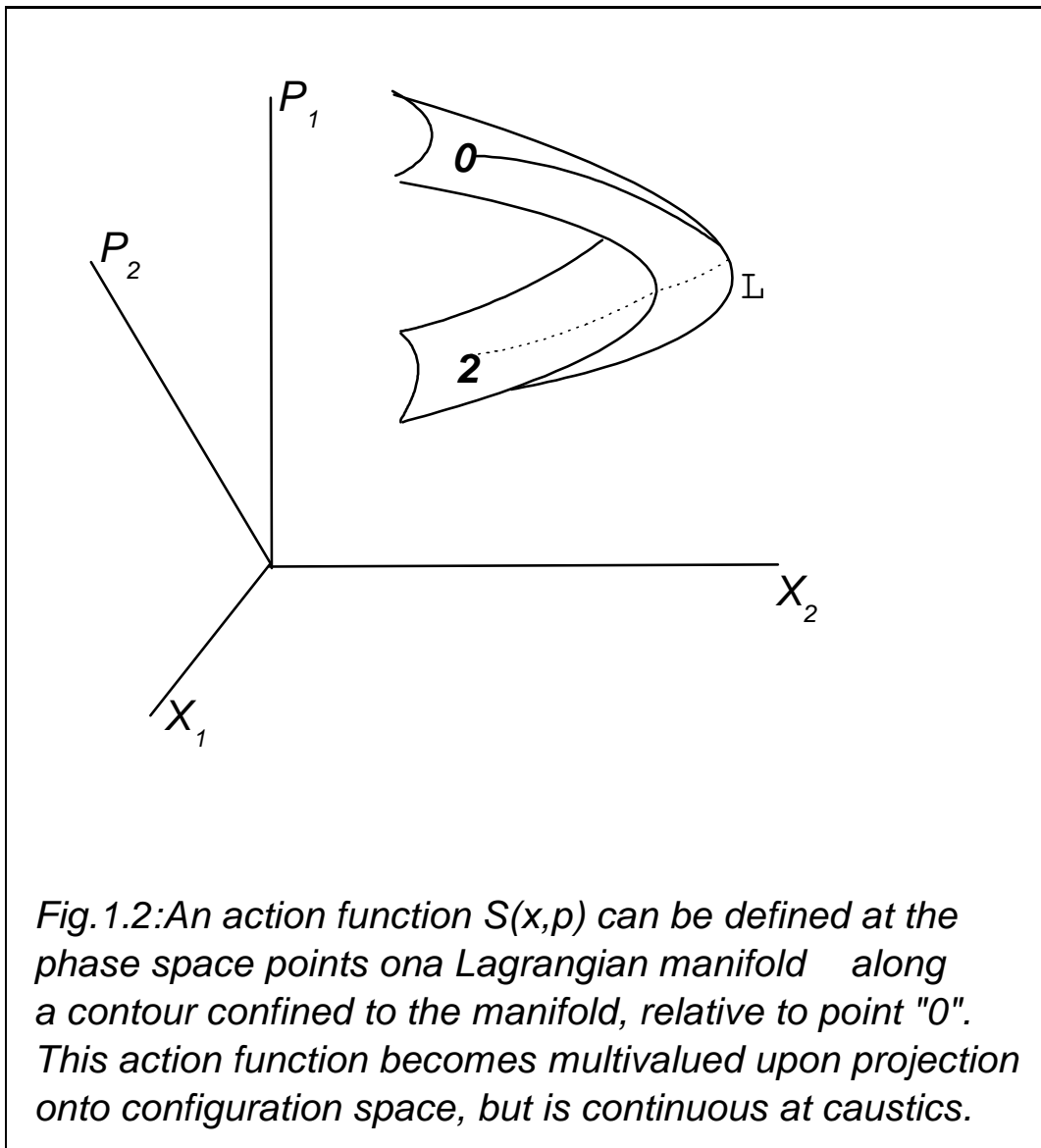
Theorem 1 *A region of Λ which is free of singular points if projected on configuration space gives curl-free momentum field.[4, 7]*

Since flow preserves the symplectic structure (cf. Liouville Theorem) Λ evolves into another Λ' under time evolution. Any function $S(\mathbf{q})$ which satisfy $\mathbf{p}(\mathbf{q}) = \partial S / \partial \mathbf{q}$ on Λ will now be called *generating function* of Λ .

Theorem 2 *On a region of Λ , free of singular points, one can define unique generating function up to additive constant.[7]*

This additive constant is usually associated with phase conventions in semi-classical applications. For Λ , having region of singular points, one can divide Λ into sub-regions which extend up to and separated by the caustics as shown in Fig.1.1. Each such region corresponds to a distinct branch of the momentum field $\mathbf{p}_b(\mathbf{q})$ and associated generating function $S_b(\mathbf{q})$ up to its own additive constant. One can define action function $S(\mathbf{q}, \mathbf{p})$ on Λ itself, as the line integral $\int p \cdot dq$ along the contour belonging to the Λ and taken relative to an arbitrary initial point, see Fig. 1.2. This can be done by demanding that the different functions $S_b(\mathbf{q})$ approach one another at the caustic dividing branches. In this way one can also link some or all of the additive constants together. The function $S(\mathbf{q}, \mathbf{p})$ will be multi-valued not only due to caustics but also due to non-trivial (e.g. *multi-connectedness*) topology of Λ . The generating function in general is specific to the choice of co-ordinates. Some Λ consist entirely of caustic points (e.g. $x = \text{const.}$ in 1-dimension). Such manifolds do not have generating function $S(x)$. However, with respect to other co-ordinate systems one can define a generating function for such





surfaces. The locations of the caustic points are relative to the representation being used. This fact plays important role in the WKB theory. It is possible to cover every Λ (Fig.1.3) with overlapping regions such that every region is caustic free in some representation obtained from a commutating mixture of \mathbf{q} 's and \mathbf{p} 's. A whole family of wave functions, such as a complete set of commutating observables, will reproduce a whole family of Λ manifolds parameterized by some set of parameters $\lambda = (\lambda_1, \lambda_2, \lambda_3, \dots, \lambda_f)$. Thus phase space is foliated up into f -parameter family of f -dimensional Λ manifolds. The function $S(\mathbf{q}, \lambda)$ is one of the generating functions of canonical transformations in classical mechanics.

1.2.2 Solution of H-J and Amplitude Transport Equations:

Now consider an initial Lagrangian manifold Λ' , free of singular points, obtained from initial action $S(\mathbf{q}', t') = S_0(\mathbf{q}')$ and $\mathbf{p}(\mathbf{q}', t') = \partial S(\mathbf{q}', t')/\partial \mathbf{q}'$. Each point of Λ' evolves under Hamilton's equations, mapping into another Λ'' at time t'' . If Λ'' is also free of singular points then one can define a generating function $S(\mathbf{q}'', t'')$, which is also a solution of H-J equation, as

$$S(\mathbf{q}'', t'') = S(\mathbf{q}', t') + R(\mathbf{q}'', t'' : \mathbf{q}', t') \quad (1.7)$$

where $R(\mathbf{q}'', t'' : \mathbf{q}', t') = \int_{\mathbf{q}', t'}^{\mathbf{q}'', t''} [\mathbf{p} \cdot d\mathbf{q} - Hdt]$ is Hamilton's principal function.

As $t'' \rightarrow t'$, one gets $R \rightarrow 0$ and $S(\mathbf{q}'', t'') \rightarrow S(\mathbf{q}', t')$ thus satisfying required initial conditions.

Since the particle density is conserved one can write $\rho(\mathbf{q}'', t'')d\mathbf{q}'' = \rho(\mathbf{q}', t')d\mathbf{q}'$, and since $\rho = |A|^2$, we get

$$A(\mathbf{q}'', t'') = A(\mathbf{q}', t') \left| \det \frac{\partial \mathbf{q}'}{\partial \mathbf{q}''} \right|^{1/2}. \quad (1.8)$$

Here the absolute sign in this equation required only when one considers many branches.

Thus the WKB solution to the Cauchy problem can be written as

$$\Psi(\mathbf{q}'', t'') = A(\mathbf{q}', t') \left[\det \frac{\partial \mathbf{q}'}{\partial \mathbf{q}''} \right]^{1/2} \exp \left\{ \frac{i}{\hbar} [S(\mathbf{q}', t') + R(\mathbf{q}'', t'' : \mathbf{q}', t')] \right\} \quad (1.9)$$

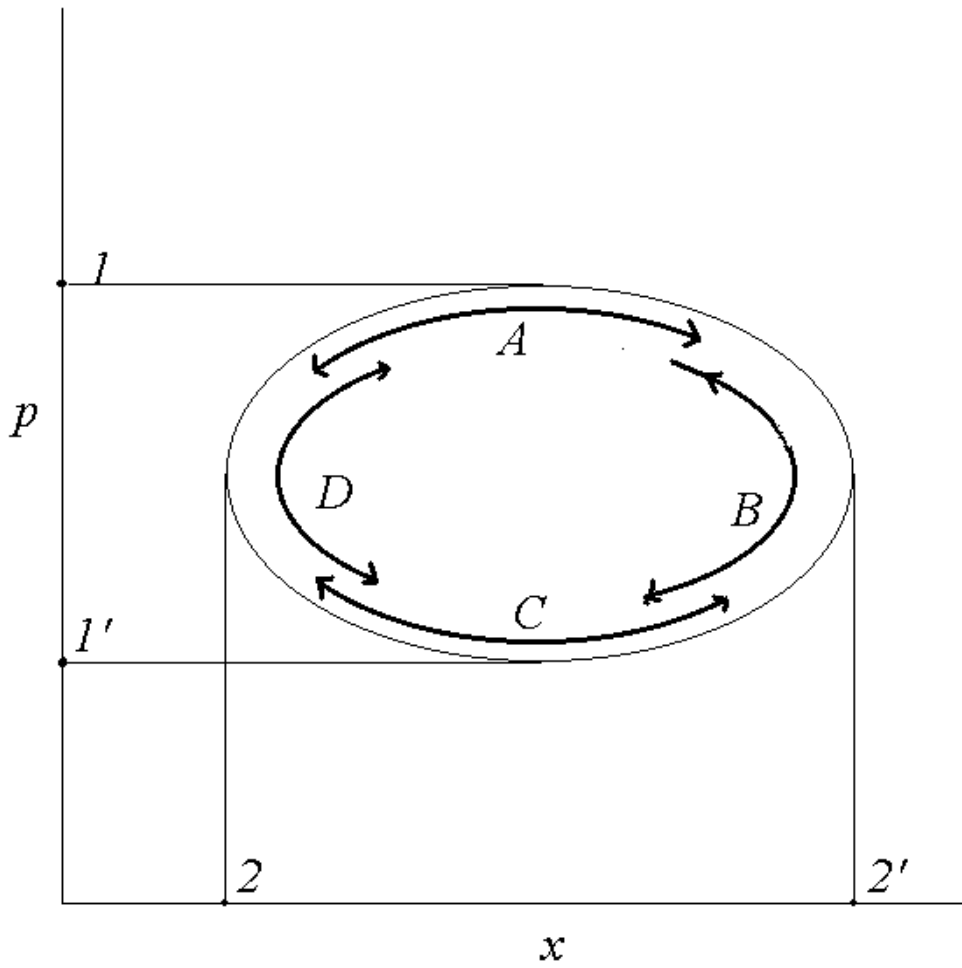


Fig. 1.3: In one degree of freedom, configuration space caustics (2&2') and momentum space causics (1&1') never occur at the same place. In higher degrees of freedom also there always exist a representation in which a given point is caustic free. Thus a Lagrangian manifold can always be covered by overlapping regions (e.g. A,B,C,D) that are caustic-free.

This expression diverges when \mathbf{q}'' is at caustic (i.e. $\det \partial\mathbf{q}'/\partial\mathbf{q}''$ diverges) of Λ'' . This is illustrated in Fig. 1.4 for one degree of freedom. This divergence represents a non uniformity in the variables (\mathbf{q}'', t'') of Ψ in \hbar , since the error in $\Psi, \rightarrow 0$, like \hbar , as $\hbar \rightarrow 0$ for fixed (\mathbf{q}'', t'') , however it goes to infinity for fixed \hbar as (\mathbf{q}'', t'') approaches caustic. Though the solution near caustic is not valid one can continue the solution through the divergence. However, function $\mathbf{q}'(\mathbf{q}'', t', t'')$ is then multi-valued. By passing through caustic the determinant changes sign via divergence. Thus $[\det \frac{\partial\mathbf{q}'}{\partial\mathbf{q}''}]^{1/2}$ becomes imaginary after first caustic pass. One can absorb this imaginary part into a phase factor as $\exp(-i\eta\pi/2)$, forcing A to be positive. The η here is well known as *Maslov index*. Considering multiplicity of orbits arriving at \mathbf{q}'' at time t'' , one can write

$$\Psi(\mathbf{q}'', t'') = \sum_b A_b(\mathbf{q}'', t'') \exp \left\{ \frac{i}{\hbar} S_b(\mathbf{q}'', t'') - i\eta_b \frac{\pi}{2} \right\}. \quad (1.10)$$

To compute indices η 's one needs to consider momentum-space wave function which is Fourier transform of a configuration-space function. The Fourier transform integral is evaluated by *stationary phase approximation*. This leads to the momentum-space function

$$\Phi(\mathbf{p}) = \exp \left(i\alpha \frac{\pi}{4} \right) |\det \underline{\underline{M}}(\mathbf{q})|^{-\frac{1}{2}} \exp \left\{ \frac{i}{\hbar} [S(\mathbf{q}) - \mathbf{q} \cdot \mathbf{p}] \right\} \quad (1.11)$$

where the symmetric matrix $\underline{\underline{M}}(\mathbf{q}) = \partial\mathbf{p}/\partial\mathbf{q} = \partial^2 S(\mathbf{q})/\partial\mathbf{q}\partial\mathbf{q}$ and α is an integer given by the *index of inertia of $\underline{\underline{M}}$* (i.e. number of positive eigenvalues minus number of negative eigenvalues). If Λ do not have singular points in say, X -representation but do have a caustic in P -representation, then at the momentum-space caustic $\det \underline{\underline{M}}(\mathbf{q}) \rightarrow 0$, hence α changes discontinuously across the caustic by $\pm 2 \cdot n$, since number of eigenvalues of $\underline{\underline{M}}$ which vanish at caustic is same as the order "n" of the caustic. Therefore relative phase shift between the two branches will have form $\exp(-i\eta\pi/2)$, and

$$\Phi(\mathbf{p}) = \exp \left(i\alpha_0 \frac{\pi}{4} \right) \sum_b \tilde{A}_b(\mathbf{p}) \exp \left\{ \frac{i}{\hbar} [\tilde{S}_b(\mathbf{p}) - i\eta_b \frac{\pi}{2}] \right\} \quad (1.12)$$

where α_0 is index of inertia of one of the branches for which $\eta = 0$, and $\tilde{S}_b(\mathbf{p}) = S_b(\mathbf{q}) - \mathbf{q} \cdot \mathbf{p}$, $\tilde{A}_b = (\tilde{\rho}_b(\mathbf{p}))^{1/2}$ with $\tilde{\rho}_b(\mathbf{p}) = \rho_b(\mathbf{q}) |\det \partial\mathbf{q}/\partial\mathbf{p}|$.

Thus the relative phase shifts between branches can be determined by switching to a representation which is caustic free. Considering any two

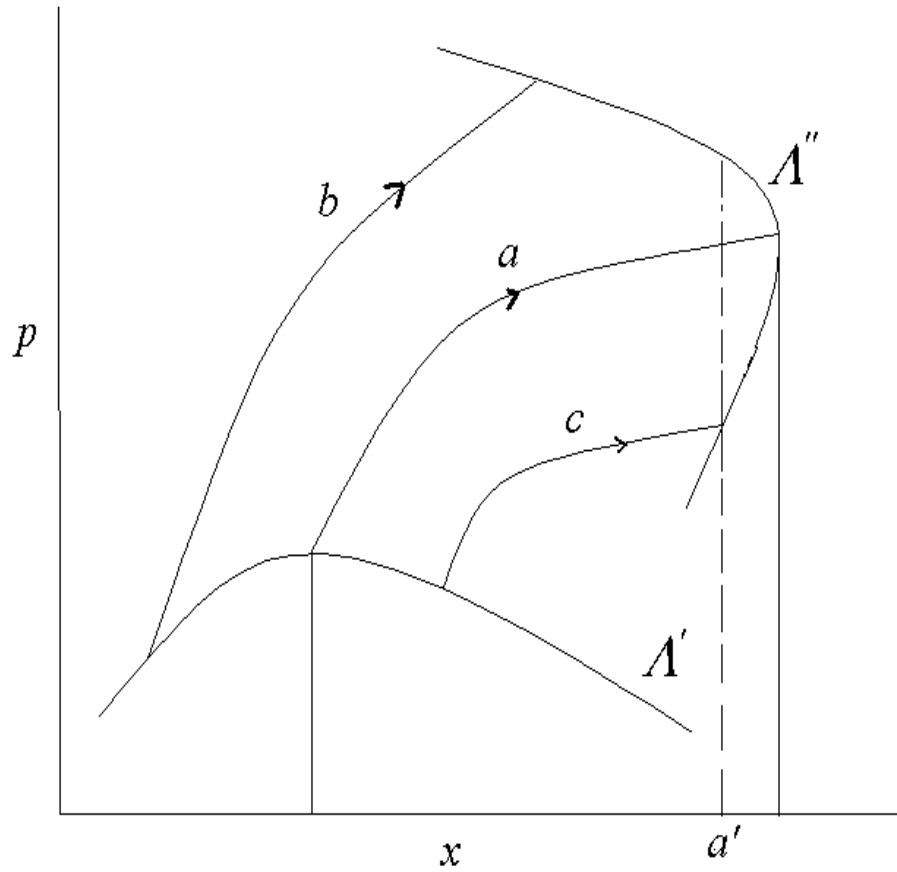


Fig. 1.4: The orbit a , has reached a caustic, b has not yet while c , has already passed one . After caustic deveoped x and p at corres ponding point (e.g. a') becomes multivalued .

branches the phases of the two branches of $\Phi_b(\mathbf{p}'', t'')$ can be written as η $\tilde{S}_b(\mathbf{p}) - i\eta_b\pi/2 + i\alpha_b\pi/4$. Demanding continuity of phases across caustic in caustic free representation, we get

$$\eta_2 = \eta_1 + \frac{\alpha_2 - \alpha_1}{2}. \quad (1.13)$$

The bounds on $\Delta\eta$, change in η across a caustic is then $-n \leq \Delta\eta \leq +n$, n being order of caustic. By extending process, it is possible to associate total $\Delta\eta$ measured between the end points of a curve segment on Λ , which may cross a number of caustic and straddle several branches. The quantity $\Delta\eta$ associated with a directed curve segment of Λ is the Maslov index of that segment. The index depends only on the geometry of Λ and its' projection on configuration space. It also depends on the representation chosen.

The method discussed in this section is simple and allows us to derive several important expressions. However, caustics are causing such difficulties that formulation has restricted applicability. The determinant $\det(\partial\mathbf{p}/\partial\mathbf{q})$ plays an important role in the formulation which becomes singular at caustic. At caustic, the method of matching mentioned above uses different equations than preceding ones. This method is also difficult to apply for higher order terms in \hbar expansion. For this reason it is advantageous to reformulate the problem in terms of Path Integrals.

1.3 Path Integrals and Semi-classical Limit

An alternate semi-classical quantization technique *via* Feynman Path Integral gained momentum due to problems discussed in the previous section. The first hint regarding this comes from the work of Selberg[8] who obtained a path integral formulation for a particle moving on a Riemann surface of negative curvature. On the short time scales path integrals had been used to study semi-classical integrable systems[9, 10]. After overcoming the problem with caustics the semi-classical path integral was extended to long times[11]. These efforts culminated in *the trace formulae* of Gutzwiller, Balian and Bloch, as well as Berry and Tabor [12, 13, 14]. The trace formulas are among the very few theoretical results of any generality that connects quantum mechanics with classical mechanics *via* semi-classical approximation for quantal density of states of a bound quantum system, in terms of a sum over the periodic orbits of corresponding classical system. In this section we briefly outline these developments.

1.3.1 The resolvent operator and its' singularities

Consider [15] time evolution of equation (1.1), which is linear in nature. Therefore we can define a linear operator $\hat{U}(t, t')$ such that

$$\Psi_t(\mathbf{q}) = \hat{U}(t, t')\Psi_{t'}(\mathbf{q}) \quad (1.14)$$

The operator \hat{U} known as evolution operator, obeys the Schrödinger equation (1.1), with the initial condition $\hat{U}(t', t') = \hat{I}$, an identity operator on the space of state vectors. The Hamiltonian defined as

$$\hat{H}_t = - \sum_{j=1}^f \frac{\hbar^2}{2m_j} \nabla_j^2 + V(\mathbf{q}) \quad (1.15)$$

is a Hermitian operator ($\hat{H} = \hat{H}^\dagger$), which implies $\partial_t \langle \Psi_t(\mathbf{q}) | \Psi_t(\mathbf{q}) \rangle = 0$. Hence the evolution operator \hat{U} is unitary ($\hat{U}^\dagger \hat{U} = \hat{I}$). The formal solution for $\hat{U}(t, t')$ can be written as

$$\hat{U}(t, t') = \hat{I} - \frac{i}{\hbar} \int_{t'}^t ds \hat{H}_s \hat{U}(s, t') \quad (1.16)$$

In case of time-independent \hat{H}_t one can solve this equation by iterations to obtain the Dyson series for the operator which finally reduces to

$$\hat{U}(t, t') = \exp \left\{ - \frac{i \hat{H}(t - t')}{\hbar} \right\}. \quad (1.17)$$

The evolution operator also obeys group property $\hat{U}(t, t'')\hat{U}(t'', t') = \hat{U}(t, t')$. (Using this we can set $t' = 0$). One can introduce evolution operators for ‘‘forward’’ and ‘‘backward’’ propagation in time such as

$$\pm \Theta(\pm t)\hat{U}(t) = \hat{U}^\pm(t), \quad (1.18)$$

where $\Theta(t)$ is the Heaviside step function (i.e. $\Theta(t) = 1 \forall t > 0, \Theta(t) = 0 \forall t < 0$). The form of (1.17) is indication of conjugacy of energy and time variables as involved in Fourier transform. Thus one can describe a system either in the time-domain or in the energy domain. Both of these description are related by a Fourier transform.

The Fourier transform of the $\hat{U}^\pm(t)$ is

$$\begin{aligned}\hat{G}_\pm(E) &= -\frac{i}{\hbar} \int_{-\infty}^{\infty} dt \exp\left\{\frac{itE}{\hbar}\right\} \hat{U}^\pm(t) \\ &= \mp \frac{i}{\hbar} \int_0^{\infty} dt \exp\left\{\pm \frac{it(E-\hat{H})}{\hbar}\right\}\end{aligned}\quad (1.19)$$

where E is the eigenvalue of the stationary Schrödinger equation $\hat{H}|\Psi(E)\rangle = E|\Psi(E)\rangle$, obtained from taking Fourier transform of (1.1). The Integral (1.19) does not exist, hence Green operator does not have meaning as an operator-valued functions, but can be meaningful as operator-valued distribution. We can redefine $\hat{G}_\pm(E)$ by replacing $E \rightarrow E \pm i\eta, \eta > 0$ (i.e. by analytical continuation in complex E surface), then

$$\hat{G}_\pm(E) = \lim_{\eta \rightarrow 0^\pm} (E \pm i\eta - \hat{H})^{-1} \quad (1.20)$$

The object $\hat{G}(z) = (z - \hat{H})^{-1}$ is known as resolvent of \hat{H} . The operators $\hat{G}_\pm(E)$ are now called as forward and backward Green operators. The resolvent is bounded, except for the values of z which corresponds to the spectrum of Hamiltonian. Since, eigenvalues of the Hamiltonian, being a Hermitian operator, are real and $\Theta(t) + \Theta(-t) = 1$, one can write evolution operator *via* inverse Fourier transform of $\hat{G}(z)$ as a contour integral

$$\hat{U}^\pm(t) = \frac{1}{2\pi i} \int_{C^\pm} dz \exp\left\{\frac{-i+z}{\hbar}\right\} \hat{G}(z). \quad (1.21)$$

For $t > 0$ ($t < 0$), the contribution of the contour C^+ (C^-) is zero. The resolvent has two types of singularities on the real axes. The discrete spectrum of \hat{H} results in poles on the real axis below an energy threshold E_0 . The Continuous spectrum on other hand results in the branch points (in general of order two, since energy is related to momentum by relation $E = E_c + p^2/2m$) at real energies $\{E_c\}$. Thus spectral decomposition of the evolution operator can be carried out in terms of a sum over bound states $|\Psi_b\rangle$ and sum over continuous states $|\Psi_C(E)\rangle$, of different channels C , with eigenvalues $\exp\left\{-\frac{iE_b t}{\hbar}\right\}, \exp\left\{-\frac{iE t}{\hbar}\right\}$ respectively, as[17]

$$\hat{U}(t) = \sum_b |\Psi_b\rangle \exp\left\{-\frac{iE_b t}{\hbar}\right\} \langle \Psi_b| + \sum_C \int_{E_c}^{\infty} dE |\Psi_C(E)\rangle \exp\left\{-\frac{iE t}{\hbar}\right\} \langle \Psi_C(E)| \quad (1.22)$$

The eigenfunctions of \hat{U} are also the eigenfunctions of \hat{H} . The energy eigenvalues are then poles of the Green operator, and hence also of its trace [16]. Considering bounded systems only we can write the expression for the level density (or density of states) $d(E)$ as

$$d(E) \equiv \sum_{n=0}^{\infty} \delta(E - E_n) = \text{Tr} \delta(E - \hat{H}) - \frac{1}{\pi} \lim_{\eta \rightarrow 0_+} \text{Im} \text{Tr} \frac{1}{E + i\eta - \hat{H}}. \quad (1.23)$$

The level density is derivative of the staircase function defined as the number of eigenvalues below energy E : $N(E) = \text{Number} \{E_n < E\} = \sum_n^{\infty} \Theta(E - E_n)$. The singularities of the level density on the real axis give eigenvalues of the discrete spectrum of \hat{H} . It is difficult to establish exact quantum mechanical expression for the evolution operator. The path integral formulation is proved to be quite useful in establishing an expression for the evolution operator and a propagator.

1.3.2 A Propagator and Path Integral

In position representation equation (1.14), can be written as

$$\begin{aligned} \Psi_t(\mathbf{q}) &= \langle q | \hat{U}(t, t') | \Psi_{t'} \rangle \\ &= \int dq' \langle q | \hat{U}(t, t') | q' \rangle \langle q' | \Psi_{t'} \rangle \\ &= \int dq' K(qq' : tt') \Psi_{t'}(q') \end{aligned} \quad (1.24)$$

where $K(qq' : tt') = \langle q | \hat{U}(t, t') | q' \rangle$ is propagator, which gives wave function at time t and position q once the wave function at t' , q' is known. It may be noted that equation (1.24) is in fact the expression of Huygens principle of the wave propagation. The propagator satisfies Schrödinger equation (1.1) along with initial condition

$$\lim_{t \rightarrow t'} K(qq' : tt') = \delta(q - q'). \quad (1.25)$$

It also follows from the group composition properties of the evolution operator and definition of the propagator that the propagator also satisfies the semi-group property *e.g.*

$$K(qq' : tt') = \int dq'' K(qq'' : tt'') K(q''q' : t''t') \quad (1.26)$$

Thus transition from $(q', t') \rightarrow (q, t)$ involves all the possible points, hence all possible paths. This notion of propagation over all possible path is very important in the path integral formulation of quantum mechanics[18].

Consider a transition between two space-time points (q_i, t_i) and (q_f, t_f) . Divide the time interval $\tau = t_f - t_i$ in N equal pieces of length $\Delta t = \tau/N$. The semi-group property implies (with $q_N, t_N = q_f, t_f$ and $q_0, t_0 = q_i, t_i$)

$$K(q_f q_i : t_f t_i) = \int \cdot \int dq_1 dq_2 \cdots dq_{N-1} \prod_{n=0}^{N-1} K(q_{n+1} q_n : \Delta t) \quad (1.27)$$

The paths entering in the above equation are not necessarily classical trajectories, and in general continuous but non-differentiable. Formally, these paths are similar to those of Brownian motion, which are Markovian Processes. Using equation(1.17), the propagator for the Hamiltonian of form (1.15), over a small time interval Δt can be written as

$$K(q_{n+1} q_n : \Delta t) = \langle q_{n+1} | \exp\left\{-\frac{i\hat{H}\Delta t}{\hbar}\right\} | q_n \rangle. \quad (1.28)$$

Using identity $\exp\{\hat{A} + \hat{B}\} = \exp\{\hat{A}\} \exp\{\hat{B}\} \exp\left\{-\frac{1}{2}[\hat{A}, \hat{B}]\right\} \cdots$, where commutator $[\hat{A}, \hat{B}] = \hat{A}\hat{B} - \hat{B}\hat{A}$ and dots represents higher order commutators, one can write

$$\exp\left\{-\frac{i\hat{H}\Delta t}{\hbar}\right\} \simeq \exp\left\{-\frac{i\Delta t \hat{T}}{\hbar}\right\} \exp\left\{-\frac{i\Delta t \hat{V}}{\hbar}\right\} \left(1 + \frac{1}{2} \left(\frac{\Delta t}{\hbar}\right)^2 [\hat{T}, \hat{V}]\right) \quad (1.29)$$

In the limit $N \rightarrow \infty$, Δt becomes small enough so that $O(\Delta t^2)$ terms can be neglected. Therefore, equation (1.28) becomes

$$K(q_{n+1} q_n : \Delta t) = \langle q_{n+1} | \exp\left\{-\frac{i\hat{T}\Delta t}{\hbar}\right\} | q_n \rangle \exp\left\{-\frac{i\Delta t \hat{V}}{\hbar}\right\},$$

which can be rearranged in form

$$K(q_{n+1} q_n : \Delta t) = \left(\frac{m}{2\pi i \hbar \Delta t}\right)^{-\frac{f}{2}} \exp\left\{\frac{i\Delta t}{\hbar} \left[\frac{m}{2} \left(\frac{\mathbf{q}_{n+1} - \mathbf{q}_n}{\Delta t}\right)^2 - V\right]\right\}.$$

Thus in limit $N \rightarrow \infty$, equation (1.27) becomes

$$K(\mathbf{q}_N \mathbf{q}_0 : \Delta t) = \lim_{N \rightarrow \infty} \int \cdots \int \left(\frac{m}{2\pi i \hbar \Delta t}\right)^{-\frac{1}{2}} \prod_{j=1}^{N-1} d\mathbf{q}_j (2\pi \hbar \Delta t)^{-\frac{f}{2}} \exp\left\{\frac{i}{\hbar} \int_{t_i}^{t_f} dt \mathcal{L}(\mathbf{q}, \dot{\mathbf{q}})\right\} \quad (1.30)$$

where, $\mathcal{L}(\mathbf{q}, \dot{\mathbf{q}}) = T - V$, is the classical Lagrangian. In the phase of above equation we have Hamilton's Principal Function

$$R[\mathbf{q}(t)] = \int_{t_1}^{t_f} \mathcal{L}(\mathbf{q}, \dot{\mathbf{q}}) dt. \quad (1.31)$$

The physical path (or classical trajectory) will be realized only if one extremizes $R[\mathbf{q}]$.

We are now interested in the semi-classical limit of equation(1.30). The semi-classical limit is obtained via method of stationary phase approximation, which amounts to an expansion about the classical path.

1.3.3 Stationary Phase Approximation:

The kernel of the propagator (1.30) is complex exponential of the type $(\exp(\frac{iR}{\hbar}))$. The stationary phase approximation [19] is an asymptotic approximation of the Feynman Path Integral where \hbar is considered as a small parameter.

Consider a simple example, i.e. the evaluation of following integral

$$F(\frac{1}{\hbar}) = \int_{-\infty}^{\infty} dx \exp\left(\frac{if(x)}{\hbar}\right) \quad (1.32)$$

When $\hbar \rightarrow 0$, the exponential becomes highly oscillatory function of x and the integral becomes nearly zero. However there are points where the oscillations stop. These points are located where the variation of $f(x)$ slow down. Therefore phase become stationary at these points, i.e. $f'(x_c) = 0$. The set of points $\{x_c\}$ are called set of stationary points. The idea is to find stationary points in the domain of integration, including boundaries, and calculate their contribution to the integral separately.

This is done by expanding $\exp\left(\frac{if(x)}{\hbar}\right)$ around each of the stationary point x_c . Then equation (1.32) can be written as

$$F(\frac{1}{\hbar}) = \int_{-\infty}^{\infty} dx \exp\left(\frac{i}{\hbar} \left[f(x_c) + \frac{f''(x_c)}{2} (x - x_c)^2 + \dots \right]\right). \quad (1.33)$$

In most of the examples $f''(x) \neq 0$, and gives dominant contribution hence, one can neglect cubic or higher order terms. If integrand is analytically continued into the complex plane of x , one needs to consider complex critical

points. Integral can then be performed by a steepest-descent method. Tunneling is one of the physical phenomenon in which complex critical points are important.

By considering only quadratic terms equation (1.33) can be transformed into an imaginary Gaussian integral, which can be evaluated to give

$$F\left(\frac{1}{\hbar}\right) = \sqrt{\frac{2\pi\hbar i}{f''(x_c)}} \text{Exp}\left(\frac{if(x_c)}{\hbar}\right) \quad (1.34)$$

Turning back to equations(1.30) and (1.31), the stationary points (or paths) are solutions of equation

$$\delta R(\mathbf{q}(t)) = 0,$$

which therefore are the classical trajectories satisfying boundary condition $\mathbf{q}(0) = \mathbf{q}_0, \mathbf{q}(t) = \mathbf{q}$, as well as Newton's equations. We can expand action W around the critical path (i.e. classical orbit) $\mathbf{q}^c(t)$

$$R[\mathbf{q}^c + \delta\mathbf{q}] = R[\mathbf{q}^c] + \frac{\delta R}{\delta\mathbf{q}}[\mathbf{q}^c]\delta\mathbf{q} + \frac{\delta^2 R}{2!\delta\mathbf{q}^2}[\mathbf{q}^c]\delta\mathbf{q}\delta\mathbf{q} + \dots$$

It may be recalled that the type of extremum for the classical orbit and hence linear stability of the orbit depends on the nature of second variation. Thus the information about the stability of the classical orbit enters into the semi-classical framework via second variation of the action functional. The second variation of the action is given by

$$\delta^2 R[f] = \int_0^t dt \delta\mathbf{q}^\top(t) (\mathcal{L}[f]) \delta\mathbf{q}(t); \quad \delta\mathbf{q}(0) = \delta\mathbf{q}(t) = 0 \quad (1.35)$$

where $\mathcal{L} = -\frac{d^2}{dt^2}\delta\mathbf{q} - \partial_{qq}^2 V[f]\delta\mathbf{q}$. A solution of $\delta^2 R[f] = 0$ is a Jacobi field along the classical path. The equation of motion for the variation under this Lagrangian \mathcal{L} is of the form of Jacobi-Hill equation. With stipulated boundary conditions, we have a Sturm-Liouville problem for the operator $\hat{D} = -\frac{d^2}{dt^2} - \partial_{qq}^2 V$, over the time interval $(0, t)$. The operator \hat{D} is real symmetric so that it has real eigenvalues μ_n corresponding to real eigenfunction

\mathbf{u}_n , forming a complete basis on which it is possible to expand any variation satisfying boundary conditions as

$$\delta\mathbf{q} = \sum_{n=0}^w a_n \mathbf{u}_n \quad (1.36)$$

with $\hat{D} \cdot \mathbf{u}_n = \mu_n \mathbf{u}_n$, $\mathbf{u}_n(0) = \mathbf{u}(t) = \mathbf{0}$, and $\int_0^t dt \mathbf{u}_m^\top(t) \cdot \mathbf{u}_n(t) = \delta_{nm}$. The second variation becomes diagonal in this new basis.

$$\delta^2 R = \frac{1}{2} \sum_{n=1}^{\infty} \mu_n a_n^2 \quad (1.37)$$

The nature of the classical path depends on the sign of the quadratic form of the second variation, which in turn depends on the number of negative eigenvalues of the operator \hat{D} . In general variation of eigenvalues is either negative or zero for solutions of equation (1.36). Therefore with increasing time interval μ_n will decrease crossing zero at time say T_n . The equation $\hat{D} \cdot \delta\mathbf{q} = 0$ admits a nontrivial solutions at this times satisfying b.c. $\delta\mathbf{q}(T_n) = 0$. At other times no such solution exist. The conjugate points corresponds to the times $T = T_n$.

Both sides of equation (1.36) are then differentiated with respect to T and the integral (1.35) can be solved.

There exist several classical paths $\mathbf{q}_l(t)$ that goes from \mathbf{q}_0 to \mathbf{q} during time t , and each of these stationary solution contribute to the propagator. From above comments we can write equation (1.30) as

$$K(\mathbf{q} \mid \mathbf{q}_0 : t) = \sum_l \left(\frac{m}{2\pi i \hbar \Delta t} \right)^{\frac{Nf}{2}} \exp \left\{ \frac{i}{\hbar} R(\mathbf{q}_l^c) \right\} \int d^{(N-1)f} [\delta\mathbf{q}] \exp \left\{ \frac{i}{2\hbar} (\partial_{qq}^2 R) \delta\mathbf{q} \delta\mathbf{q} \right\}. \quad (1.38)$$

The higher order terms are obtained in [15]. The matrix of the second derivatives $\underline{D} = \partial_{qq}^2 R[\mathbf{q}]$ is a $(N-1)f \times (N-1)f$ matrix given by

$$\underline{D} = \frac{1}{\Delta t} \begin{bmatrix} A_1 & -1 & 0 & 0 & \cdots & 0 \\ -1 & A_2 & -1 & 0 & \cdots & 0 \\ 0 & -1 & A_3 & -1 & \cdots & 0 \\ \vdots & \vdots & \vdots & \vdots & \ddots & \vdots \\ 0 & 0 & 0 & \cdots & -1 & A_{N-1} \end{bmatrix}$$

where A_n are $f \times f$ matrices given by $A_n = A_{\alpha\beta}(n\Delta t) = 2\delta_{\alpha\beta} - \Delta t^2 \partial_{\alpha\beta}^2 V$. In the limit $\Delta t \rightarrow 0$ the matrix \underline{D} is related to the Jacobi-Hill operator \hat{D} . The

propagator can be obtained evaluating all the Gaussian integrals and their moments. Finally one gets

$$K(\mathbf{q}, \mathbf{q}_0 : t) = \sum_l \left(\frac{m}{2\pi i \hbar} \right)^{\frac{f}{2}} \left| \det_{ij} \frac{\partial^2 R_l}{\partial q_0^i \partial q^j} \right|^{1/2} \exp \left\{ \frac{i}{\hbar} R_l(\mathbf{q}_0, \mathbf{q}; t) - \frac{i\pi\nu_l}{2} \right\}. \quad (1.39)$$

where ν_l is the Morse index.

As mentioned earlier a Fourier transform establishes the bridge between the energy and time domain, the energy Green function can be obtained by taking Fourier transform of equation (1.39):

$$G(\mathbf{q}, \mathbf{q}_0) = \frac{1}{i\hbar} \int_0^\infty dt \exp\left(\frac{iEt}{\hbar}\right) K(\mathbf{q}, \mathbf{q}_0; t). \quad (1.40)$$

This integral can again be evaluated using stationary phase approximation. Here the stationary phase condition is $\partial_t [Et + R_l] = 0$. If we define the reduced action $S_l(\mathbf{q}_0, \mathbf{q}; E) = Et + R_l(\mathbf{q}_0, \mathbf{q}; t(\mathbf{q}_0, \mathbf{q}; E)) = \int_{q_0}^q \mathbf{p} \cdot d\mathbf{q}$ we obtain a quantity independent of time, $\partial_t S_l = 0$. This stationary phase condition picks up all the classical trajectories l from \mathbf{q}_0 to \mathbf{q} at given energy E . The following steps are same as above and as a result we get

$$G(\mathbf{q}_0, \mathbf{q}; E) = \frac{1}{i\hbar(2\pi i \hbar)^{(f-1)/2}} \sum_l |\det D|^{1/2} \exp \left\{ \frac{iS_l(\mathbf{q}_0, \mathbf{q}; E)}{\hbar} - \frac{i\nu_l\pi}{2} \right\} \quad (1.41)$$

where

$$D = \begin{bmatrix} \frac{\partial^2 S}{\partial q_0 \partial q} & \frac{\partial^2 S}{\partial q_0 \partial E} \\ \frac{\partial^2 S}{\partial E \partial q} & \frac{\partial^2 S}{\partial E^2} \end{bmatrix}.$$

Finally, to obtain semi-classical density of states as in equation(1.23), we take trace of above Green function. The contributions to the trace mainly comes from two sources: (i)very short paths for which the propagator is delta function [20]. In fact these are equilibrium points of the system. (ii) periodic orbits of non-zero length. The contribution of paths that are closed but not periodic, is negligible as a result of destructive interference among themselves. The former leads to Thomas-Fermi term for the average density of states

$$d_{av}(E) = \frac{1}{\hbar^f} \int d\mathbf{p} d\mathbf{q} \delta(E - H(\mathbf{p}, \mathbf{q})). \quad (1.42)$$

The second source leads to the oscillatory contribution for the density of states, which in general form can be written as

$$d_{osc}(E) = \sum_l \sum_r A_{l,r}(E) \cos(r(S_l(E) - \alpha_l)) \quad (1.43)$$

where l, r denotes the primitive periodic orbits and their repetitions respectively, and S_l, α_l denotes action and phase. The amplitudes $A_{l,r}$ depend on two aspects of the periodic orbit-whether they are stable and whether they are isolated. The total density of states is sum of these contributions,

$$d(E) = d_{av}(E) + d_{osc}(E). \quad (1.44)$$

1.4 Density of States for Pseudo-integrable Billiards

In the pseudo-integrable billiards almost all(in sense of Lebesgue measure) periodic orbits are marginally stable and non-isolated (i.e. occur in bands.). The density of states is given by [21]

$$d(E) = \frac{m}{2\pi\hbar^2} \operatorname{Re} \sum_i \int \int d\mathbf{q} H_0^{(1)}\left(\frac{l_i}{\hbar}\sqrt{2mE}\right) \exp(i\alpha_i\pi). \quad (1.45)$$

where m is mass of the particle(billiard ball) and l is length of the periodic orbits. The index α_i (half of Maslov indices ν) represents number of specular reflections at the boundary of the billiard. And $H_0^{(1)}$ is a Bessel Function of third kind (Hankel function). Since periodic orbits form continuous families on the invariant surface and each orbit in the family has the same value of l_i , independent of \mathbf{q} , integration in (1.45) is trivial. The oscillatory contribution to the density of states in the asymptotic form ($\hbar \rightarrow 0$) is then given by

$$d_{osc}(E) = \left(\frac{m}{2\pi^2\hbar^2}\right)^{3/4} E^{-1/4} \sum_i \frac{A_i}{l_i^{1/2}} \cos\left(\frac{l_i}{\hbar}\sqrt{2mE} + (\alpha_i - \frac{1}{4})\right), \quad (1.46)$$

where A_i represents area of the bands of the periodic orbits. The summation here is over all primitive periodic orbits and their repetitions. The average contribution from zero length periodic orbit gives the Wyle area[22] contribution to the level density

$$\begin{aligned} d_{av}(E) &= \frac{mA_R}{2\pi\hbar^2} \operatorname{Re}(A_R H_0^{(1)}(0)) + \text{higher.order.terms.} \\ &= \frac{mA_R}{2\pi\hbar^2} J_0(0) + h.o.t. = \frac{mA_R}{2\pi\hbar^2} + h.o.t. \end{aligned} \quad (1.47)$$

where, A_R is configuration space area of the billiard and higher order terms include corrections from boundary and corners of the configuration space.

Integrated density of states or mode number $N(E) = \text{Number} \{E_n < E\} = \sum_n^\infty \Theta(E - E_n)$ is then given by

$$N(E) = \int_0^E dE' \ d(E') \quad (1.48)$$

Once the complete information about classical variables such as l, A is obtained, equations (1.46) and (1.47) can be used to study various spectral fluctuation properties in which we are interested.

In this chapter, we have attempted to give brief sketch of the developments in semi-classical techniques taken place during last few decades. In particular the problem begun by Selberg of finding semi-classical properties of a quantum particle moving on a constant negative curvature Riemann surface, has enjoyed a flurry of new activity in recent years. An extensive development of concepts by Gutzwiller and other workers have resulted in many applications in laser spectroscopy, Rydberg states of atoms or molecules, electronic semiconductor devices etc. The success for the path integral approach is in the fact that in all these systems periodic orbits can be classified, their actions computed, and the path integrals can be summed. Many techniques have been developed to carry out this task. The Gutzwiller trace formula, however, gives only leading order terms in the \hbar expansion. Higher order terms also have been computed recently by Gaspard[15].

Bibliography

- [1] A.Einstein, Verh. Dtsch. Phys. Ges. **19**, (1917)82.
- [2] P.Ehrenfest, Verh. Deut. Phys. Ges. **15**, (1913)451; Ann. der Phys. **51**, (1916)327.
- [3] G.Wentzel, Z.Physik **38**, (1926)518; H.A.Kramers, Z.Physik **39**, (1926)828; L.Brillouin C.R. Acad. Sci. Paris **183**, (1926)24.
- [4] V.P.Maslov and M.V.Fedoriuk, Semi-Classical Approximation in Quantum mechanics(Reidel, Boston, MA, 1981).
- [5] J.B.Delos, Adv. Chem. Phys. **65**, (1986)161.
- [6] I.C.Percivel, Adv. Chem. Phys. **36**, (1977)1.
- [7] R.G.Littlejohn, J. Stat. Phys. **68**, (1992)7.
- [8] A.Selberg, J.Indian Math. Soc., **20**, (1956)47.
- [9] C.Morette, Phys. Rev. **81**, (1951)848.
- [10] Ph.Choquard, Helv. Phys. Acta, **28**, (1955)89.
- [11] L.S.Schulman, Techniques and Applications of Path Integration, (Wiley-Interscience, New York, 1956).
- [12] M.C.Gutzwiller, J.Math. Phys. **8**, (1967)1979; **10**, (1969)1004; **11**, (1970)1791; **12**, (1971)343.
- [13] R.Balian and C.Bloch, Ann. Phys. **60**, (1970)401; **63**, (1971)592; **64**, (1971)271; **69**, (1972)76; **85**, (1974)514.

- [14] M.V.Berry and M.Tabor, Proc. Roy. Soc. Lond. Ser **A349**, (1976)101; J.Phys. A:Math. and Gen. **10**, (1977)371.
- [15] P.Gaspard, D.Alonso, I.Burghardt, Adv. in Chem. Phys. vol. **XC**, (1995)105.
- [16] W.Thirring, Quantum Mechanics of Atoms and Molecules, Springer, New York, 1981.
- [17] C.J.Joachain, Quantum Collision Theory, North-Holland, Amsterdam, 1975.
- [18] R.P.Feynman and A.R.Hibbs, Quantum Mechanics and Path Integrals, McFraw-Hill, New York, 1965.
- [19] N. Bleistein and R.A.Handelsman, Asymptotic Expansion Of Integrals, Dover, New York, 1986.
- [20] M.V.Berry and K.E.Mount, Rep. Progr. Phys. **35**, (1972)315.
- [21] P.J. Richens and M.V.Berry, Physica **2D**, (1981)495.
- [22] H.P.Baltes and E.R.Hilf, Spectra of finite systems, (B-I, Wissenschaftsverlag, Mannheim, 1978).

Chapter 2

Billiards - Classical Dynamics

2.1 Introduction

Billiards are dynamical systems corresponding to the motion of a point like particle in a bounded domain Q , which is a compact Riemannian manifold with piecewise smooth boundary ∂Q . We assume $Q \subset Q_0$, Q_0 being a closed C^∞ Riemannian manifold. The boundary ∂Q consists of a finite number of smooth compact C^∞ sub-manifolds $\partial Q_1, \partial Q_2, \dots, \partial Q_r$ of co-dimension 1. The points of the boundary $\mathbf{q} \in \partial Q$ are singular of order n if ∂Q is only C^n at \mathbf{q} . The points which are not singular are called regular and represented by a set $\partial \tilde{Q} = \partial Q \setminus \{\mathbf{q} \text{ of order } < \infty\}$.

The particle reflect from the boundary according to law of elastic reflections. The motion between reflections corresponds to the geodesic flow G_t , associated to a Hamiltonian H_0 with Q_0 as configuration space. The reflection of the particle trajectories from a singular point of the boundary is not well defined. Being of measure zero (in Lebesgue sense) these trajectories are of little importance from the point of view of ergodic theory. These trajectories may play important role in semi-classical theories, rendering diffraction effects. Before turning to specific types of billiards we are interested, few relevant terminologies, definitions are given below.

2.1.1 Phase space

The phase space of the billiards is the set of all tangent vectors of fixed length, $M = \{\mathbf{x} = (\mathbf{q}, \mathbf{v}) | \mathbf{q} \in Q, \mathbf{v} \in S^{d-1}(\mathbf{q})\}$ where $d = \dim Q$ and $S^{d-1}(\mathbf{q})$

is the unit sphere of dimension $d - 1$ over \mathbf{q} . The reflections of $\mathbf{x} \in \partial\widetilde{M} = \{\mathbf{x} = (\mathbf{q}, \mathbf{v}) \in M \mid \mathbf{q} \in \partial\widetilde{Q}\}$ where $\partial\widetilde{Q} = \partial Q \setminus \{\mathbf{q}\}$ of order 0, are defined by $R : (\mathbf{q}, \mathbf{v}) \rightarrow (\mathbf{q}, \mathbf{v} - 2\langle \mathbf{n}_\mathbf{q}, \mathbf{v} \rangle \mathbf{n}_\mathbf{q})$. Here, $\mathbf{n}_\mathbf{q}$ is the unit inward normal to ∂Q at \mathbf{q} . Let $\pi : M \rightarrow Q$ (equivalently, $\mathbf{x} = (\mathbf{q}, \mathbf{v}) \mapsto \mathbf{q}$) be the natural projection on Q . Since $\pi^{-1}(\mathbf{q}) = \mathbf{q} \otimes S^{d-1}(\mathbf{q})$, we have $\dim M = 2d - 1$. For $\mathbf{x} \in M$, the point $\mathbf{q} = \pi(\mathbf{x})$ is said to be carrier of \mathbf{x} . M possesses a natural involution sending each point $\mathbf{x} = (\mathbf{q}, \mathbf{v}) \in M$ into a point $\mathbf{x}' = (\mathbf{q}, -\mathbf{v}) \in M$.

Definition 2 *The measure μ on M is defined as*

$$d\mu = d\rho(\mathbf{q})d\omega(\mathbf{q}) \quad (2.1)$$

where $d\rho(\mathbf{q})$ is the element of volume generated by the Riemannian metric into Q and $d\omega(\mathbf{q})$ is the Lebesgue measure into $S^{d-1}(\mathbf{q}) \ni \mathbf{v}$.

The flow G_t of the billiard corresponds to a vector field $\{G_t(\mathbf{x}), \mathbf{x} \in M_0\}$, where $G_t(\mathbf{x})$ is a tangent vector to M_0 at \mathbf{x} . (M_0 being unit tangent bundle over Q_0). The flow G_t thus determines the motion of a particle with unit velocity along geodesic lines. We define flow Φ_t at the moment of a reflection from boundary ∂Q as follows

$$\Phi_{\tau(\mathbf{x})} = \begin{cases} G_{\tau(\mathbf{x})}, & \text{if } \mathbf{x} \notin M_- \\ G_{\tau(\mathbf{x})} \circ R, & \text{if } \mathbf{x} \in M_- \end{cases} \quad (2.2)$$

where, $M_- = \{\mathbf{x} = (\mathbf{q}, \mathbf{v}) \in \partial\widetilde{M} \mid \langle \mathbf{n}_\mathbf{q}, \mathbf{v} \rangle \leq 0\}$ and $\tau(\mathbf{x})$ is the nearest strictly positive moment of a boundary reflection of the trajectory issued from \mathbf{x} .

Let N_{ij} be the set of all interior points $\mathbf{x} \in M$ such that the segment of the geodesic line in the direction of \mathbf{x} intersect ∂Q on $\partial Q_i \cap \partial Q_j$. Denote by $N^{(1)}$, the set of all points $\mathbf{x} \in M$ which will be contained in $\cup_{i \neq j} N_{ij}$ at some step of construction of the geodesic flow. Denote by $N^{(2)}$, a set all \mathbf{x} for which process of construction of a geodesic leads to an infinite number of reflection in finite time. Then

Definition 3 *If for almost every (in the sense of measure μ) $\mathbf{x} \in M' = M \setminus (N^{(1)} \cup N^{(2)})$, we have a geodesic segment of a finite length with end point located at a regular point, the billiards are said to be proper.*

We will consider here proper billiards only. Dynamics of billiards is of Hamiltonian nature. However, due to the reflections on the boundary its dynamics cannot be completely described by a Hamiltonian, unlike a particle moving under the influence of a conservative force. There are many examples of dynamical system that can equivalently be described in a billiard. For example system of two particles of masses m_1, m_2 moving in a unit interval $[0, 1]$, bouncing off from boundary as well as from each other elastically is equivalent to a triangular billiard. Another example is of three hard rods sliding along a frictionless ring and making elastic collisions which is also equivalent to a billiard on triangular table[1]. One can also deform a Hamiltonian system mathematically into a billiard.[2, 3, 4]

The billiards can exhibit all features of dynamical systems, from integrability to chaotic behaviour. The behaviour of course depends on the geometry of the billiard table. Billiards can be classified according to their behavioural pattern as: 1) Hyperbolic billiards or dispersing billiards, e.g., polygons with smooth obstacles[5], some billiards with convex boundary[6], 2)Elliptical billiards with strictly positive curvature convex tables[7]. 3) Parabolic billiards, e.g., polygonal billiards. Here we shall concentrate on polygonal billiards in the Euclidean plane.

2.2 Polygonal billiards

Let P be closed, connected, non-self intersecting polygon in the Euclidean plane, $P \subset \mathbb{R}^2$, whose boundary ∂P consist of a finite number of line segments(edges), we denote them in arranged order $\partial P_1, \partial P_2 \dots \partial P_r$ (some times we will use notations $a_1, a_2 \dots$ etc. for convenience) such that $\partial P_{i \pm 1}$ are neighbour of ∂P_i . The points $\partial P_i \cap \partial P_{i \pm 1}$ are vertices of P . We thus have a set of regular points $\partial \tilde{P} = \partial \tilde{\tilde{P}} = \{\mathbf{q} \in \partial P \mid \mathbf{q} \notin \partial P_i \cap \partial P_{i \pm 1}\}$. It is obvious that $\mathbf{q} \in \partial P_i \cap \partial P_{i \pm 1}$ are zero order singular points. We denote its phase space by $M(P)$. At each regular point $\mathbf{q} \in \partial P_i$, the unit normal vector is same and shall be denoted by \mathbf{n}_i .

Consider the one-parameter group $\{T^t\}$ of transformations on M (for $\mathbf{x} = (\mathbf{q}, \mathbf{v}) \in \mathbf{M}', -\infty < t < \infty$) defined as follows: $T^t \mathbf{x}_o$ is obtained by starting at \mathbf{q}_o and drawing a continuous path inside P consisting of straight line segments and of total length $|t|$ and ending at $\mathbf{x}_t = (\mathbf{q}_t, \mathbf{v}_t)$. The straight line segments (except first and last) begin and end on ∂P and is called as the link of trajectory a given trajectory. The direction change at the boundary in

passing from one link to the next is made in accordance with laws of elastic reflections. This is done via a map $\sigma_i : S^1 \longrightarrow S^1$ at each point $\mathbf{x} = (\mathbf{q}, \mathbf{v})$, $\mathbf{q} \in \partial P_i$ which acts according to the formula $\sigma_i \mathbf{v} = \mathbf{v} - 2 \langle \mathbf{n}_i, \mathbf{v} \rangle \mathbf{n}_i$. If path hits vertex we stop trajectory there. The set of the form $\pi(\{T^t \mathbf{x} : -\infty < t < \infty, \mathbf{x} \in M'\})$ represents configuration trajectory of P . If trajectories hit vertices of P both in the future and in the past then trajectory is finite, we call it a *generalized diagonal* of P .

The procedure of unfolding polygons can be applied now (see Fig. 2.1). The configurational trajectory $\pi(\{T^t \mathbf{x}\})$ has vertices on ∂P_i . Starting from any reference point $(\mathbf{q}_0, \mathbf{v}_0)$ on the trajectory, let trajectory has successive vertices on the boundary segments of $a_1, a_2, a_3 \dots$ of P . Then reflections of P with respect to these faces transform broken line to the trajectory into a straight line intersecting the polygons $P, P_{a_1}, P_{a_1, a_2}, \dots$. Here, P_{a_1, a_2, \dots, a_i} is the polygon obtained by reflecting P with respect to the sides a_1, a_2, \dots, a_i . The velocity of the motion on the part of trajectory after k^{th} reflection is $\mathbf{v}_k = (\sigma_{a_k} \sigma_{a_{k-1}} \dots \sigma_{a_1}) \mathbf{v}_0$. Let G_P be the sub-group of the isometry group of the unit circle S^1 generated by the isometries $\sigma_1 \sigma_2 \dots \sigma_r$. In the analysis of billiard dynamics, the singularities produced by the vertices play a major role. The vertex angles and the relative lengths of the edges are important characteristics of P as far as dynamics is concerned. If all the angles of P are commensurable with π then we call P a *rational billiard*. The group G_P is finite for rational billiards. The problem of billiard dynamics deals with behaviour of the billiard trajectory. The question mainly falls into two categories, one concerning statistics which belong to ergodic theory and other concerning the topology of trajectories. Here we are more interested in the topological properties than the ergodic properties of the polygonal billiards. Most of the information we need for semi-classical study can be extracted from techniques developed in these areas. As shown in the previous chapter semi-classical properties of a system depends mainly on the periodic orbits. We shall therefore simply state some well known facts about ergodic properties of polygonal billiards. And discuss topological properties that mainly concerns about periodic orbits of polygonal billiards.

The billiard in a typical polygon is ergodic [8]. A prevailing opinion in the mathematical community is that polygonal billiards are never mixing, but this has not been established yet. However there is a conjecture about existence of *weakly mixing* polygonal billiards [9] which is stronger property than ergodicity but weaker than mixing. The rational polygonal billiards are however, proved to be not mixing. Some of the important facts relevant to

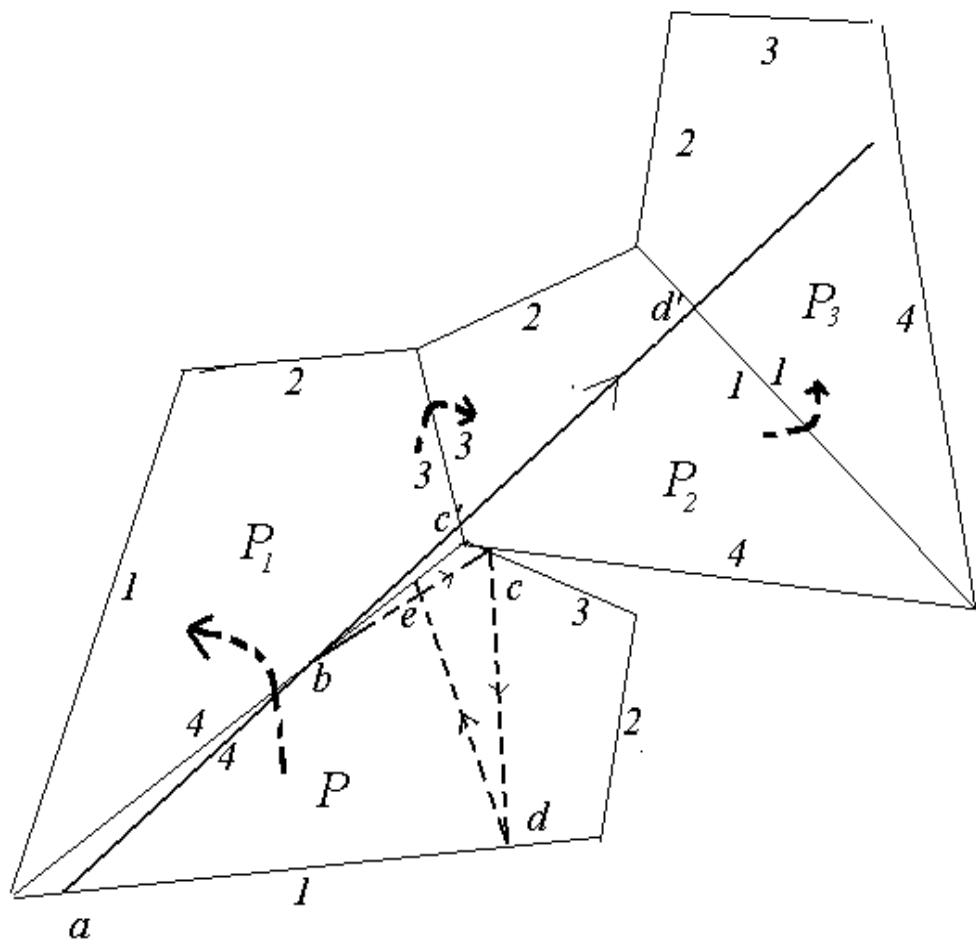


Fig. 2.1: Unfolding of a polygon P . Boundary segments are denoted by nos. 1,2,3,4. A trajectory starting from 'a' in P hits sides 4-3-1-4 at b-c-d-e respectively. A straightened trajectory $a-b-c'-d'-e'$ is obtained by reflecting P in side 4 to get P_1 and so on.

our work are presented below.

Proposition 1 *The set of generalized diagonals of P is countable.[10]*

Proof: Let X be the set of polygons obtained by unfolding along all billiard trajectories in P . Then X belongs to the set of polygons $\{gP : g \in G_P\}$ which is countable because the group G_P has finite number of generators and hence countable. This implies that set of pairs of vertices of any two polygons in X is also countable. \bullet

Theorem 3 *For any $\mathbf{q} \in P \subset \mathbb{R}^2$ and almost all (w.r.t. Lebesgue measure) $\mathbf{v} \in S^1$ the closer of the configurational trajectory of the point $\mathbf{x} = (\mathbf{q}, \mathbf{v})$ with respect to the billiards flow $\{T^t\}$ contains at least one vertex of the polygon.*

Let γ be periodic trajectory (of length L) in P with m links $\gamma_0, \gamma_1, \dots, \gamma_{m-1}$ such that γ_0 is the reflection of γ_{m-1} . Unfolding of γ then results in set of polygons $P_0 = P, P_1, \dots, P_{m-1}, P_m$. Choose a link γ_0 and let l be the line through γ_0 . The element $g \in G_P$ that moves P into P_m , also moves γ_0 into $\tilde{\gamma}_m$ (*tilde* here represents link in the unfolded polygon that corresponds to the link in original polygon) which belongs to the same line l as γ_0 . For example in Fig 2.1, γ is $abcd\dots$, links $\gamma_0, \gamma_1\dots$ are simply segments $ab, bc\dots$ so on and links in the unfolded polygons are $bc', c'd'$ etc.

Thus g preserves the line l , hence g is either a parallel translation along l preserving orientation, or a sliding reflection with axis l reversing the orientation. Since $gP = P_m$, g is the product of m reflections, m is even if g preserves orientation and odd if reverses orientation.

Corollary 1 *If m is even, γ extends to a band of periodic trajectories of length L parallel to γ . Both boundaries are unions of the generalized diagonals. If m is odd, every trajectory γ' starting close to γ and parallel to it comes back after m reflections to the same edge, at the same distance from γ and in the same direction but on the opposite side of γ .*

Proof: It is convenient to denote γ by γ_0 . unfolding P along γ_0 we obtain: 1)the sequence $P = P_0, P_1, \dots, P_m$, 2)the line l_0 and 3) the motion g such that $P_m = gP$. Let the point x_0 on the edge a of P be the starting point of γ_0 and let $y_0 = gx_0$ be the corresponding point on the edge $b = ga$ of P_m . The periodicity of γ_0 implies that l_0 goes from x_0 to y_0 .

Let γ be the trajectory starting at $x \in a$ close to x_0 and parallel to γ_0 . If γ is close enough to γ_0 , unfolding along γ we obtain the line l through x parallel to l_0 and passing by the same sequence $P = P_0, P_1, \dots, P_{m-1}$ of polygons. Let l intersect b at y .

If γ_0 is even, by previous discussion, the quadrangle formed by a, b, l_0 , and l is a parallelogram, thus $y = gx$, i.e. γ comes back to x in the same direction. Hence, γ is periodic. Now start moving γ_0 to the right parallel to itself. We then get γ_t , $t \geq 0$. For small t , γ_t is periodic of the same length as γ_0 . Increasing t we come to the moment $t = t_1$ such that $\gamma_1 = \gamma_{t_1}$, hits the vertex of P . Since γ_{t_1} is the limit of the periodic trajectory, it is also a generalized diagonal or union of such. The same argument works for $t \leq 0$.

When γ_0 is odd, the quadrangle above is a trapezoid and the point $x_1 = g^{-1}y$ on the side a where γ returns after m reflections is symmetric to x with respect to x_0 . •

Theorem 4 *In any rational polygonal billiard there is at most a finite number of prime periodic orbits of odd periods.*

Consider convex rational polygon P with r vertices. Its interior angles $\alpha_1, \alpha_2, \dots, \alpha_r$ being commensurable with π , can be written in form $\alpha_i = (k_i/n)\pi$, where $n \geq 1$ and the greatest common divisor of the numbers n, k_1, k_2, \dots, k_r is 1. Then we have following lemma for group G_P .

Lemma 1 *The group G_P is isomorphic to the symmetry group of a regular polygon with n vertices.*

Proof: Note that in the velocity space S^1 the composition of the symmetries corresponding to the sides bounding the angle α_i is a rotation $R_{2\alpha_i}$ of the circle S^1 by an angle $2\alpha_i = (2k_i/n)\pi$. Hence, for any family of integers s_0, s_1, \dots, s_r , the group G_P contains the rotation by an angle $\alpha = (s_0n + s_1k_1 + \dots + s_rk_r)(2\pi/n)$. But it follows from our assumptions that there exist a family s_0, s_1, \dots, s_r , for which $s_0n + s_1k_1 + \dots + s_rk_r = 1$. Hence the group G_P contains the rotation $R_{2\pi/n}$ and all rotations by angles which are multiples of $2\pi/n$. Moreover, the group G_P contains n symmetries with respect to the axes of the form $R_{2\pi/n}l$, $k = 0, 1, \dots, n-1$, where l is any of the axes of symmetry of $\sigma_1, \sigma_2, \dots, \sigma_r$. The transformations indicated above generate the symmetry group of a regular polygon of n sides. •

The group G_P is thus isomorphic to the *dihedral* group D_n . The group G_P therefore has $2n$ elements and the circle $0 \leq \theta \leq 2\pi$ is divided by the

action of G_P into $2n$ intervals $\pi(i-1)/n \leq \theta \leq \pi i/n$, $i = 1, \dots, 2n$. Every θ , $0 \leq \theta \leq 2\pi$ is equivalent by action of G_P to a unique θ_1 , $0 \leq \theta \leq \pi/n$, so that set of orbits of G_P is parametrized by $[0, \pi/n]$. The orbit of every θ , $0 \leq \theta \leq \pi/n$ has $2n$ elements, the orbits of $\theta = 0$ and $\theta = \pi/n$ have n elements each.

2.3 Invariant Surface of Polygonal Billiards

Theorem 5 *If G_P is a finite group, then the billiards in the polygon P are not ergodic. Moreover, to each orbit of the natural action of the group G_P on S^1 (i.e., to the set $\Omega = \Omega(\mathbf{v}_0) = \{g\mathbf{v}_0 \in S^1 : g \in G_P\}$), corresponds to the set A_Ω , invariant with respect to $\{T^t\}$, consisting of all $\mathbf{x} = (\mathbf{q}, \mathbf{v}) \in M$ such that $\mathbf{v} \in \Omega$. [20]*

Proof: Suppose $\mathbf{x} = (\mathbf{q}, \mathbf{v}) \in A_\Omega$, i.e., $\mathbf{v} = g_0\mathbf{v}_0$, $g_0 \in G_P$. Then any $t \in \mathbb{R}$, we have $(\mathbf{q}_t, \mathbf{v}_t) = T^t\mathbf{x} \in A_\Omega$. Since the group G_P is finite we can find a set of orbits of the group $G_P : C \subset S^1/G_P$ whose measure differs from zero or one. The set $A = \bigcup_{\Omega \in C} A_\Omega$ is invariant w.r.t. $\{T^t\}$ and $\mu(A)$ differs from zero or one.●

This theorem states that for a finite group G_P , only a finite number of directions may be obtained when we move along billiards trajectories from the given initial direction.

It may be noted that any vector $\mathbf{v} \in S^1$ can equivalently expressed in terms of angle θ . From the discussion of previous section for any θ , $0 \leq \theta \leq \pi/n$, the set $R_\theta \equiv A_\Omega$ is invariant under the billiard flow. The invariant surface R_θ are *level surfaces* of the function $\psi = M(P) \rightarrow [0, \pi/n]$, defined as $\psi(x, \eta) = \theta$, where $0 \leq \theta \leq \pi/n$ and $\eta = g\theta$ [10, 11, 12, 13]. The function ψ is independent of the Hamiltonian H that gives rise to the flow of the billiard and is a constant of motion.

2.3.1 Construction of the invariant surface

The invariant surfaces R_θ for $0 \leq \theta \leq \pi/n$ are isomorphic to a surface R which can be geometrically constructed the polygon P (see Fig. 2.2 for an example). To construct R which is made up of $2n$ copies of P , say $P_1, P_2 \dots, P_{2n}$, choose θ_1 , $0 \leq \theta_1 \leq \pi/n$ and denote $\theta_2, \theta_3, \dots, \theta_{2n}$ the elements of the G_P -orbit of θ_1 in the natural order. Now take polygon P_1 remove it from list

of $2n$ copies of P_1 and consider any trajectory in direction θ_1 , it hits a side say a_{ij} of P_1 . Reflect P_1 on the plane about a_{ij} , join the reflected P_1 (say P_1') to the figure under construction (i.e. R) resulting in a combined figure $P_1 + P_1' = P_1'$ and remove a copy of P_1' from set of $2n$ copies of P . Repeat the whole process with P_1' , for trajectory in the same direction θ_1 but not necessarily along the same line. Each time trajectory meets a side a_{ij} , carry out reflection. If $P_{i'}$ is still in the list of $2n$ polygons join it to the figure under construction and remove it from the list. If $P_{i'}$ is not in the list then identify side a_{ij} and corresponding side of $P_{i'}$ in the P_i' which are already drawn and transfer a trajectory to $P_{i'}$. Repeat the procedure until all the $2n$ polygons are exhausted from the list, and resulting in a polygonal surface R . In the case of overlapping between P_i' we consider them belonging to the different copies of the plane. There are many possible surfaces R for a given P . The polygon R has an even number of sides and they are divided in pairs, each side of any pair differs from the other one by a parallel translation. The billiard flow have simple realization on R . Consider a trajectory in any direction θ , suppose it meets boundary segment a of R . Since sides of R comes in a pair, let b be pair of a . The trajectory meeting a gets instantly transferred to b by the parallel translation that identifies a and b . The trajectory then starts anew in the same direction θ from the side b .

If each identified pair glued together one gets the invariant surface R (we keep here same notation R for simplicity reason). It is therefore clear that R is a closed surface without any boundary. It can also be shown that R is orientable. The gluing or identifying sides preserve the orientation of the side.

2.3.2 Topology of the invariant Surface

The topological type of a closed orientable surface R is determined by its genus $g(R)$. The surface of genus g looks like a pretzel with g holes or equivalently a sphere with g handles.

Again, let $\pi m_i/n_i$, $i = 1, \dots, r$, be the vertex angles between the sides of P . From discussion above one can see that each vertex a_i of P with angle $\pi m_i/n_i$ gives rise to n/n_i singular points a_{ij} of the flow on R . Each a_{ij} has $2m_i$ equally spaced throngs and the flow lines in a small neighbourhood of such singular point are shown in Fig.(2.3). Singular points of this type are called multisaddles, the flow lines coming into and going from the singular point are called the incoming and the outgoing separatrices. Thus a vertex a_i gives

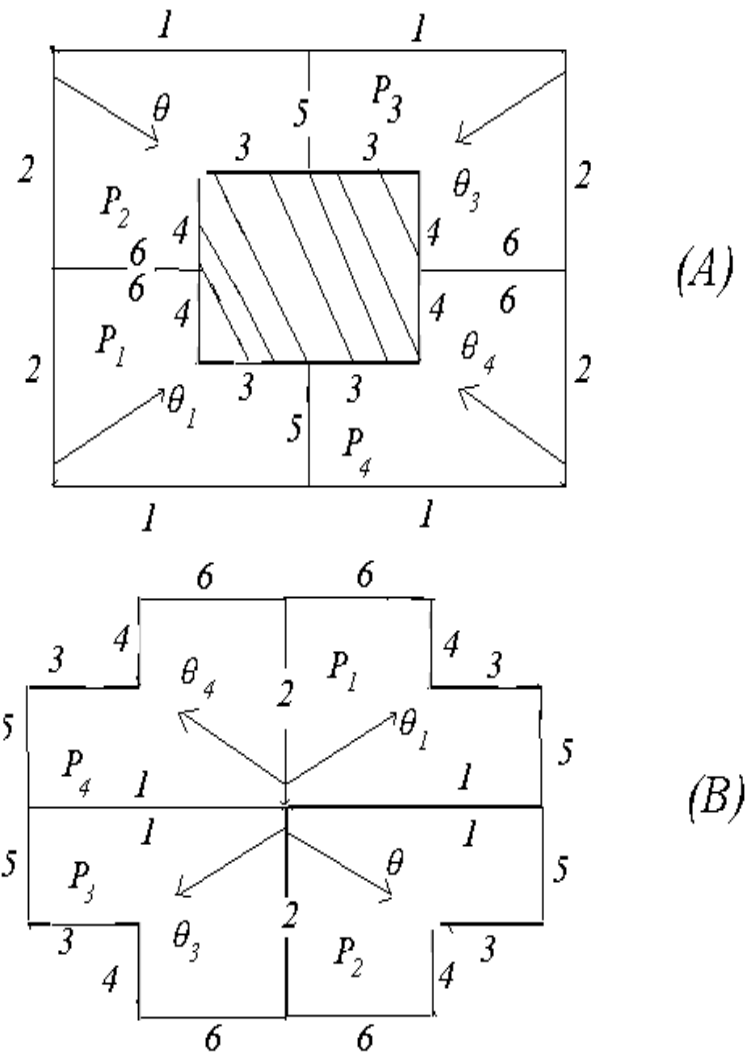


Fig. 2.2: (A) and (B) shows two different surfaces ' R' of a 'L' shaped billiard P_1 . Here since ' n ' = 2, we require four copies of P_1 , i.e. $P_1 P_2 P_3$ and P_4 . Respective identification of the sides are shown by nos. 1, 2...

rise to n/n_i multisaddles on R with m_i number of incoming and outgoing separatrices each. Varying θ does not change the position of multisaddles a_{ij} but uniformly rotates the separatrices around a_{ij} . The index of a multisaddle a with $2m$ separatrices is equal to $m - 1$. The index formula for the Euler number gives

$$\chi(R) = \sum_{i=1}^r \frac{n}{n_i} (1 - m_i) = 2 - 2g(r) \quad (2.3)$$

and hence the genus of the surface R is

$$g(R) = 1 + \frac{n}{2} \sum_{i=1}^r \frac{m_i - 1}{n_i}. \quad (2.4)$$

Thus the topology of R is thus determined by the angles of P . The surfaces $R_0, R_{\pi/n}$ are called exceptional invariant surfaces. Their topology, is not determined by the angles of P [14].

The topology of the invariant surface determines whether the system is completely integrable or not. We will now discuss this in a dynamical sense.

2.4 Integrability and beyond:

The dynamics of classical Hamiltonian system is completely described by the Hamilton's equations of motion

$$\dot{q}_i = \frac{\partial H}{\partial p_i}; \quad \text{and} \quad \dot{p}_i = -\frac{\partial H}{\partial q_i}$$

where symbols have their usual meaning i.e. H is the Hamiltonian and (q_i, p_i) are the canonical coordinate-momentum pair.

Consider a system of f degrees of freedom with the Hamiltonian H . The Hamiltonian induces the flow Φ_t on the phase space M . The dynamical system is integrable (in the sense of Liouville)[15, 16] if there exists a canonical transformation such that the new momenta are the constants of motion. A necessary and sufficient condition for this transformation to exist is that it should be possible to find f analytic functions $\{F_i\}_{i=1\dots f}$ on M satisfying following conditions :

- The Poisson bracket, $\{F_i, H\} = 0$ for all i , which implies $F_i(\Phi_t x) = F_i(x)$ for all $x \in M$,

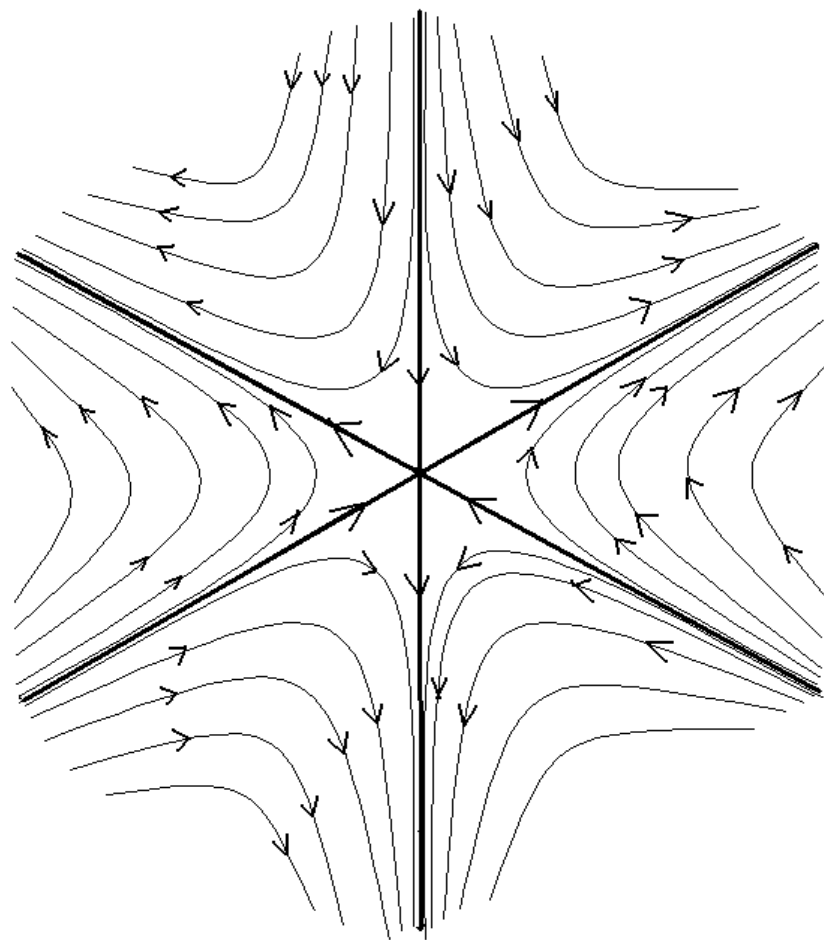


Fig. 2.3 Vector field near singular point with $m=3$

- all F are in involution with each other i.e. $\{F_i, F_j\} = 0$ for all $i, j = 1 \dots f$,
- all $\text{grad}(F_i)$ are linearly independent.

Here the Poisson bracket $\{A, B\} = \sum_{i=1}^f \left(\frac{\partial A}{\partial q_i} \frac{\partial B}{\partial p_i} - \frac{\partial A}{\partial p_i} \frac{\partial B}{\partial q_i} \right)$, and $\text{grad} = (\nabla_q, \nabla_p)$. One can then define a level set of the functions $\{F_i\}$ as $M_k = \{x \in M | F_i(x) = k_i, i = 1 \dots f\}$. This level set is invariant under flow Φ_t . Furthermore if M_k is compact and connected, then it is diffeomorphic to the f -dimensional torus[16]. The vector field $\{\mathbf{V}_i\}$; $\mathbf{V}_i = (\nabla_p F_i, -\nabla_q F_i)$ is linearly independent, tangent to M_k , and commutating. According to the Noether's theorem [17, 18] these constants of motion (or isolating integrals) result from the symmetries of the dynamical system.

Polygonal billiards are examples of dynamical systems where there exist one or two constants of motion depending upon the angles and ratio of the sides of the polygon. For some rational polygons with a rational ratio of their sides, there exist two constants of motion satisfying all integrability conditions except one i.e. $\{F_i, F_j\} \neq 0$ at the vertices of the polygon. Thus the vector field \mathbf{V} becomes singular at countable number of points in the phase space. Hence it is not possible to obtain global action-angle variables or constants of motions. Following Richens and Berry[13], we call these systems a pseudo-integrable.

2.5 Birkhoff-Poincaré Maps and Interval Exchange Maps

The Birkhoff-Poincaré map is first return map for billiards. For simplicity let P be simply connected billiard. We enumerate the vertices of P counterclockwise $A_0, \dots, A_{n-1}, A_n = A_0$. Denote by $a_i = [A_{i-1}, A_i], i = 1, \dots, n$ the edges of P . The boundary ∂P with length coordinate x is isomorphic to the circle of perimeter equal to the length(L) of ∂P . The set $\Omega \subset M(P)$ of vectors with footpoints in ∂P can be parameterized by coordinates $0 \leq x \leq L$ and $-\pi/2 \leq \theta \leq \pi/2$. The vector (x, θ) has foot points in $x \in a_i \subset \partial P$ and angle θ between it and the inner normal to a . Set $L_k = |a_1| + \dots + |a_k|$, $k = 0, \dots, n$. The coordinates θ in (x, θ) is not well defined for $x = L_k$ because these x are vertices of P and the angle θ can be

measured with respect to any of the two normals. The set Ω with points excluded is isomorphic to the cylinder $[0, L) \times [-\pi/2, \pi/2]$ with deleted intervals $L_0 \times [-\pi/2, \pi/2], \dots, L_{n-1} \times [-\pi/2, \pi/2]$ (see Fig. 2.4). The Birkhof-Poincaré map $F : \Omega \rightarrow \Omega$ is defined as follows: consider a trajectory from x in direction θ , $(x, \theta) \in \Omega$. When trajectory hits ∂P the first time and bounces off, it determines another point $(y, \eta) = F(x, \theta)$ to Ω . The mapping F is not well defined on the deleted intervals $L_0 \times [-\pi/2, \pi/2], \dots, L_{n-1} \times [-\pi/2, \pi/2]$ as well as on the boundaries $\theta = \pm\pi/2$. Fix an edge $a_i = [A_{i-1}, A_i]$ and a vertex A_j , $j \neq i-1, i$. Points (x, θ) , $x \in a_i$, such that the ball goes to the corner A_j form a curve in Ω on which map F is not well defined. Each rectangle of Ω is divided by these curves into the domains of continuity of F . Thus, the set of discontinuities of F is the union of a finite number of curves in Ω , F is obviously invertible and F^{-1} is the Birkhof-Poincaré map for the billiards with time reversed. The F -invariant Lebesgue measure is $\cos \theta d\theta dx$. The properties of the billiard flow are easily translated into the properties of the mapping F .

2.5.1 Interval exchange Map For Rational Billiards

Since the billiard flow G^t decomposes into the family G_θ^t of flows, $0 \leq \theta \leq \pi/N$, the Birkhof-Poincaré map F also decompose into the one parameter family $F_\theta : \Omega_\theta \rightarrow \Omega_\theta$ mappings, where $\Omega_\theta = \Omega \cap R_\theta$ is set of vectors with foot points on ∂P with directions equivalent to θ and $F_\theta = F | \Omega_\theta$. The family $\{F_\theta\}$ is the family of interval exchanges [19, 20, 21].

Suppose the space I is semi-interval $[0, 1)$ and $\xi = (I_1, \dots, I_r)$ is a partition of I into $r \geq 2$ disjoint semi-intervals $I_1 = [0, d_1), \dots, I_r = [d_{r-1}, 1)$, $0 < d_1 < \dots < d_{r-1} < 1$. Let $\omega = (\omega_1, \dots, \omega_r)$ be permutation of the number $\{1, \dots, r\}$.

Definition 4 Suppose the transformation $T : I \rightarrow I$ is a translation $T_{\alpha_i}x = x + \alpha_i (\text{mod } 1)$ on each of the semi-intervals I_i (the number α_i depends on i) and exchanges the semi-intervals according to permutations ω i.e. The semi-intervals $T^{-1}I_i = T_{\alpha_i}I_i = I'_{\omega_i}$ adhere to each other in the order $I'_{\omega_1} \dots I'_{\omega_r}$: then T is said to be interval exchange transformation corresponding to the partition ξ and the permutation ω .

Thus if I is piece of wire then the transformation T essentially is the cutting of I into pieces I_1, \dots, I_r , rearranging them according to permutation ω and welding them together again. Identifying I with the circle we can think

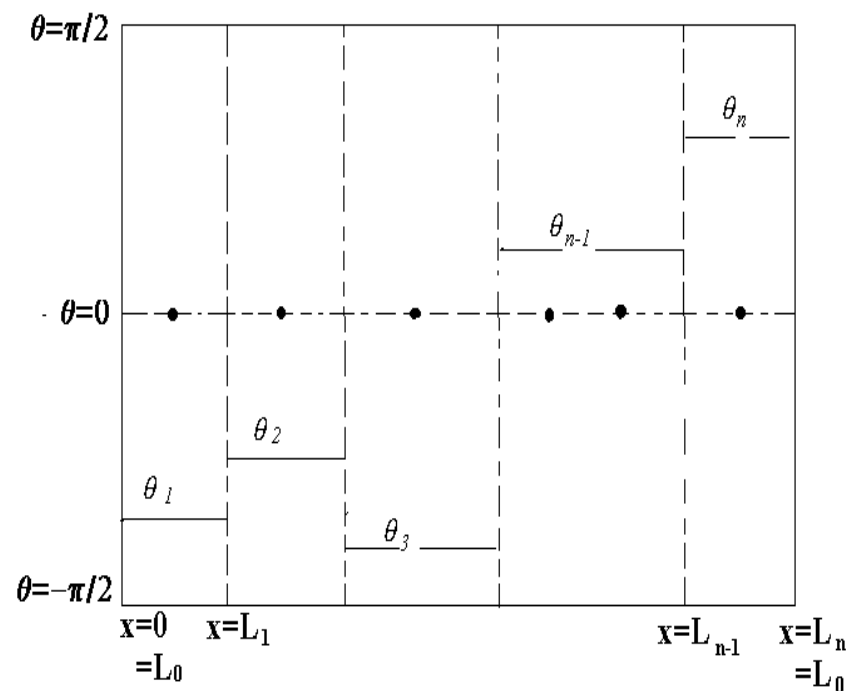


Fig. 2.4: Domain of Birkhoff-Poincaré map F . Vertical dashed lines (corresponding to $x=L_0\dots x=L_n$) are deleted intervals from the domain. See text.

of T as an interval exchange on the circle. An exchange of two intervals is given by one number $0 < \alpha < 1$ and it is simply rotation by angle α . It is clear that interval exchanges are invertible transformations of I preserving the Lebesgue measure ρ and the numbers $\alpha_1, \dots, \alpha_r$ are well defined (mod 1) by the pair (ξ, ω) .

Now to see that the family $\{F_\theta\}$ is the family of interval exchanges recall that in coordinates (x, θ) the set Ω is $[0, L) \times (-\pi/2, \pi/2)$ and $F(x, \theta) = (y, \eta)$ where η locally depends only on θ . The map F preserves $dm = \sin \theta dx$ which is interpreted as the mass element carried by the flow in direction θ . Fix a direction θ and for each side a_i of P let $-\pi/2 < \theta_{i_1} < \dots < \theta_{i_N} < \pi/2$ be the directions D_N -equivalent to θ (they depend on i because a_i determines angle of reference). The set Ω_θ is the union $a_1 \times \{\theta_{1_1}, \dots, \theta_{1_N}\} \cup \dots \cup a_p \times \{\theta_{p_1}, \dots, \theta_{p_N}\}$ of horizontal intervals. The mapping F preserves the set Ω_θ which is union of pN horizontal intervals (they can be glued into one interval) and the length element dm on Ω_θ . The positive orientation of P induces orientation of Ω_θ (each interval oriented from left to right), the map F reverses the orientation. Thus, the restriction F_θ of F to Ω_θ is an interval exchange with the flipping of intervals. Multiplying F_θ by the trivial orientation reversing map $J : (x, \theta) \rightarrow (L - x, \theta)$ we obtain honest interval exchange. Dividing by total length m_θ of Ω_θ which is

$$m_\theta = |a_1| (\sin \theta_{1_1} + \dots + \sin \theta_{1_N}) + \dots + |a_p| (\sin \theta_{p_1} + \dots + \sin \theta_{p_N})$$

we normalize F_θ to an interval exchange on $[0, 1)$ (with flipping). For a fixed polygon P the parameter of F_θ i.e. the number of exchanged intervals, the permutation ω and the length of interval depends only on θ . The obvious upperbound on the number of exchanged intervals is $p^2 N$.

The interval exchange maps has been used to prove many statistical and topological properties of polygonal billiards[20, 21]. Our main interest is in enumeration, classification of the periodic orbits. In the next chapter we will use modified form of interval exchange to carry out this task in case of some specific examples.

Bibliography

- [1] S.L.Glashow, L. Mittag, J. of Stat. Phys. **87**(1997)937.
- [2] G.D.Birkhoff, Acta. Math. **50**(1927)359.
- [3] P.Dahlqvist, G.Russberg, **24**(1991)4763.
- [4] P.Collas, D.Klein, H.P.Schwabler, Chaos, **8**(1998)466.
- [5] Y.G.Sinai, Russ. Math. Surveys, **33**(1978)229.
- [6] L.A.Bunimovich, Comm. Math. Phys., **65**(1976)295.
- [7] V.F.Lasutkin, Math. of USSR-Izv., **7**(1973)185.
- [8] S.Kerckhoff,H.Masur and J.Smillie, Ann. Math. **124** (1986)293.
- [9] E.Gutkin, A.Katok, in *Holomorphic Dynamics*, (Springer-Verlag, Berlin,1989).
- [10] A.N.Zemlyakov and A.B.Katok, Math. Notes **18** (1975)760.
- [11] R.H.Fox and R.B.Kerhner, Duke. Math. J. **2**, (1936)147.
- [12] M.Keane, Proc. Int. School Of Math. Phys., Univ. Camerino, 1974.
- [13] P.T.Richens and M.V.Berry Physica **2D**, (1981)495.
- [14] A.Katok, Commun. Math. Phys. **111**, (1987)151.
- [15] V.I.Arnol'd and A. Avez, Ergodic Problems of Classical mechanics, (Benjamin, New York, 1968).
- [16] V.I.Arnol'd, Mathematical Methods of Classical Mechanics, (Springer, New York, 1967).

- [17] E.Noether, Nachrichten Gesell. Wissenschaft, **2**, (1918)235.
- [18] L.E.Reichl, Transition to Chaos, In Conservative Classical System: Quantum Manifestations, Springer-Verlag, New York, 1992.
- [19] C.Boldrighini, M.Keane,F.Marchetti, The Annals of Probability, **6**, (1978)532.
- [20] I.P.Korneld, S.V.Fomin, Y.G.Sinai, Ergodic Theory, Springer, Berlin,1982.
- [21] A.Katok and B.Hasselblatt, Introduction to the Modern Theory of Dynamical systems, (Cambridge University Press, Cambridge, 1995).

Chapter 3

Periodic Orbits in Some Pseudo-integrable Billiards

3.1 Introduction

In this chapter we take up first task to study spectral fluctuations of pseudo-integrable billiards within semi-classical framework, i.e. to enumerate and classify all the periodic orbits of some typical pseudo-integrable billiards and also define their respective actions. We shall consider $\pi/3$ -rhombus billiard for this purpose. This specific example serves as a paradigm model as there are hardly any general results known in the literature. Furthermore the methodology we develop here, being based on interval exchange transformation, may be used to enumerate and classify periodic orbits in many rational polygonal billiards.

3.2 Periodic orbits of the $\pi/3$ -rhombus billiard

The $\pi/3$ -rhombus billiard is an example of an almost integrable system. As discussed before, billiard flow for a particle inside an almost integrable polygon is called an almost integrable billiard. The most fascinating mathematical questions are related to the periodic orbits of these billiards. For complete analytical semi-classical study of such systems one needs to enumerate and classify all the periodic orbits and also able to compute actions of periodic

orbits of the given system. The example where the enumeration and classification of periodic orbits is analytically carried out are very rare. Apart from the trivial enumeration of the orbits for a separable barrier billiard there is no instance where a complete study exists.

3.2.1 Enumeration

To begin with, let us briefly recapture how the motion of a particle inside $\pi/3$ -rhombus shaped encloser can be visualized as motion on an equivalent barrier billiard [1, 2]. It is simple to see (ref. Fig. 3.1) that after three successive reflections ($A \rightarrow B \rightarrow C$) of the rhombus A around a vertex of angle $2\pi/3$, the rhombus returns upon itself but with reversed orientation with vertices 2 and 4 interchanged. In other words, we obtain the final configuration of vertices as if we have reflected the rhombus about the shorter diagonal of the rhombus joining the vertices 1 and 3. If we continue the reflections, it will take exactly three more, or equivalently, another reflection about the shorter diagonal, for the rhombus to identify itself with original orientation. In this picture, due to double-valuedness of configuration of vertices per direction (by direction we mean one of the three directions the rhombus is facing in Fig. 3.1), one can visualize three rhombus-orientations in Fig. 3.1 on one sheet(or,plane) and the subsequent three orientations (required to obtain the original configuration of vertices in rhombus-A) on another sheet(or, plane). One can visualize a trajectory of particle reflecting from a wall of the rhombus by letting the particle move straight and appropriately reflecting the rhombus about the wall. It is this way of analysing that turns out to be more fruitful and hence the discussion on the tessellation of plane by rhombi. Due to its equivalence to the Riemann surface of $z^{1/2}$, z being a complex variable, we notice that the two sheets discussed above are joined along straight lines (The complex counterparts are branch cuts) that cannot be crossed; we call these barriers. Furthermore, as we have seen above, going to the next plane is to compensate for a phase π , the trajectory must reflect from the barrier. Alternatively, after three reflections, we can reflect third rhombus back onto itself (hence compensating for the phase in the third step), i.e. the fourth rhombus comes to lie under the third rhombus. If we continue reflections now, the sixth rhombus will come to lie under the first rhombus. In this picture the point in Fig. 3.2 will become a (monkey) saddle point. Continuing the process of reflections, we can get planes connected by cuts between the saddle points. This construction, projected onto two dimen-

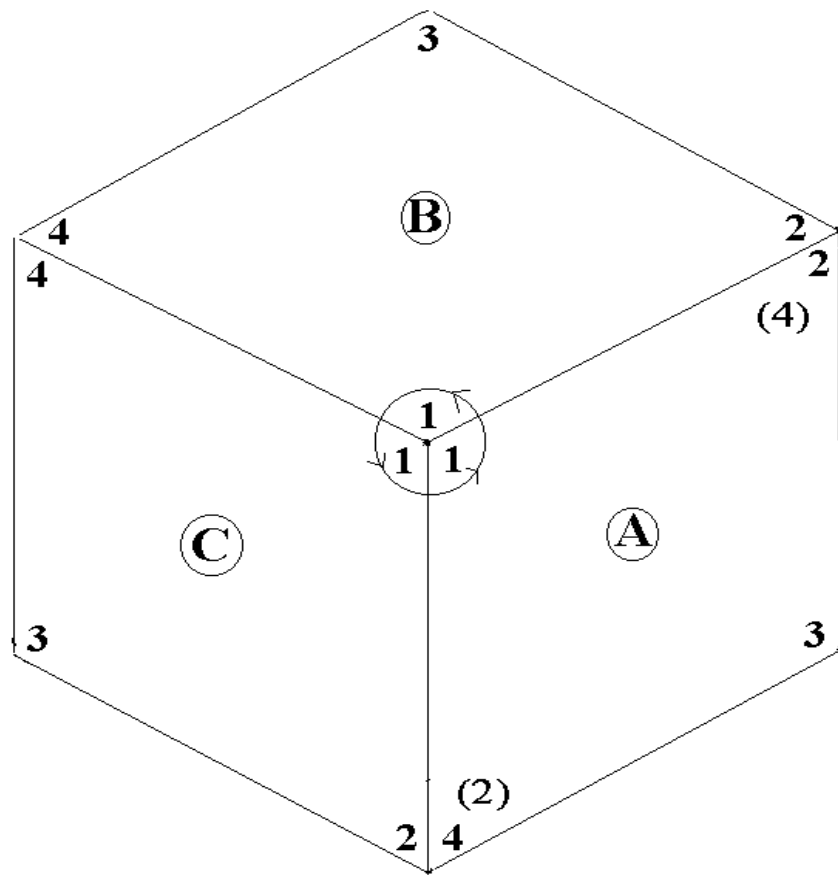


**Fig. 3.1: Refection of the rhombus about a $2\pi/3$ -vertex.
The vertices 2 and 4 are interchanged on third
reflection.**

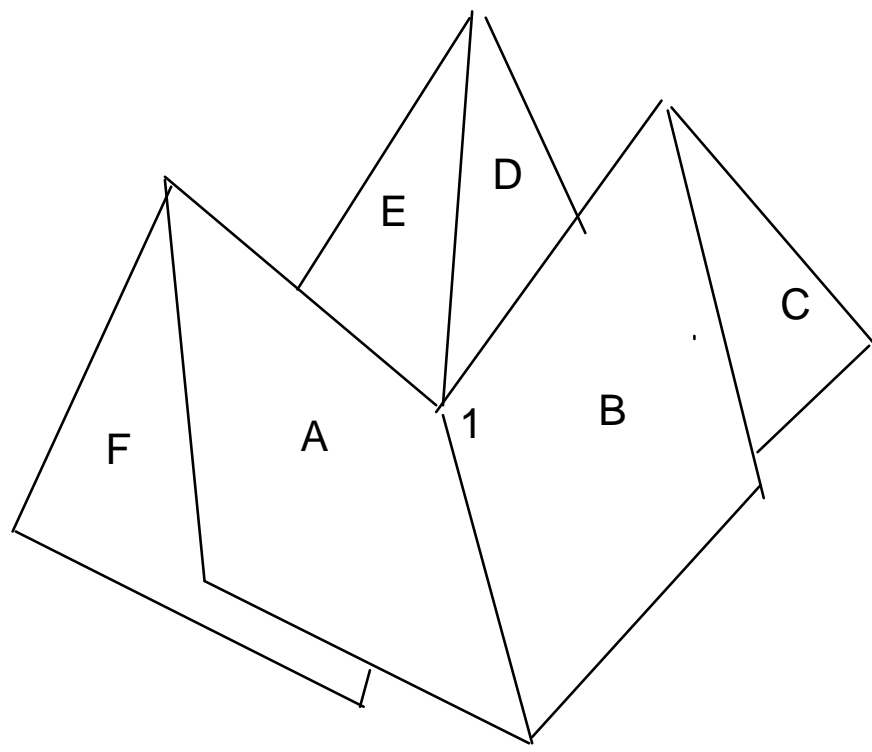


Fig3.2: Appearance of a saddlepoint at the vertex 1, that results in the cuts in fig. 3.3

sions, entails an orbit looking like a zig-zag line. We can now construct the fundamental region using six replicas of rhombus, and subsequently tessellate the two-dimensional plane by staking the fundamental regions side by side, exploiting the translational symmetry. On doing so, we will generate a barrier billiard shown in Fig 3.3 with two sets of planes (call them top and bottom) interspersed with each other.

Now concentrate our attention on the barrier billiard where the barrier to gap ratio is two. the barrier constituted of contributions from two rhombi and hence, there are two distinguishable sub-barriers giving rise to a single barrier of length twice that of gap. Classification of the periodic orbits had been carried out for a barrier billiard with barrier to gap ratio equal to unity[3]. It must be noted that the barrier billiard corresponding to the rhombus problem is more general than the barrier billiard studied in [3]. since the barrier to gap ratio is two and moreover the barriers appear in an oblique manner at an angle of $\pi/3$.

First, we observe that bifurcations of the orbits take place at the two ends of the barriers and at the center of the barrier (e.g. one example of such bifurcation is shown in Fig. 3.3, where two neighbouring trajectories on the opposite side of a trajectory $OABC$ bifurcate at end of a barrier near vertex C). This is due to the fact that each half of the barrier is contributed from two different rhombi in the fundamental region, and the point of bifurcation actually corresponds to a vertex.

The single connected surface is made up of two planes - a top and bottom. Under the covering of the surface by fundamental regions (double hexagons), the surface divides into alternate arrays of both planes containing barriers. Obviously, it does not matter which plane is called top(or bottom). This argument allows us to choose an origin which, for obvious reasons, dictated by symmetry of the barriers, is chosen to be the center of the barrier, denoted by O in Fig.3.3. Calling the length of a side of the rhombus by L , the barrier length is $2L$ and gap length is L . On the vertical axis, the perpendicular distance between adjacent arrays of a (top/bottom) plane is $\sqrt{3}L$. Since the factor of $\sqrt{3}$ is common in the vertical axis, we choose to measure the length in this direction in terms of $\sqrt{3}$, thereby making the ordered pairs labeling the points purely consisting of integers, (q, p) . For instance, a point O' in the Fig. 3.3 will be labeled by $(3, 2)$. A typical trajectory on this surface will be made up of alternate motions in the top and the bottom planes via barriers (i.e. when a trajectory hits a barrier on a upper plane it simply appears on the lower plane and vice versa). Since every plane consist of an identical

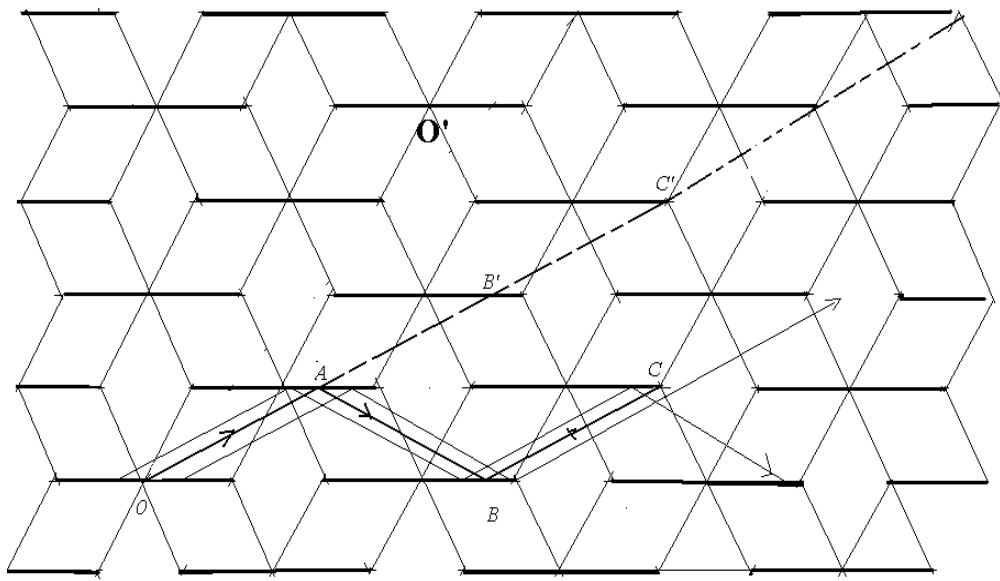


Fig. 3.3: Tesselation of the plane by stacking the fundamental regions exploiting the translational symmetry. Barriers are shown by thick lines. Trajectory OABC... can be straighten as O'A'B'C'... . Two nearby trajectories parrallel to OABC are also shown. Owing to the symmetry of the barriers, the integer labelling can be done, e.g. the point O' can be labelled as (3,2).

array of barriers, the trajectory starting at an angle with the plane from an initial point and ending on an equivalent point on the same plane constitutes a periodic orbit (see e.g. Fig. 3.4). Instead of following the zig-zag path, we can unfold the trajectory into an exactly equivalent straightened version as shown in Fig. 3.3. As stated above this straightened trajectory will lie on both planes, crossing planes at the barriers. Subsequently, we must decide which directions lead to periodic orbits. By virtue of the integer labeling, it is clear that all those directions that end on (integer, integer) ordered pair correspond to periodic orbits. Leaving apart a factor of $\sqrt{3}$ in the vertical direction, these directions correspond to rational gradients on each (top, bottom) plane. Also, starting from origin, we must consider only those end points such that q and p are co-prime, since only such pairs results in primary periodic orbits. If q and p are not co-prime but have g.c.d. k , then orbit ending at (q, p) represents k^{th} repetition of a primary periodic orbit ending at $(q/k, p/k)$. By the symmetry of the barriers on the plane, we need to restrict ourselves to an upper-half region only. Further taking care of geometry of our system, we restrict further to either $p \leq q$ or $q \leq 3p$, obviously then, three classes emerge, *viz.* (q, p) can be (i)(odd,odd), or, (ii)(odd,even), or, (iii)(even,odd). Next, we have to classify the number of bands or families of periodic orbits that correspond to each direction.

For equal barrier to gap ratio, it was shown that any trajectory with irrational gradient can be approximated arbitrarily well by trajectories with rational gradients, utilizing Klein's string construction or the continued fraction expansion. However, those trajectories never close in position and momentum both, rather they form a curious zig-zag path, for quadratic irrational gradients, has a fractal dimension. For the barrier in our case, same holds. Hence, we conclude that the trajectories with any irrational gradient do not close. It, therefore follows that if we take into account all the rational gradients avoid over-counting and classify different families/bands, we would have enumerated all the periodic orbits.

We shall now use modified form of interval exchange transformations and name it polar construction for the reasons of clarity and easy generalization.

3.2.2 Polar Construction

Exploiting the periodicity of barrier-gap-barrier-gap... string, we wrap the basic string of skewed sets of barrier-gap-barrier on two circles representing two different planes. Each circle has three basic divisions, coming out of

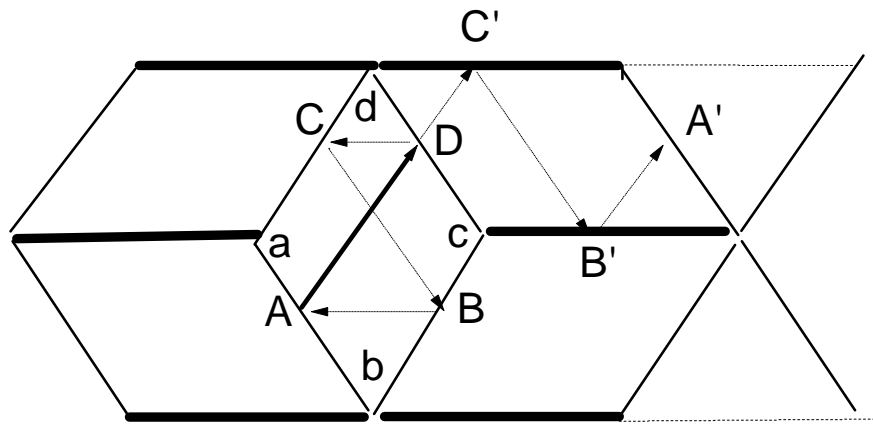


Fig.3.4: The periodic orbit $(ADCBA)$ in the rhombus $abcd$ is equivalent to the periodic orbit $(ADC'B'A')$ in the barrier billiard, which closes on equivalent point on the other plane.

two barriers (from two rhombi, joined together) and a gap. Each division now corresponds to an angle $2\pi/3$. The fact that barriers on two planes are stacked in a skewed manner is accounted for giving appropriate phase difference between equivalent points on two circles (see. Fig. 3.5). A (q, p) direction can be represented by these circles by the following procedure.

Divide each segment of the inner (outer) circle into p parts, after fixing the origin at the point joining the two sub-barrier segments. The origin of the outer (inner) will be at an angle of $\pi q/3p$ from the origin of the inner (outer) circle moving along the circular arc in a definite sense (we use anticlockwise movement). After fixing the origin, the outer circle has to be divided into $3p$ parts of equal length with one division at the origin. Since there are two gradients, positive and negative, we adopt the convention of marking outside (inside) of the circle as a representative of positive (negative) gradient.

To follow a trajectory, we start with an arbitrary point on one of the p sub-segments of the barrier segment on the right of the origin, on the inner circle. Next point will be on the outer circle just at the same distance (number of sub-segments) from the origin (of the outer circle) as the previous point was from its respective origin. As is clear from earlier discussion, these points must alter between the outer and the inner circles. The following point comes on the inner circle q segments away from the original one, and the next on the outer circle q segments away from the earlier one, and so on. Going on in this way, after a finite number of points, we will reach the starting point on the inner circle and that would make one periodic point. Although this is generally valid, in some cases it may not lead to the minimal length of the orbit. Such would be the case when, exactly after half the number of reflections, the trajectory will close, i.e., reach a point corresponding to the same respective sub-segment as it started with, on the other circle. At first sight, it might seem erroneous to consider this as a periodic orbit. However, it may be recalled that though the procedure of erecting barriers and subsequent polar construction is a way leading to an easy classification of orbits; however, more fundamental idea is the straightening of a trajectory-reflecting the domain about the edge on which the particle is incident. For the cases where the length of an orbit turns out to be double by polar construction, one can easily see that using the domain-reflection method, one gets the correct length. Thus, without ambiguity, the trajectory in the polar construction must be considered periodic even if it seems to be closing on the other plane (see, for example illustration in Fig. 3.4). With this clarification, we need only think in terms of the polar construction. Different sequences of barriers

and gap correspond to the different orbits.

3.2.3 Classification

As we have seen above, the most elementary classification is in (q, p) being (odd, odd) , $(odd, even)$ and $(even, odd)$. Having set the origin at the center of the barrier, the trajectory sets off in some rational direction and reaches either a center of some barrier or end (left or right) of some barrier. It is rather obvious to see that for each of the three cases written above there are subclasses which we shall call: the center-to-center(CC) case and the center-to edge(CE) case. Our Procedure of classification is in following steps:

(i) using the polar construction, we depict the trajectory on the circles, with an opening and an ending point on one of the sub-segments of the segment. We go on to the other to other sub-segments of the same segment, exploring the positive and negative gradients till both sides of the circles are filled. In all, we must fill $12p$ points.

(ii)check if the orbit has already closed a half-way on the outer circle or, equivalently, on the other plane.

With these steps in mind, we now take up each class separately and classify the bands of periodic orbits in full.

Case 1: Odd-Odd CE

We first describe through a simple example as to how we would arrive at general conclusions. Our approach would be to make a conclusion based on empirical data obtained by "brute force". At the end, we will provide with a rationale supporting and explaining the conclusion obtained.

Let us consider the case of $(q, p) = (1, 3)$. The corresponding polar construction is shown in Fig.3.5. As can be seen, point 1 and point 10 identify with each other, forming a periodic orbit after six bounces. Also, there is an orbit with negative gradient. It should be noted that all the sub-segments are visited by just these two orbits. The orbit close a half-way of $(3q, 3p)$, on the other plane and, there are two bands of orbits. Drawing the polar construction for other odd-odd CE cases, it can be seen that there are only two bands of orbits as seen above.

Now we come to discuss the rationale behind this classification of orbits. Due to the polar construction, each sub-segment is an arc of angle $2\pi/3p$. Translating the formation of periodic orbit by the polar construction into an

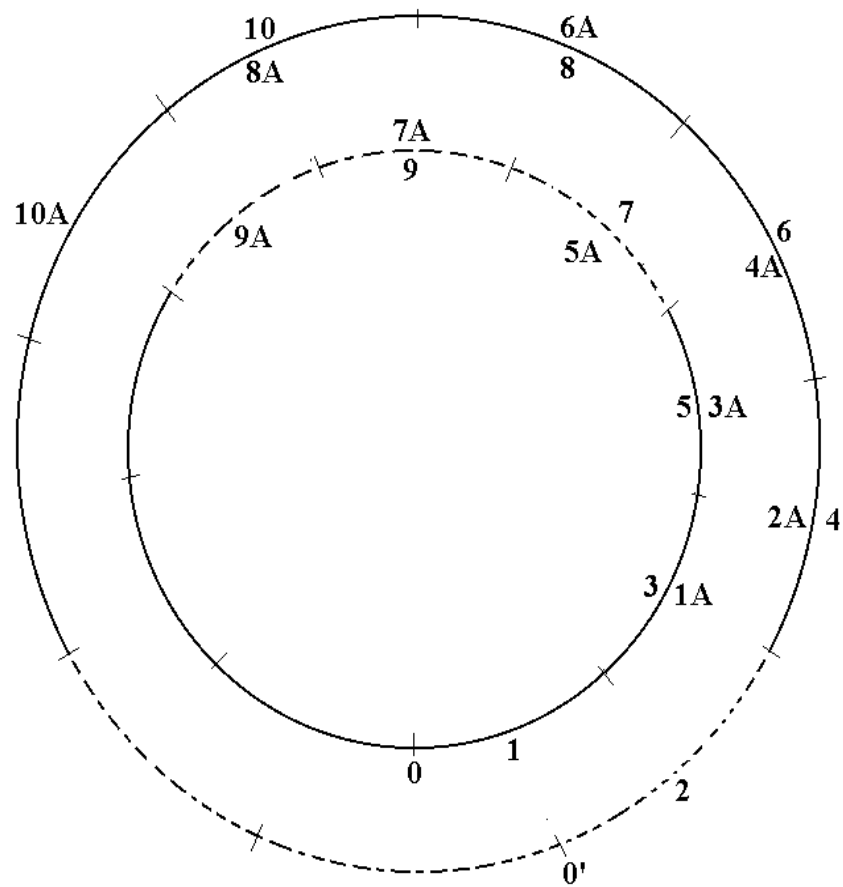


Fig. 3.5: Polar map for the odd-odd center-edge case

$$(q,p) = (1,3)$$

equation, we trivially get

$$N(2\pi/3p)q = 2\pi M \quad (3.1)$$

where N denotes the number of sub-segments and M denotes the number of rotations by 2π . Henceforth, we call N by the "crossing index" and M by the "rotation number" eq.(3.1) is simply

$$Nq = 3Mp \quad (3.2)$$

where M, q, p are positive integers. Since this is a CE case, q is not a multiple of three, i.e. $q \neq 3l, l \in \mathbb{Z}$. Thus, the only way in which eq.(3.2) can be satisfied is if $q = M$ and $3p = N$. Note that M and N will be odd as both q and p are odd. The crossing-index on one circle is $3p$ implying that the total crossing-index is $6p$ after which the orbit closed. In all, there are $12p$ sub-segments and hence there are exactly two bands of periodic orbits.

In general, the crossing-index is given by

$$N = [q, 3p]/q \quad (3.3)$$

and the rotation number is given by

$$M = [q, 3p]/3p \quad (3.4)$$

where $[a, b]$ denotes the lowest common multiple of a and b . Trivially, for the CE case, $N = 3p$ and $M = q$, for the CC case, $N = p$ and $M = q/3$.

Case 2: Odd-Odd CC

Firstly, all the rational directions pointing toward an infinite number of avenues correspond to the bands of periodic orbits. Points (q, p) corresponding to avenues are of the form $(3(2k - 1), 1), k \in \mathbb{Z}_+$. For each direction there will be two bands corresponding to positive and negative gradients.

We go over to a representative of a general case, viz., $(q, p) = (3, 5)$. The polar construction is depicted in Fig. 3.6. There are three strings of points corresponding to three bands of periodic orbits. Including the opposite gradients, there are four distinct bands in all. The string starting with point 1 and ending with point 11 closes after six reflections. Same is the case for $1B - 11B$ orbit. The opposite gradient counterpart of $1 - 11$ ($1B - 11B$) is equivalent to itself, starting from the outer circle (at $6(6B)$). So these strings give us two bands of periodic orbits. Care must be taken for the periodic orbit starting with the point 1A. The orbit closes at 6A

as this is the subsequent corresponding to $1A$ on the inner circle and the gradient matches. The orbit $1A - 6A$ closes after four reflections and occurs in a band. Taking the opposite gradient, we get two bands of periodic orbits here. For other odd-odd CC cases, we obtain the same results as in the above mentioned case. Let us now see the reason for the occurrence of four bands of periodic orbits in this case.

From eqs (3.3) and (3.4), $M = q/3$ and $N = p$. For each orbit, the crossing-index will be $2p$ accounting for the other circle also. In total, there are $12p$ segments and it clearly follows that there must be six bands of periodic orbits. Subtracting the two equivalent bands, we are left with four bands.

Case 3: Odd-Even CE

Consider $(q, p) = (1, 2)$. The polar construction is drawn in Fig. 3.7. There is a bifurcation in the band of trajectories starting with point 1, and further continue the two bands, primed and unprimed, to eventually close at $13'$ and 13 respectively. This feature, which can be succinctly put as bifurcation of the vector fields at vertices and continuation of trajectories in the form of bands (a signature of zero Liapunov exponent), is typical of pseudo-integrable system. The points 1 and $6'$ are, indeed, identical. Orbits emanating from 1 and $6'$ ($1A$ and $6A'$) will be the same. Consequently, on allowing the opposite gradients, we get just two bands of periodic orbits. All other examples of this class give rise to same number of bands and the orbit-types are also similar. Of course, the lengths and other details will be different.

As the arguments for justification follow on the same lines, we do not repeat them for this and further cases.

Case 4: Odd-Even CC

For this case, consider $(q, p) = (3, 2)$, polar construction for the same is drawn in Fig. 3.8. Due to bifurcations, we have drawn double the marks, thus, making explicit that we have to fill $24p$ points in all. As can be seen from the diagram, there are four bands of periodic orbits: an orbit corresponding to the string $12\dots 9$; another orbit corresponding to the string $1A2A\dots 9A$; and a positive-negative gradient pair, $1'2'\dots 5'$ (plus the opposite gradient). It is interesting to see that bifurcations of these vector fields take place at all possible places, viz. Z_1, Z_2 and Z_3 . Considering other odd-even cases, one can easily see that the same conclusions about the number of bands etc. will hold, leaving apart the finer details.

Case 5: Even-Odd CE

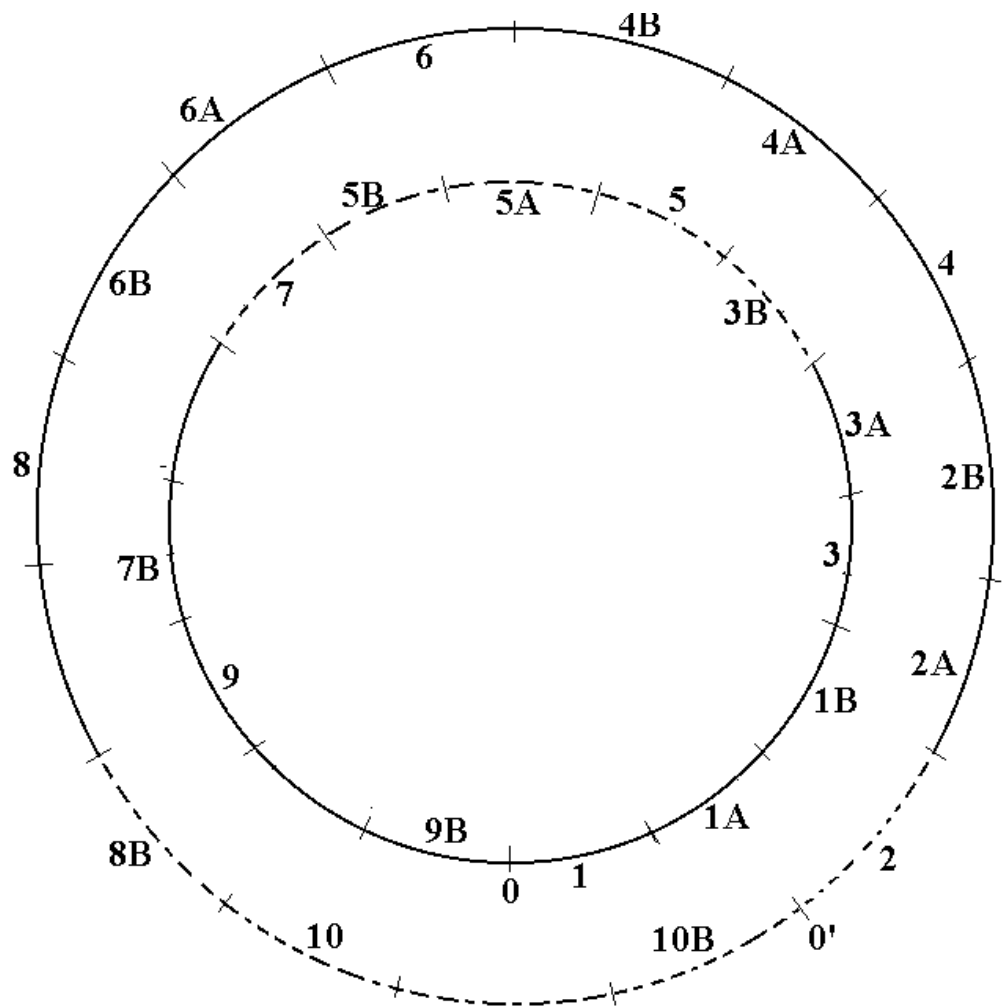


Fig. 3.6 : Polar map for the odd-odd center-center case

$$(q,p) = (3,5)$$

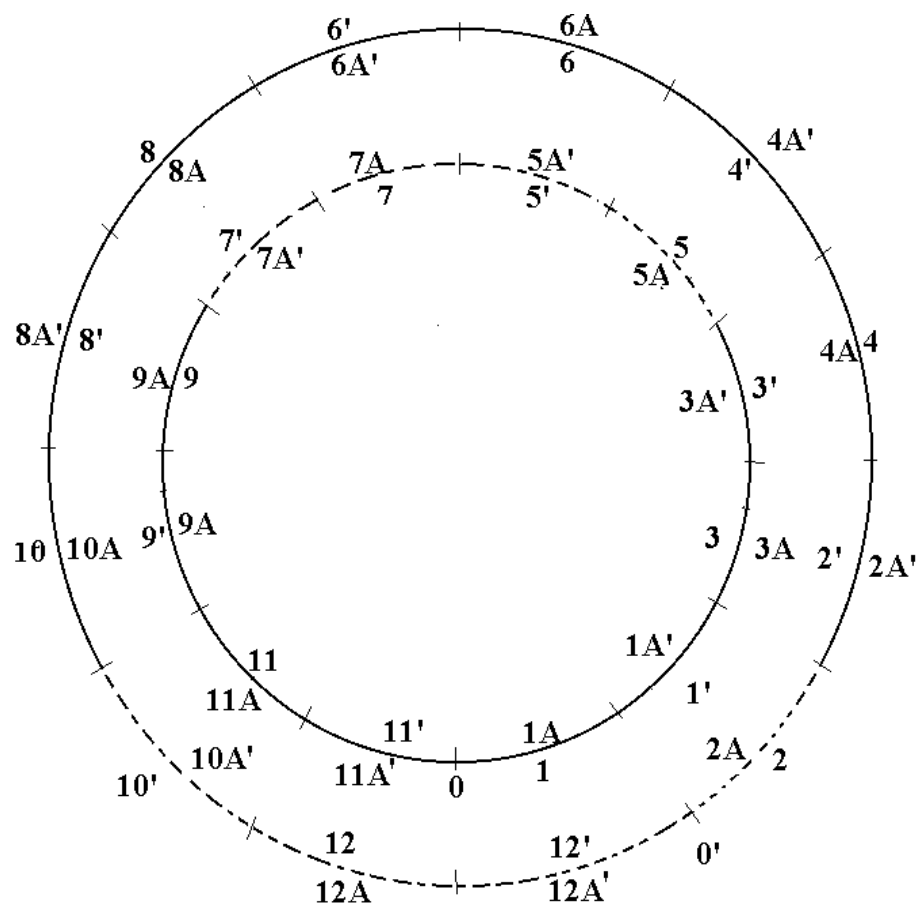


Fig. 3.7 : Polar map for the odd-even center-edge case $(q,p) = (1,2)$

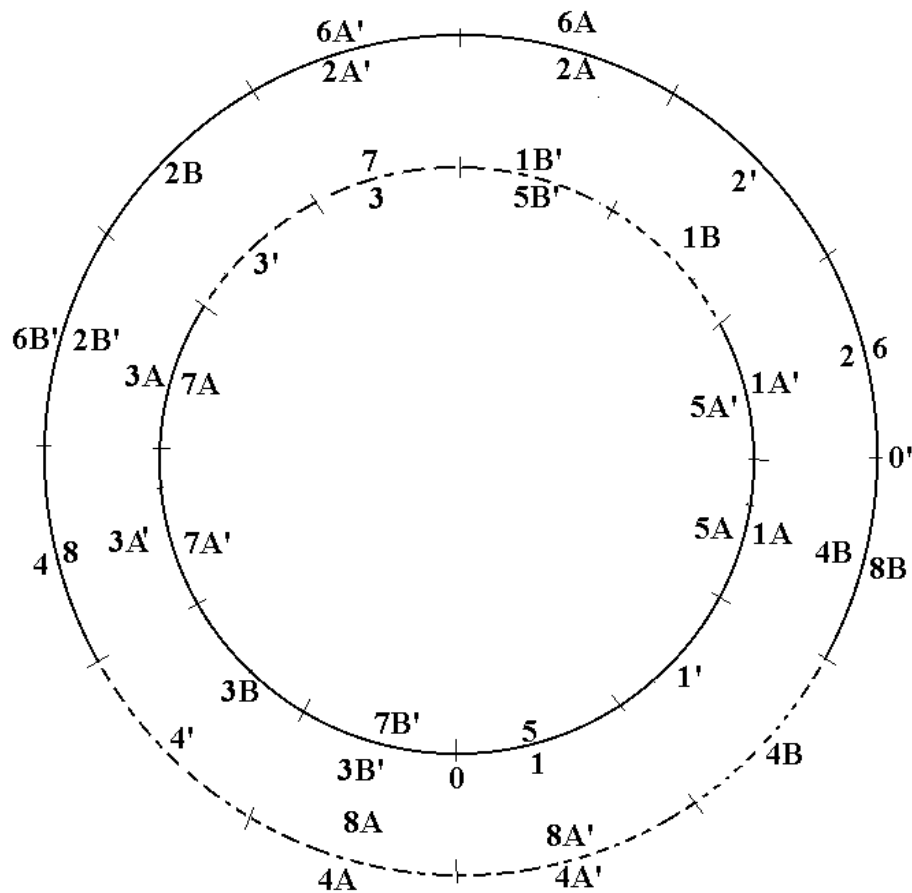


Fig. 3.8 : Polar map for odd-even center-center case

$$(q,p) = (3,2)$$

Consider $(q, p) = (2, 1)$, the polar construction is shown in Fig. 3.9. There are two bands of periodic orbits. In fact, the periodic orbit formed with opening point as the negative-gradient-equivalent of the point 1 is identical to the orbit $1A2A\dots7A$, starting from $2A$. Thence, strings $1 2\dots7$ and its negative gradient counterpart are the two bands in this case. **Case 6: Even-Odd CC**

A general case can be studied through the example of $(q, p) = (6, 5)$, polar construction being depicted in Fig. 3.10. Although the diagram is getting rather complicated, in the same manner as discussed earlier, it can be concluded that there are four bands of periodic orbits. General validity of this conclusion can be verified without undue hardship. The results of this section, along with the lengths of the periodic orbits and the phase space areas of the bands in which they occur are summarized in Table I. This concludes our discussion on the enumeration and classification of the periodic orbits in $\pi/3$ -rhombus billiard. The periodic orbits of other billiards such as Hannay-McCraw billiard [3] or rectangle billiard with slit at the center can also be enumerated and classified in the same way.

3.3 The H-M Billiard

The particle moves here in a configuration space where a hard line-segment barrier is placed at the center parallel to one of the sides of the periodic cell of side length L , and the length of the barrier is half of the side length(i.e. $L/2$). The invariant integral surface of this system has genus equal to two ($g = 2$). The fundamental region consist of two cells, due to presence of a barrier (see, Fig. 3.11). The opposite boundaries of the fundamental region are identified topologically resulting in one handle of a sphere. The barriers in each cell of the fundamental region has to be identified topologically which results in another handle of the sphere. By stacking the domains of the billiard side by side in both the orthogonal directions, one obtains an infinite lattice of barriers and gaps, with barrier to gap to ratio unity. One can label the end points of barriers by integer-pairs which form lattice points. It can be easily seen that the straightened version of a rational gradient ($= |p/q|$) trajectory will initially meet lattice point (q, p) and then repeat itself by meeting lattice points (mq, mp) where $m \in \mathbb{Z}$. On the other hand, the irrational gradient trajectory will never visit any lattice point though it will come arbitrarily close to many lattice points, hence will never be periodic. Thus the periodic

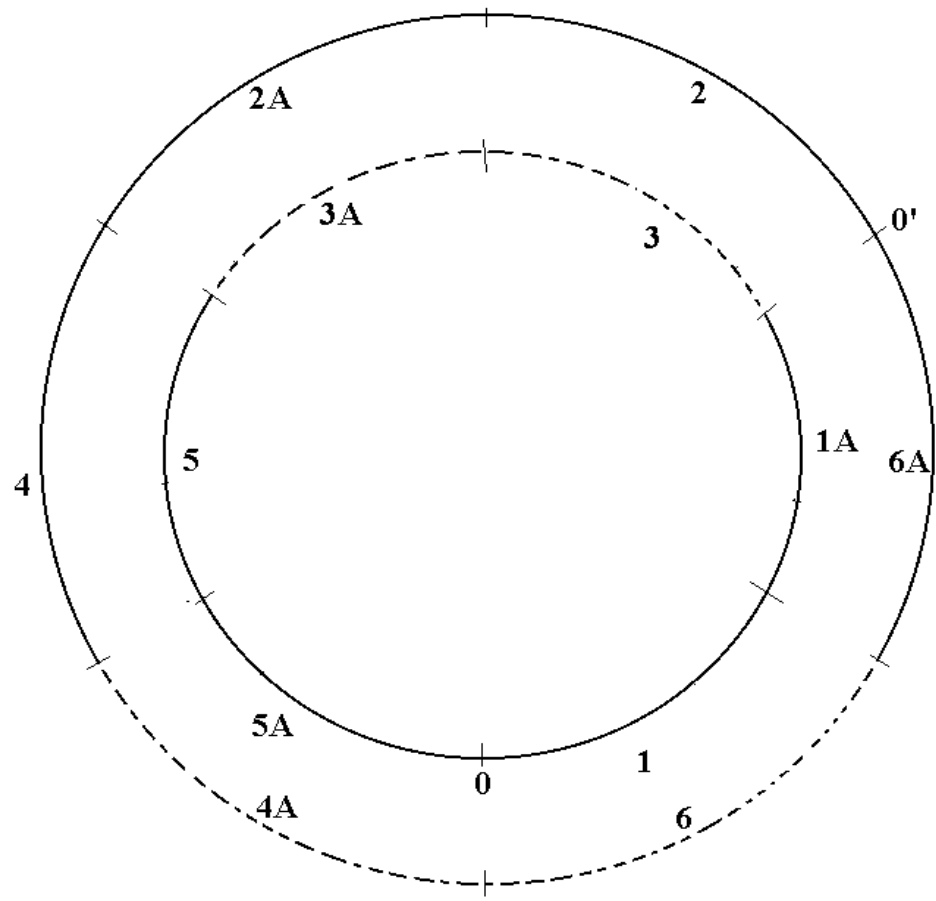


Fig. 3.9 :Polar Map for the even-odd center-edge case

$$(q,p) = (2,1)$$

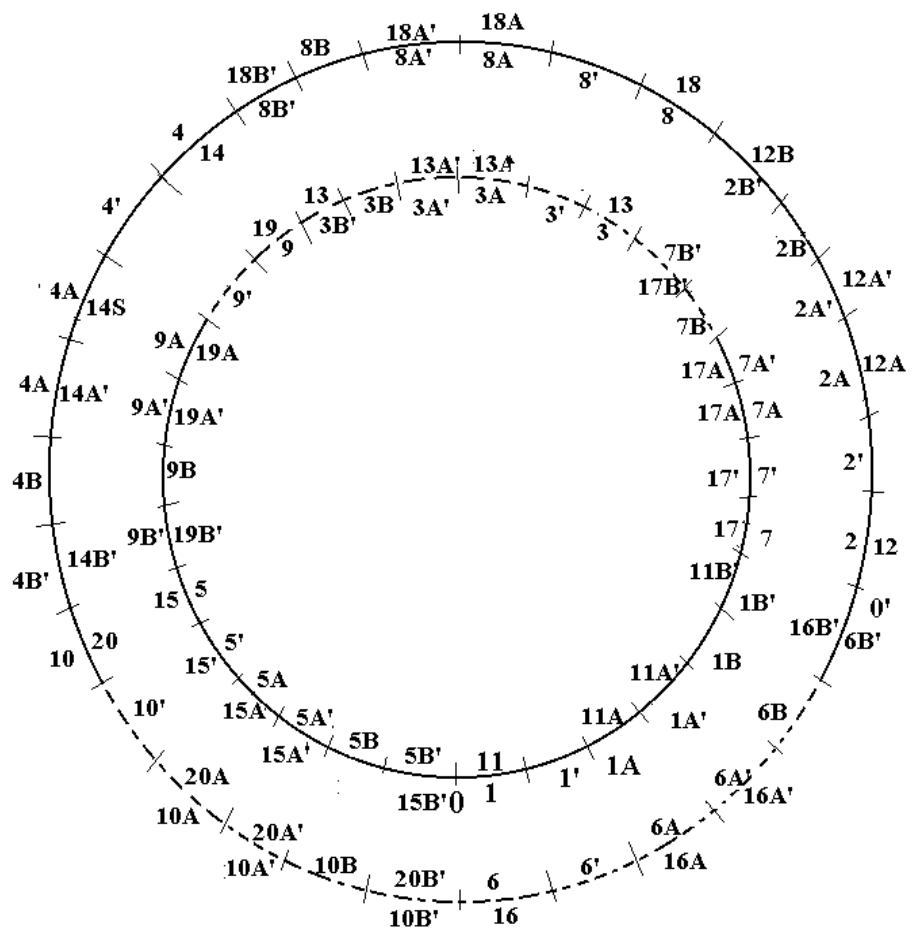


Fig. 3.10: Polar Map for the even-odd center-center case

$$(q, p) = (6, 5)$$

orbits in the system are the ones which hit any lattice point (q, p) in this array of barriers, the gradient of such trajectories will be given by $|p/q|$. By above arguments, we need to consider only the pairs (q, p) such that q and p are co-prime since they only give a primitive periodic orbits, and points (mq, mp) , where $m \in \mathbb{Z}$, gives m repetitions of a primitive periodic orbit corresponding to (q, p) . Each such (q, p) gives different number of bands or families of periodic orbits, depending on whether the pair is odd-odd (o, o) or even-odd (e, o) or odd-even (o, e) . The length of periodic orbit in a given family corresponding to a lattice point (q, p) is given by

$$l = cL\sqrt{(q^2 + p^2)}$$

where c depends on the number of families of periodic orbits. The periodic orbits can now be enumerated and classified exactly same way as done in the case of the $\pi/3$ -rhombus billiard[3]. The result is summarised in the table 3.2.

3.4 The Single Slit Rectangle billiard

Another simple example of pseudo-integrable billiard is a simple modification of H-M billiard, where instead of periodic cells one can consider a linear barrier of length L placed at the center of the rectangle $(L, 2L)$, parallel to longer side. This simple modification results in the pseudo-integrable billiard whose invariant surface is topologically equivalent to a sphere with three handles(genus, $g = 3$). The fundamental region now consist of four replicas of the configuration space instead of two as in the H-M billiard. Opposite sides of the fundamental region are identified as well as each pair of barrier lying one above each other has to be identified separately which results in genus 3 surface (see Fig. 3.12). By stacking the domains of the billiard side by side in both the orthogonal directions, one obtains an infinite lattice of barriers and gaps, with barrier to gap to ratio unity, which is exactly same as the lattice of barriers and gaps one obtains in the case of H-M billiard. One can proceed in the same way as before to label lattice point. The periodic orbits can then be enumerated and classified using polar maps. The result is summarised in table 3.3. In this chapter we have developed a methodology to enumerate and classify periodic orbits of some pseudo-integrable billiards. The same methodology can be used to study large number of rational polygonal billiards in particular one can apply technique to rectangular billiard

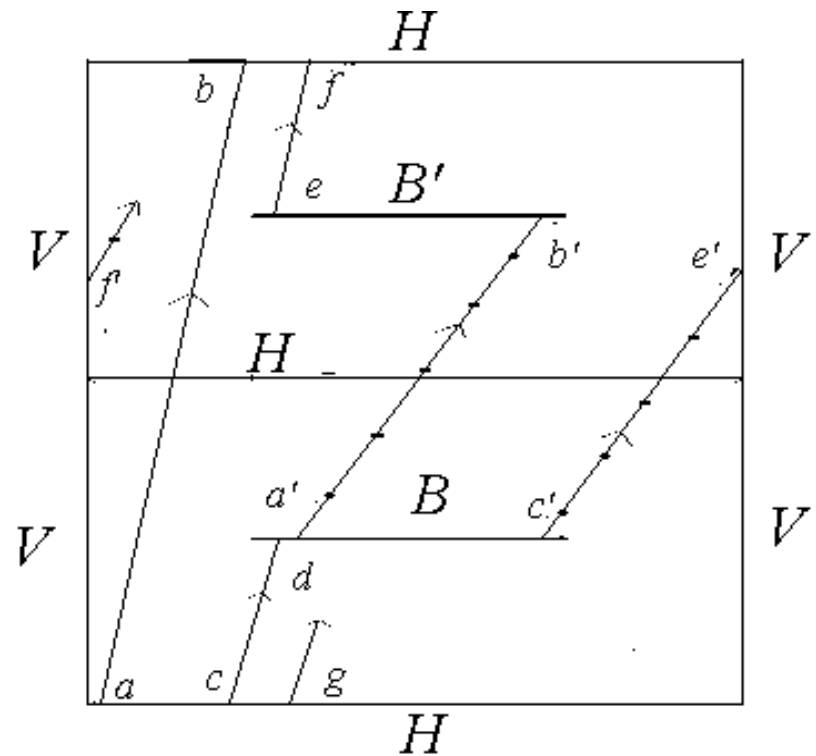


Fig. 3.11: H-M billiard (pqrs). Fundamental region requires two replicas as shown. V, H represents identified sides of a periodic cells. B, B' are barriers in respective cells. A trajectory $abcdefg\dots$ starts at 'a', meet H at 'b', due to identification it is then transferred to 'c' and so on. Note that 'd' is equivalent to 'e' since lower side of B is identified with upper side of B' and vice versa.

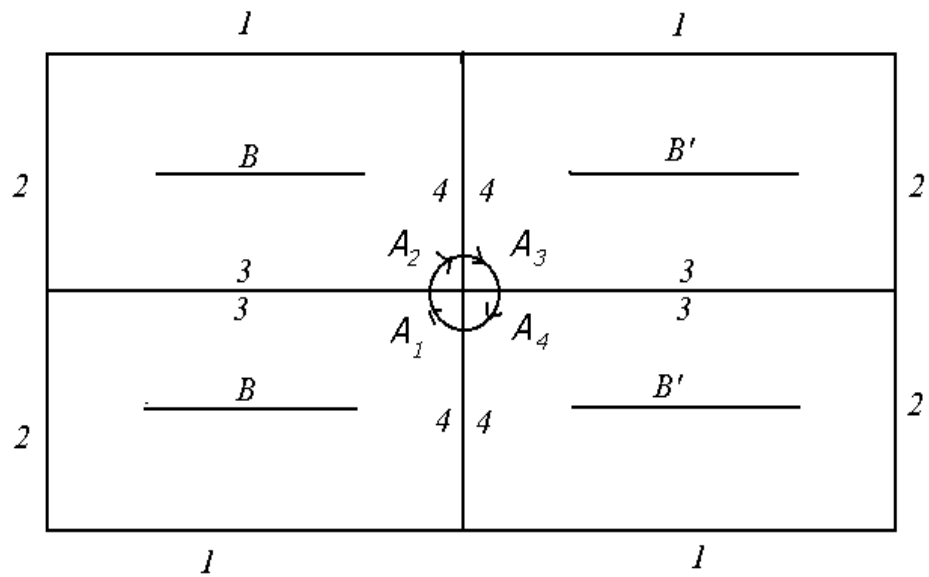


Fig. 3.12: The fundamental region of a single slit rectangle billiard which requires four copies of configuration space A_1 . Side identification is indicated by 1,2,3,4 and barriers by B and B' .

with many slits(or barriers) or L-shaped billiards.

Type	Classes	No. of Families	Closing Point	Length	Band Areas
Center-center	odd-odd	1-1	$(q/2, p/2)$	$Lf_{pq}/2$	A_R
		2	(q, p)	Lf_{pq}	$2A_R$
	odd-even	1-1	(q, p)	Lf_{pq}	A_R
		2	$(2q, 2p)$	$2Lf_{pq}$	$2A_R$
Center-edge	even-odd	1-1	(q, p)	Lf_{pq}	A_R
		2	$(2q, 2p)$	$2Lf_{pq}$	$2A_R$
	odd-odd	1-1	$(3q/2, 3p/2)$	$3Lf_{pq}/2$	$3A_R$
Center-edge	odd-even	1-1	$(3q, 3p)$	$3Lf_{pq}$	$3A_R$
	even-odd	1-1	$(3q, 3p)$	$3Lf_{pq}$	$3A_R$

Table 3.1: Summary of the results obtained in this chapter about periodic orbits of $\pi/3$ -rhombus billiard. The symbol $f_{pq} = (q^2 + 3p^2)^{1/2}$, L and $A_R = 3^{1/2}L^2/2$ are length and area of the billiard. Note that total band area occupied by periodic orbits assigned to a single lattice point is always $6A_R$ (i.e. the phase space area of the billiard).

Classes	No. of Families	Closing Point	Length	Band Areas
odd-odd	1	$(4q, 4p)$	$4Lf_{pq}/2$	$2A_R$
even-odd ¹	1-1	(q, p)	Lf_{pq}	$A_R/2$
even-odd ²	1	$(2q, 2p)$	$2Lf_{pq}$	A_R
odd-even	2	$(2q, 2p)$	$2Lf_{pq}$	A_R

Table 3.2: Summary of results for single H-M billiard, The symbol $f_{pq} = (q^2 + p^2)^{1/2}$, L and $A_R = L^2$ are length and area of the billiard. Again here total band area occupied by periodic orbits assigned to a single lattice point is always $2A_R$ (i.e. the phase space area of the billiard).

Classes	No. of Families	Closing Point	Length	Band Areas
odd-odd	2	$(4q, 4p)$	$4Lf_{pq}/2$	$2A_R$
even-odd ¹	2	$(2q, 2p)$	$2Lf_{pq}$	A_R
even-odd ²	2	$(2q, 2p)$	$2Lf_{pq}$	A_R
odd-even	2	$(4q, 4p)$	$4Lf_{pq}$	$2A_R$

Table 3.3: Summary of results for single slit rectangle billiard, The symbol $f_{pq} = (q^2 + p^2)^{1/2}$, L and $A_R = 2L^2$ are length and area of the billiard. Here also total band area occupied by periodic orbits assigned to a single lattice point is always $6A_R$ (i.e. the phase space area of the billiard).

Bibliography

- [1] B. Eckhardt, J. Ford and F. Vivaldi, *Physica* **13D**, (1984)339.
- [2] S.R.Jain and H.D. Parab, *J. Phys. A:Math. Gen.* **25**, (1992)6669.
- [3] J.H.Hannay and R.J. McCraw *J. Phys. A* **25** (1990)887.

Chapter 4

Growth Rate of Periodic Orbits

4.1 Introduction

An important characteristic of a dynamical system is the asymptotics of the number of periodic orbits(or growth rate of periodic orbits) having lengths less than or equal to l . We denote this function by $F(l)$. From the point of view of application, semi-classical theory of spectral statistics can be carried out only after knowing the exact form of this law. The problem addressing the distribution of the periodic orbits with the period of the orbits is discussed in this chapter. The answer to the problem is known only for the chaotic dynamical systems which possess only unstable, isolated periodic orbits. In such cases growth rate of periodic orbits is known to be exponential[1, 2]. e.g. For so called axiom A systems $F(l)$ is given by

$$F(l) = \exp \{ \kappa l \} / \kappa l \quad \text{as } l \rightarrow \infty$$

where $\kappa > 0$ is the topological entropy of the system. For the pseudo-integrable and their special cases, the almost integrable billiards(A polygon P is called almost integrable if the group G_P generated by the reflections in the side of P is a discrete subgroup of the group of motions of the Euclidean plane R^2), there are some conjectures and incomplete results.

For example a theorem due to [3, 4] states that in case of any arbitrary polygon P , the function $F(l)$ grows slower than any exponential, as $l \rightarrow \infty$. By Corollary (2.1), $F(l)$ is bounded above by the number of generalized diagonals of length less than l . The sub-exponential growth rate of the number of generalised diagonals is estimated from above by the entropy of the billiard,

which is zero [5, 6]. The above theorem is the only known upper bound on the periodic orbits in general polygons. As for a lower bound, no result has been established yet. On the other hand, periodic orbits in rational polygons have efficient bounds from below and from above. The proofs of these estimates use the theory of holomorphic quadratic differentials on Riemann surface. We state here a theorem [7, 8] regarding this,

Theorem 6 *Let P be a rational polygon. Then there are positive constants $0 < c_1 < c_2$ such that for all sufficiently large values of l , we have*

$$c_1 l^2 \leq F(l) \leq c_2 l^2. \quad (4.1)$$

These quadratic bounds are not likely to hold for general (irrational) polygons. The expectation is that, for general polygons there are polynomial bounds on $F(l)$.

Conjecture 1 *Let P be an arbitrary polygon. then there exist positive constants c_1, c_2 and integers $1 \leq n_1 \leq n_2$ such that for sufficiently large l we have*

$$c_1 l^{n_1} < F(l) < c_2 l^{n_2}. \quad (4.2)$$

For arbitrary rational polygons condition (4.1) may well give best possible estimates on the $F(l)$. However, there are non-trivial examples when the asymptotics of $F(l)$ can be computed exactly.

Our investigations on some models are carried out analytically with comparisons shown with the numerical results. We sharpen the existing theorem on proliferation law for almost-integrable systems in a significant manner. Our analysis enables us to give a general law of proliferation of the periodic orbits in the pseudo-integrable billiards.

If we consider an integrable system, Δ corresponding to an almost integrable system, P and let g be the genus of the surface R corresponding to P , denote by $|\Delta|$ and $|P|$ the respective areas of Δ and P , Gutkin [9] proved that there exists a constant c_1 such that

$$F(l) = c_1 \frac{\pi g}{|P|} l^2 + o(l). \quad (4.3)$$

The constant $c_1 \varepsilon [1, \frac{|P|}{|\Delta|}]$.

4.2 Law of Proliferation of Periodic Orbits in Pseudo-integrable Billiards

Our results in the previous chapter clearly showed that there are countable number of families of periodic orbits. By a family of periodic orbit, we mean an isolated trajectory closing after an odd number of reflections, or a band of trajectories closing after an even number of reflections. We have also seen that the periodic trajectories only occur in bands for the $\pi/3$ -rhombus billiard due to its equivalence with the barrier billiard. The number of families of periodic orbits of length less than x is finite for any x ; we shall call this number by Counting Function, $F(x)$ now on.

In the subsections below, the law for an almost integrable and a pseudo-integrable billiard [10, 11] is derived.

4.2.1 The $\pi/3$ -Rhombus Billiard

We now present number-theoretic arguments to obtain $F(x)$ for the $\pi/3$ -rhombus billiard. Subsequently, we shall discuss and compare our results with the above-mentioned results by Katok [3] and Gutkin [9]. The length of periodic orbits in the given family corresponding to the lattice point (q, p) where q, p are co-prime is given by

$$l = c_2 L \sqrt{(q^2 + 3p^2)} \quad (4.4)$$

where c_2 depends on family of periodic orbits as seen in the Table 3-1 of chapter (3). If $l < x$ for a given family of points (q, p) should be counted in $F(x)$. We can draw a circle of radius $l_1 (= q_0 L)$ then, all points (q, p) having family of periodic orbit with length $c_2 l_1 \leq x$ (or $l_1 \leq x/c_2$) should be considered for the calculation of $F(x)$. Referring to Fig. 4.1, area of a quarter circle is $(\pi l_1^2/4)$ and the area of the square OABC is (l_1^2) . We shall denote the integer (fractional) part of a number by $[...](\{...\})$. The number of lattice points in OABC is

$$\begin{aligned} N &= (q_0 + 1) \left[\frac{(q_0 + 1)}{\sqrt{3}} \right] \\ &= (q_0 + 1)^2 / \sqrt{3} - (q_0 + 1) \left[\frac{(q_0 + 1)}{\sqrt{3}} \right] \end{aligned} \quad (4.5)$$

On an average, $[(q_0 + 1)/\sqrt{3}]$ is $1/2$ (obviously); hence

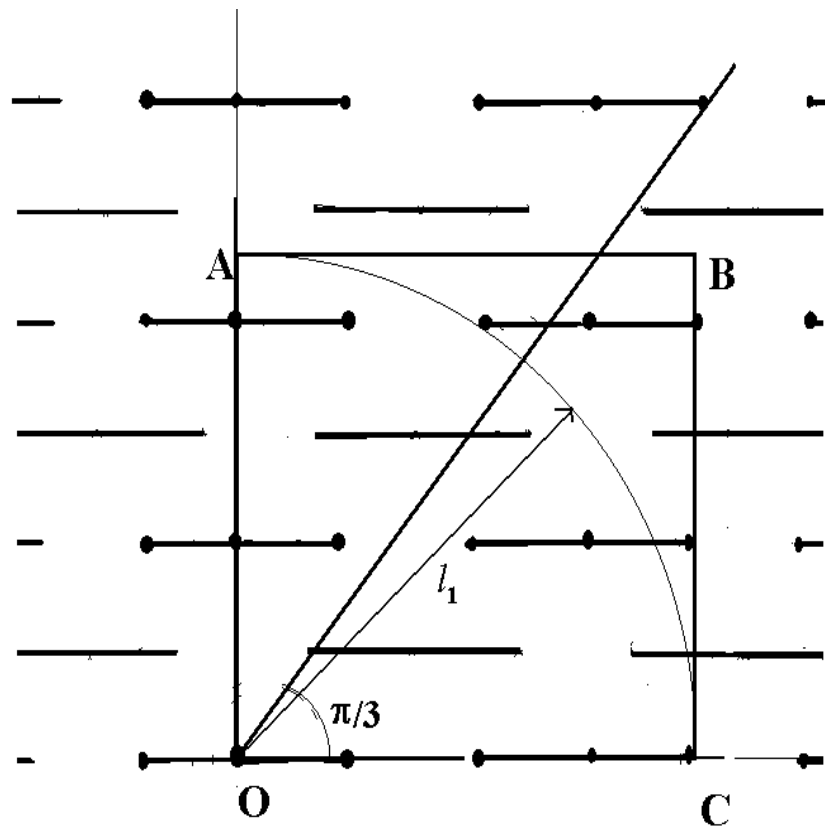


Fig. 4.1: Lattice points of $\pi/3$ -rhombus billiard. Area of $OABC$ is l_1^2 . We count points lying in $\pi/3$ sector only.

$$N \sim \frac{q_0^2}{\sqrt{3}} + \frac{(2q_0 + 1)}{\sqrt{3}} - \frac{(q_0 + 1)}{2} \quad (4.6)$$

Therefore, number of lattice points in a quarter circle is

$$N_q = N(\pi l_1^2/4)/l_1^2 = \frac{\pi N}{4} \quad (4.7)$$

Since the probability that two randomly chosen numbers are co-prime is $(6/\pi^2)$ [13], the number of co-prime lattice points is

$$N_c = \left(\frac{6}{\pi^2}\right)\left(\frac{\pi N}{4}\right) \sim \frac{\sqrt{3}l_1^2}{2\pi L} + \frac{A\sqrt{3}}{4\pi} \quad (4.8)$$

where

$$A = (4 - \sqrt{3})l_1/L + 2 - \sqrt{3}. \quad (4.9)$$

For reasons discussed in the previous section, we are concerned in finding the number of points in a $(\pi/3)$ sector, the area of which is two-thirds that of a quarter circle. Hence, for $(\pi/3)$ sector,

$$N'(l_1) \sim \frac{l_1^2}{\sqrt{3}\pi L^2} + \frac{A}{2\sqrt{3}\pi} \quad (4.10)$$

Taking only the dominant contribution $(O(l_1^2))$, with the help of Table (3.1) (cf. chapter 3), we can write for the number of periodic orbits whose length is $\leq x$ as

$$\begin{aligned} F(x) \sim & 2(P_{oocc}N_{oocc}(2x) + P_{oocc}N_{oocc}(x) + P_{oecc}N_{oecc}(x) \\ & + P_{oecc}N_{oecc}(x/2) + P_{eooc}N_{eooc}(x) + P_{eooc}N_{eooc}(x/2) \\ & + P_{ooce}N_{ooce}(2x/3) + P_{ooce}N_{ooce}(x/3) + P_{ooce}N_{ooce}(x/3)) \end{aligned} \quad (4.11)$$

where (P_{oocc}) is the probability that given co-prime lattice point is of odd-odd, centre-centre type and so on, $N_{oocc}(l)$ is total number of odd-odd, centre-centre type co-prime lattice points contained in the sector. Out of the four points, only one is odd-odd (or even-odd or odd-even), also two out of three points are of centre-edge type and one is of centre-centre type. Therefore, we have

$$P_{oocc} = P_{oecc} = P_{eooc} = \frac{1}{9} \quad ,$$

$$P_{ooce} = P_{oece} = P_{eoce} = \frac{2}{9}.$$

Thus we can write

$$F(x) = 2((4 + 1 + 1 + \frac{1}{4} + 1 + \frac{1}{4})(\frac{x^2}{9\sqrt{3}\pi L^2}) + (\frac{4}{9} + \frac{1}{9} + \frac{1}{9})(\frac{2x^2}{9\sqrt{3}\pi L^2}))$$

or

$$= \left(\frac{53}{27\sqrt{3}\pi L^2} \right) x^2.$$

In terms of $|P|$ this can be written as

$$F(x) = 0.049\ 733 \left(\frac{2\pi}{|P|} \right) x^2. \quad (4.12)$$

Of course, apart from the dominant term that is quadratic in x , there will be terms of $O(x)$ and $O(1)$. It is, however, important to note here that term of $O(x)$ is not related to the orbits periodic after an odd number of reflections (hence, isolated). These terms only present more exact expression for $F(x)$ arising from the above arguments. Their origin is in the points contributing to $F(x)$ lying on the boundary of the sector. On the same lines as above, terms of $O(x)$ and $O(1)$ are found to be $(26/81\pi)(4\sqrt{3} - 3)(x/L)$ and $(12/27\pi)(2\sqrt{3} - 3)$ respectively. Thus the counting function is of form

$$F(x) = \left(\frac{53\sqrt{3}}{81\pi L^2} \right) x^2 + \left(\frac{26}{81\pi L} \right) (4\sqrt{3} - 3)x + \left(\frac{12}{27\pi} \right) (2\sqrt{3} - 3). \quad (4.13)$$

4.2.2 The H-M Barrier Billiard:

We now present our calculation for the Hannay-McCraw billiard [12]. Recall the discussion about this billiard in the previous chapter where we have argued that the periodic orbits in this system are the ones which hit any lattice point (q, p) in this array of barriers, the gradient of such trajectories will be given by $|p/q|$. Therefore we consider only the pairs (q, p) such that q and p are co-prime since they only give a primitive periodic orbits, and points (mq, mp) , where $m \in \mathbb{Z}$, gives m repetitions of a primitive periodic

orbit corresponding to (q, p) . Each such (q, p) gives different number of bands or families of periodic orbits, depending on whether the pair is odd-odd (o, o) or even-odd (e, o) or odd-even (o, e) . The length of periodic orbit in a given family corresponding to a lattice point (q, p) is given by

$$l = cL\sqrt{(q^2 + p^2)}$$

where c depends on the number of families of periodic orbits. It can be seen from table (3.2) of chapter 3, that, for (q, p) as [12]

$$c = \begin{cases} 4 & \text{one band, closing at } (4q, 4p) \text{ for } (o, o) \\ 2, 2 & \text{two bands, each closing at } (2q, 2p) \text{ for } (o, e) \\ 1, 1, 2 & \text{two bands closing at } (q, p) \text{ and one at } (2q, 2p) \text{ for } (e, o) \end{cases} \quad (4.14)$$

If $l \leq x$ for a given family of points (q, p) , the contribution from this family of (q, p) should be counted in $F(x)$. Drawing a quarter circle of radius l_1 in the quadrant under consideration, all points (q, p) having family of periodic orbits with length $cl_1 \leq x$ (or $l_1 \leq x/c$) must be considered for the calculation of $F(x)$. The quarter circle is inscribed in a square OABC with side length l_1 (Fig.4.2). thus the area of this square is l_1^2 and the area of the quarter circle OAC is $\pi l_1^2/4$. We shall denote the integer (fractional) part of a number by $[] \{ \}$. The number of lattice points in the square OABC is given by

$$N = \left(\left[\frac{l_1}{L} \right] + 1 \right)^2 \left(\left(\frac{l_1}{L} - \left\{ \frac{l_1}{L} \right\} + 1 \right)^2 \right)$$

Taking fractional part of l_1/L , on an average as $1/2$, we can write

$$N = \left(\frac{l_1}{L} \right)^2 + \left(\frac{l_1}{L} \right) - \frac{1}{4}$$

Then the number of lattice points in a quarter circle is just

$$N_q = \left(\frac{N}{l_1^2} \right) \left(\frac{\pi l_1^2}{4} \right) = \frac{\pi N}{4} \quad (4.15)$$

Since the probability that two randomly chosen numbers are co-prime is $(6/\pi^2)$ the number of co-prime lattice points in quarter circle is

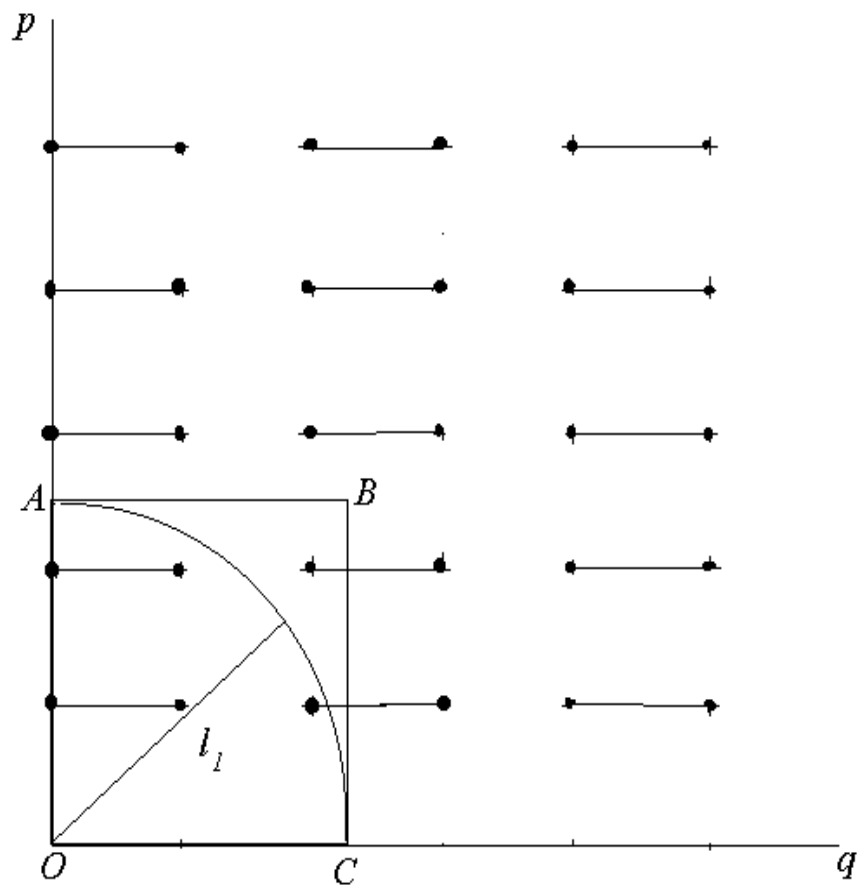


Fig. 4.2: Lattice structure of H-M billiard and single slit rectangular billiard is same though fundamental regions are not. End points of the barriers can be assigned integer labelling.

$$\begin{aligned} N_c &= \left(\frac{6}{\pi^2}\right) \left(\frac{\pi N}{4}\right) \\ &= \left(\frac{3}{2\pi L^2}\right) l_1^2 + \left(\frac{3}{2\pi L}\right) l_1 + \frac{3}{8\pi} \end{aligned} \quad (4.16)$$

The counting function can now be written explicitly as (using equation(4.14))

$$F(x) = P_{oo}N_{oo}\left(\frac{x}{4}\right) + 2P_{oe}N_{oe}\left(\frac{x}{2}\right) + 2P_{oe}N_{oe}(x) + P_{eo}N_{eo}\left(\frac{x}{2}\right) \quad (4.17)$$

where again e.g., P_{oo} is the probability that a given co-prime lattice point is of (*odd, odd*) type and $N_{oo}(x)$ is the total number of odd-odd co-prime lattice points contained in the quarter circle of radius x ($= N_c$). Trivially,

$$P_{oo} = P_{oe} = P_{eo} = \frac{1}{3} \quad (4.18)$$

thus

$$\begin{aligned} F(x) &= \frac{1}{3} \left[N_c\left(\frac{x}{4}\right) + 3N_c\left(\frac{x}{2}\right) + 2N_c(x) \right] \\ &\quad \left(\frac{45}{32\pi L^2} \right) x^2 + \left(\frac{15}{8\pi L} \right) x + \frac{3}{4\pi} \end{aligned} \quad (4.19)$$

This is the asymptotic law of proliferation of periodic orbits for system under consideration. How fast actual $F(x)$ converges to equation(4.19) depends on the rate of convergence of P_{oo} , P_{oe} , P_{eo} and N_c in accordance with equations(4.18) and (4.16) respectively. It can be easily seen that P converges rapidly to $1/3$. In Table (4.1), we compare the actual number of co-prime pairs with the results obtained by equation(4.16). It can be seen that (even) at $x = 50$, the % difference between the numerical and analytical results is only 2%. For similar reasons, we get an equally remarkable agreement in the case of the $\pi/3$ -rhombus billiard as seen in Fig.(4.3).

4.2.3 The Single Slit Rectangle Billiard

This billiard has been already described in the last chapter. Again we consider only the pairs (q, p) such that q and p are co-prime since they only give a primitive periodic orbits, and points (mq, mp) , where $m \in \mathbb{Z}$, gives m repetitions of a primitive periodic orbit corresponding to (q, p) . Each such (q, p) gives different number of bands or families of periodic orbits, depending on whether the pair is odd-odd (o, o) or even-odd (e, o) or odd-even (o, e). The

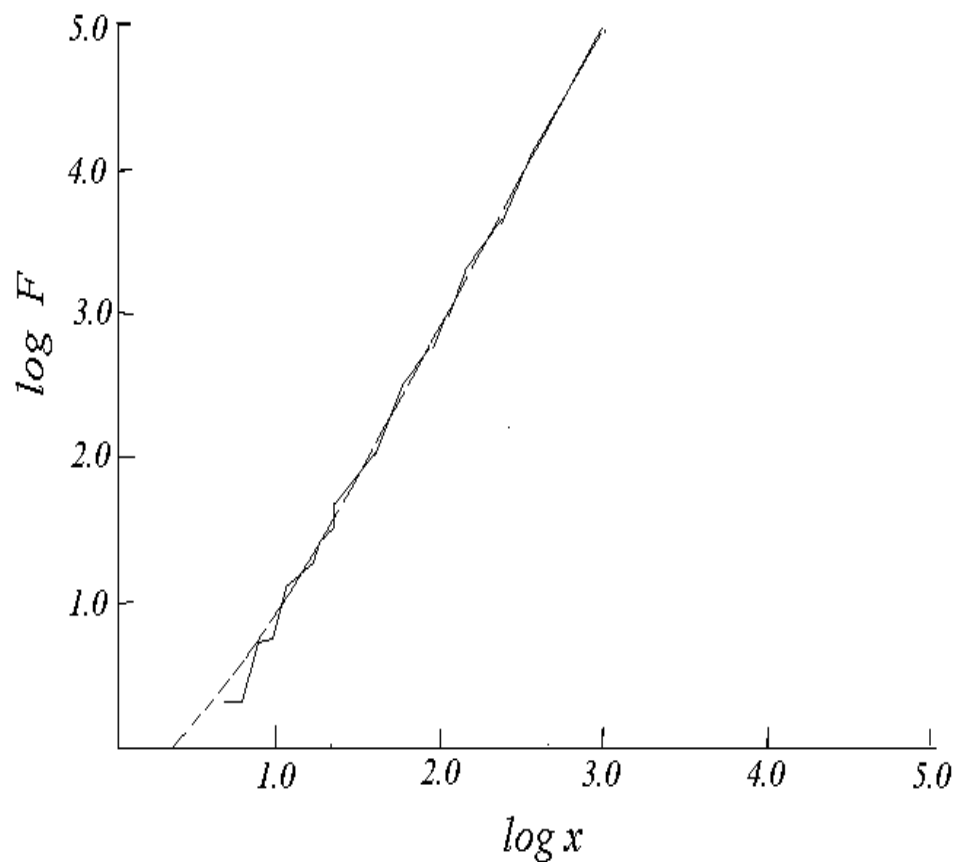


Fig. 4.3: A log-log plot of the counting function, $F(x)$ vs. the length l of the primitive periodic orbits. Dashed curve represents theoretical results eq. (4.13) and the solid curve represents actual $F(x)$ obtained numerically.

length of periodic orbit in a given family corresponding to a lattice point (q, p) is given by

$$l = cL\sqrt{(q^2 + p^2)}$$

where c depends on the number of families of periodic orbits, which is now changed due to a simple modification of H-M billiard to single slit rectangle, and is now given by (ref. Table 3.3 of chapter 3)

$$c = \begin{cases} 4 & \text{two bands, each closing at } (4q, 4p) \text{ for } (o, o) \\ 4 & \text{two bands, each closing at } (4q, 4p) \text{ for } (o, e) \\ 2, 2 & \text{four bands each closing at } (2q, 2p) \text{ for } (e, o) \end{cases} . \quad (4.20)$$

Remaining analysis is same and will not be repeated here. Proliferation law of periodic orbits can be deduced similarly and will be of same form $ax^2 + bx + c$.

The similarity of equations (4.13) and (4.19) indeed suggest an immediate generalization. However, first of all, let us discuss the reason underlying the difference between the quadratic coefficient obtained by us and the one by Gutkin in the theorem paraphrased earlier in this section. The calculations show that this difference is of an order or so. The reason is as follows. In considering the number of lattice points formed by stacking fundamental region of the corresponding integrable system, the condition of co-primality was not taken into account by Gutkin. As explained earlier an orbit labeled by a pair (mq, mp) , where $m \in \mathbb{Z}$, gives m repetitions of a primitive periodic orbit corresponding to point (q, p) where q and p are co-prime. Hence, ignoring the co-primality condition leads to an over counting of the periodic orbits. Further, due to symmetry in the tessellated two dimensional plane, calculation need to be performed for $(\pi/4)$ sector in the single slit or H-M billiard and for $(\pi/6)$ sector in the $\pi/3$ -rhombus billiard. In general, of course, for a domain with a discrete symmetry of order N , only a (π/N) sector needs consideration. Finally, one must note that a basic difference between the lattice generated by fundamental polygonal billiard and corresponding integrable system, lies in the incomplete tessellation of the plane by non-integrable billiards. For instance, the barriers are of zero width and finite length in the two examples considered in this section. It is this structure that enables us to completely classify the orbits *via* integer labeling. The relative weight (P_{oo}, P_{oe}, P_{eo}) in H-M billiard and (P_{oocc}, P_{ooce}) etc. in

the $(\pi/3)$ -rhombus billiard for different types of co-prime lattice points differ in different system and lead to a different quadratic coefficient. Hence, to give a general formula for the law of proliferation of periodic orbits exactly demands a complete enumeration and classification of periodic orbits. Although this important question cannot be answered today, a general recipe in the following is presented which comes very close to an exact formula for quadratic coefficient.

4.3 Proliferation of Periodic Orbits Considering Repetitions

We now discuss the nature of this law if repetitions of the orbits are also counted. this finds application in the semi-classical theory of spectral statistics. If we follow on the similar lines as above, we obtain the asymptotic behaviour detailed below.

If we are counting repetitions of the primitive orbits of length, $l < x$, then the primitive orbits of length between x and $x/2$ will not be repeated; the primitive orbits with length $l; x/2 < l < x/3$ will be repeated once; the primitive orbits with length $x/3 < l < x/4$ will be repeated twice and so on. Thus taking into account these repetitions, one can write an expression for number of ‘effective’ co-prime lattice points within a quarter circle of radius $x, N(x)$ as,

$$N_r(x) = N_c(x) - N_c\left(\frac{x}{2}\right) + 2\left(N_c\left(\frac{x}{2}\right) - N_c\left(\frac{x}{3}\right)\right) + \dots + n\left(N_c\left(\frac{x}{n}\right) - N_c(1)\right) \quad (4.21)$$

Here n is the largest integer less than x , we have neglected $N(l)(l < 1)$ since there are no periodic orbits of length less than 1 in the system we have considered. Equation (4.21) can be rewritten as

$$N_r(x) = N_c(x) + N_c\left(\frac{x}{2}\right) + N_c\left(\frac{x}{3}\right) + \dots + N_c\left(\frac{x}{n}\right) - nN_c(1) \quad (4.22)$$

Then, the modified counting function, $F_r(x)$, for say H-M billiard becomes

$$F_r(x) = \frac{1}{3} \left[N_r\left(\frac{x}{4}\right) + 3N_r\left(\frac{x}{2}\right) + 2N_r(x) \right] \quad (4.23)$$

substituting equation(4.22) in equation(4.23), we get

$$\begin{aligned}
F_r(x) = & \left(\frac{1}{3}\right) \left(\left(\frac{A(n_4)}{16} + \frac{3A(n_2)}{2} + 2A(n)\right) \left(\frac{3}{2\pi}\right) x^2 \right. \\
& \left. + \left(\frac{B(n_4)}{4} + \frac{3B(n_2)}{2} + 2B(n)\right) \left(\frac{3}{2\pi}\right) x - (n_4 + n_2 + n) \left(\frac{3}{\pi}\right) \right) \tag{4.24}
\end{aligned}$$

where n_4 and n_2 are the largest integers less than $x/4$ and $x/2$ respectively. A and B are given by

$$A(n) = \sum_i \frac{1}{i^2}; \quad B(n) = \sum_i \frac{1}{i}$$

Asymptotically ($n \rightarrow \infty$), $A(n) = \pi^2/6$ and $B(n) = \log(n) + \gamma$ where (γ) is the Euler-Mascheroni constant, equal to 0.5772157..... The proliferation law with repetitions for other billiards considered above can similarly be deduced.

The rate of convergence of actual $F_r(x)$ to equation(4.24) depends upon the rate of convergence of actual $N_r(x)$ to equation(4.22). In Table(4.1), we compare actual number of 'effective' co-prime pairs $N_r(x)$ with that given by equation (4.22). Note that the % difference between actual 'effective' co-prime numbers and those obtained from equation(4.22) at $x = 50$, is 5% (it may be recalled that this figure is almost 2.5 times the one observed for N_c). It is for this reason that the convergence to the quadratic law (equation(4.24)) is much slower if one considers repetitions.

To conclude, we have shown analytically that the rate of proliferation of the periodic orbits is exactly quadratic (in length) asymptotically. We have seen that this is in complete agreement with extensive numerical calculations on two model pseudo-integrable systems. The reason underlying the asymptote, $ax^2 + bx + c$, to the counting function is clearly related to the tessellation of the two dimensional plane by the fundamental region of the billiards.

4.4 Generalization

It is well known that a rational polygon can periodically tile a surface everywhere flat, in the sense of null Gaussian curvature, except at isolated vertex points of singular negative curvature. A periodic structure that tiles the almost everywhere flat surface may consist of several polygons and hence space can be assigned distinct labels (albeit complicated) taking account of

different periodicities, in a spirit similar to the one presented above. To enumerate distinct primitive periodic orbits, one needs a condition analogous to the co-primality condition required by the two systems discussed above, since out of all lattice points lying on the same line of a given slope only one will give a primitive periodic orbit. Let us denote the probability of the "co-primality condition" to be satisfied by distinct labels P_c . Furthermore, the classification entailing each distinct label will give rise to relative weights in which the orbits will be distributed, let us denote it by P_j (j denote classes). For a polygon with symmetry group of order N , the points to be considered will be restricted to a π/N sector. This number can be written as

$$N_L = \sum_i (\alpha_i x^2 + \beta_i x + \gamma_i) / N$$

where the summation is over all the periodicities. And number of "co-prime" points are $N_{LC}(x) = P_C N_L(x)$. For each class of periodic orbit for which the weight is P_j , there may be k types of periodic orbits closing at length $\xi_{kj}x$. We assume that k remains constant for given class. With this the counting function becomes

$$F(x) = \sum_j P_j \sum_k N_{LC} \left(\frac{x}{\xi_{kj}} \right)$$

and hence coefficient of $F(x) = ax^2 + bx + c$ are

$$\begin{aligned} a &= \frac{P_C}{N} \sum_i \alpha_i \sum_j P_j \sum_k \xi_{jk}^{-2} \\ b &= \frac{P_C}{N} \sum_i \beta_i \sum_j P_j \sum_k \xi_{jk}^{-1} \\ c &= \frac{P_C}{N} \sum_i \gamma_i \sum_j P_j \end{aligned}$$

Hence, counting function will quadratic and convergence will depend on both P_C and P_L . However, If k is not constant but depends on x then above analysis will have to be modified and $F(x)$ may not be quadratic.

x	N_c	N_c eq.(4.16)	/diff Col.2, 3	N_r	N_r eq.(4.22)	/diff Col.5, 6
3.0	2	5	150.0	2	4	100.0
4.0	6	9	50.0	6	9	50.0
5.0	10	14	40.0	12	17	41.6
6.0	16	19	18.7	18	23	27.7
7.0	20	26	30.0	26	34	30.7
8.0	28	34	21.4	36	46	27.7
9.0	36	42	16.6	48	59	22.9
10.0	46	52	13.0	62	75	20.9
20.0	190	200	5.2	280	313	11.8
30.0	424	443	4.4	654	707	8.1
40.0	764	782	2.3	1188	1264	6.3
50.0	1192	1217	2.0	1876	1977	5.3
60.0	1718	1747	1.6	2720	2848	4.7
70.0	2330	2372	1.8	3724	3876	4.1
80.0	3048	3093	1.4	4884	5063	3.7
90.0	3876	3910	.8	6208	6406	3.2
100.0	4770	4822	1.1	7684	7912	2.9
200.0	19088	19193	.55	31066	31593	1.7
300.0	42972	43114	.33	70162	71009	1.2
400.0	76402	76585	.24	124974	126145	.94
500.0	119372	119604	.19	195484	197005	.78

Table 4.1: Comparision between actual and theoretical values for N_c and N_r

Bibliography

- [1] W.Parry and M. Pollicott, Ann. Math. **118**, (1983)573.
- [2] W.Parry, Ergod. Throry Dynam. Syst. **4**, (1984)117.
- [3] A.Katok, Commun. Math. Phys. **111**, (1987)151.
- [4] E. Gutkin and H.Haydn, Bull. AMS, **32**, (1995)50.
- [5] I.P.Korneld, S.V.Fomin, Y.G.Sinai, Ergodic theory, Springer, Berlin, 1982.
- [6] G.Galperin, T.Krüger, S.Troubetzkoy, Local instablity of orbits in polygonal and polyhedral billiards, Forschungszentrum BiBoS, Rep. Nr. 539/1992.
- [7] H.Masur, Ergod. Theory Dynam. Syst. **10**, (1990)151.
- [8] H.Masur, Holomorphic Functions and Moduli I, (MRI, 1988)215.
- [9] E.Gutkin, Physica, **19D**, (1986)311.
- [10] S.R.Jain and H.D.Parab, J. Phys. A:Math. and General, **25**,(1992)6669.
- [11] H.D.Parab and S.R.Jain, Phys. Rev. E, **47**, (1993)R776.
- [12] J.H.Hannay and R.J. McCraw J. Phys. **A25** (1990)887.
- [13] M.R.Schroeder, Number Theory In Science and Communication, 2nded.(Sringer-Verlag, Berlin,1984).

Chapter 5

Two-Point Cluster Function and Form Factor: A Diagonal Approximation

5.1 Introduction

We Consider the discrete spectrum E_1, E_2, E_3, \dots of a f -dimensional bound quantum system. As mentioned in the chapter (1) one can define a "global" function $N(E)$ which gives number of levels less than or equal to E on the set of this discrete levels. The function $N(E)$ is obviously a staircase like function, since it jumps by unity at the occurrence of an eigenvalue E_i and remains constant otherwise. Of course if spectrum consist of degeneracies then jump in $N(E)$ at the particular degeneracy will not be unity but equal to number of degenerate levels at particular point on energy axis. Typical functional nature of $N(E)$ is therefore non-analytical. When we approximate $N(E)$ by a semi-classical expression we use approximate analytical form for the exact staircase. We use same symbol $N(E)$ for both actual staircase and its semiclassical approximation, mostly we will be talking about semiclassical approximation below.

As mentioned earlier it is possible to separate semi-classical approximation to $N(E)$ in a smooth part $N_{av}(E)$ and the fluctuating part $N_{osc}(E)$ (i.e. $N(E) = N_{av}(E) + N_{osc}(E)$). In the particular case of a particle (of mass $m = 1/2$) in polygonal box (or polygonal billiard) of area A_R , $N_{av}(E)$ is

given by

$$N_{av}(E) = \frac{A_R E}{4\pi\hbar^2} - \frac{L_D \sqrt{E}}{4\pi\hbar} + C \quad (5.1)$$

where L_D is length of the parameter of the boundary, and C is a constant containing complex information on the geometrical and topological properties of the billiard.

This average behaviour may be eliminated in order to characterize and compare the fluctuation patterns of different systems whose corresponding $N_{av}(E)$ is not same. For this purpose it is convenient to ‘‘unfold’’ the original spectrum $\{E_i\}$ through the mapping $E \mapsto r$

$$r_i = N_{av}(E_i). \quad (5.2)$$

The effect of (5.2) is that the sequence $\{r_i\}$ has on the average a constant mean spacing equal to unity, irrespective of the particular form of the function $N_{av}(E)$. By construction $r_i \simeq i - 1/2 (i = 1, 2, \dots)$ and the departures

$$\delta_i = r_i - (i - 1/2) \quad (5.3)$$

of r_i from its average value $i - 1/2$ are the level fluctuations. As a result of unfolding the spectrum in a way mentioned above it is obvious that the average part of level density of unfolded spectrum $d_{av}(y)$ is unity.

5.2 Spectral Fluctuation Measures

The level fluctuations can be characterized in a systematic way using the k -point correlation functions and measures derived from them. The k -point correlation function is defined as [1, 2]

$$R_k(x_1, \dots, x_k) = \frac{n!}{(n-k)!} \int_{-\infty}^{\infty} \dots \int_{-\infty}^{\infty} P_n(x_1, \dots, x_n) dx_{k+1} \dots dx_n. \quad (5.4)$$

where P_n is a joint probability density function of the levels $\{x_i\}_{i=1 \dots n}$ and $1 \leq k \leq n$. The R_k is thus a probability density of finding a level (regardless of labeling) around each of the points $x_1 \dots x_k$, the positions of the remaining levels being unobserved. Each function R_k ; $k > 1$ contains terms of various kinds describing the grouping of k levels into various subgroups or clusters.

In practice it is convenient to introduce k -level cluster functions obtained from R_k by subtracting out the lower-order correlation terms, as

$$T_k(x_1 \dots x_k) = \sum_G (-1)^{k-m} (m-1)! \prod_{j=1}^m R_{G_j}(x_t, \text{with } k \text{ in } G_j). \quad (5.5)$$

Here G stands for any division of the indices $[1, \dots, k]$ into subgroups $[G_1, \dots, G_m]$. For example,

$$\begin{aligned} T_1(x) &= R_1(x) \\ \text{and} \\ T_2(x_1, x_2) &= -R_2(x_1, x_2) + R_1(x_1)R_1(x_2) \end{aligned} \quad (5.6)$$

Measuring the energies in the units of the mean level spacing $\lambda = 1$ and introducing the variables $y_i = x_i/\lambda$, (this is nothing but the unfolding mentioned earlier) the cluster functions can be written as

$$Y_k(y_1, \dots, y_k) = \lim_{n \rightarrow \infty} \lambda^n T_n(x_1, \dots, x_k). \quad (5.7)$$

The Y_k 's are then well defined and finite everywhere. The cluster functions being isolated from the effects of the lower correlations, vanishes as the separation

$r = |r_1 - r_2|$ becomes larger and larger. Among these two-level cluster function Y_2 is of prime importance. When the collection of levels are treated as a classical Coulomb gas, Y_2 defines the shape of the neutralizing charge cloud induced by each particle around itself [2]. As mentioned earlier many fluctuation measures can now be expressed in terms of the Y_k 's. We shall discuss this at appropriate place.

Consider now one point measure, the energy level density function $d(y) = \sum_i \delta(y - y_i)$, where δ is usual Kronecker's delta function. The average with respect to the probability distribution function $P(y_1 \dots y_n)$ (so called ensemble average) of the level density function is given by

$$\begin{aligned} \langle \langle d(y) \rangle \rangle &= \int_{-\infty}^{\infty} dy_1 \dots \int_{-\infty}^{\infty} dy_n d(y) P(y_1 \dots y_n) \\ &= n \int_{-\infty}^{\infty} dy_1 \dots \int_{-\infty}^{\infty} dy_n \delta(y - y_1) P(y_1 \dots y_n) \\ &= R_1(y) = T_1(y) \end{aligned} \quad (5.8)$$

Also the density-density correlation function (for energy) is defined as

$$\begin{aligned}
\langle\langle d(y)d(y')\rangle\rangle &= \sum_{i=1}^n \sum_{j=1}^n \int_{-\infty}^{\infty} dy_1 \cdots \int_{-\infty}^{\infty} dy_n \delta(y - y_i) \delta(y' - y_j) P(y_1 \dots y_n) \\
&= n \sum_{i=1}^n \int_{-\infty}^{\infty} dy_1 \cdots \int_{-\infty}^{\infty} dy_n \delta(y - y_1) \delta(y' - y_1) P(y_1 \dots y_n) \\
&\quad + n(n-1) \sum_{i \neq j=1}^n \int_{-\infty}^{\infty} dy_1 \cdots \int_{-\infty}^{\infty} dy_n \delta(y - y_1) \delta(y' - y_2) P(y_1 \dots y_n) \\
&= \delta(y - y') R_1(y) + R_2(y, y')
\end{aligned}$$

Hence, from equation (5.6), we get

$$\langle\langle d(y)d(y')\rangle\rangle = \delta(y - y') R_1(y) + R_1(y) R_1(y') - T_2(y, y'). \quad (5.9)$$

Since the ensemble average is same as the spectral average (see e.g. [3]), which is defined as (for level density)

$$\langle d(y) \rangle = \frac{1}{\eta} \int_{y-\eta/2}^{y+\eta/2} dx \quad d(x), \quad (5.10)$$

we can write in an asymptotic limit

$$\langle d(y) \rangle = R_1(y) = Y_1(y) = d_{av}(y) = 1 \quad (5.11)$$

and

$$\langle d(y)d(y') \rangle = \delta(y - y') + 1 - Y_2(y, y'). \quad (5.12)$$

Thus two-point correlation function $R_2(y_1, y_2)$ or cluster function $Y_2(y_1, y_2)$ are related to the spectral average of density-density correlation function as

$$R_2(y, y') = \langle d(y)d(y') \rangle - \delta(y - y') \quad (5.13)$$

and

$$Y_2(y, y') = 1 + \delta(y - y') - \langle d(y)d(y') \rangle. \quad (5.14)$$

Equations (5.13) and (5.14) are the important relation to develop semi-classical understanding of spectral fluctuation properties in which we are

interested. Since we can write density of states as sum of average and fluctuating part ($d(y) = d_{av}(y) + d_{osc}(y)$) the density-density correlation function becomes

$$\begin{aligned}\langle d(y)d(y') \rangle &= \langle (d_{av}(y) + d_{osc}(y))(d_{av}(y') + d_{osc}(y')) \rangle \\ &= d_{av}(y)d_{av}(y') + d_{av}(y)\langle d_{osc}(y') \rangle \\ &\quad + d_{osc}(y)\langle d_{av}(y') \rangle + \langle d_{osc}(y)d_{osc}(y') \rangle,\end{aligned}$$

since $\langle d_{osc}(y) \rangle = \langle d_{osc}(y') \rangle \simeq 0$, and also $d_{av}(y) = 1$, we finally get

$$\langle d(y)d(y') \rangle = 1 + \langle d_{osc}(y)d_{osc}(y') \rangle. \quad (5.15)$$

Using this, equations (5.13) and (5.14) can be rewritten as

$$R_2(y, y') = \langle d_{osc}(y)d_{osc}(y') \rangle + 1 - \delta(y - y') \quad (5.16)$$

and

$$Y_2(y, y') = \delta(y - y') - \langle d_{osc}(y)d_{osc}(y') \rangle. \quad (5.17)$$

These are the equations that we will use below to study spectral fluctuation properties as we can substitute semi-classical expression obtained in chapter (1) for $d_{osc}(y)$. Note, existence of $\delta(y - y')$ in eqs. (5.16) and (5.17). Since R_2 or Y_2 must be free of δ -function, density-density correlation function also must contain similar δ -function. Indeed this is due to the self-correlation of a level.

All the relevant information to evaluate semi-classical periodic orbit sum is obtained in the previous two chapters. For an easy reference we will reproduce briefly those results in the following section. Further the example, we consider here ($\pi/3$ -rhombus billiard) also possesses a symmetry with respect to both the diagonals. This results in modification of the semi-classical expression for the density of states, since one can now work with decomposed state space due to symmetry. These issues are also discussed in the following section before we take up study of statistical measures.

5.3 Semi-classical Density of States

As stated in chapter (1) the oscillatory part of density of states in case of pseudo-integrable is given by[4]

$$d(E) = \frac{m}{2\pi\hbar^2} \text{Re} \sum_i \int \int d\mathbf{q} H_0^{(1)} \left(\frac{l_i}{\hbar} \sqrt{2mE} \right) \exp(i\alpha_i \pi). \quad (5.18)$$

where all symbols are as explained in chapter (1). Here we take $m = 1/2$, then by taking real part and in the asymptotic limit ($\hbar \rightarrow 0$) we get (note that α 's are integers)

$$d_{osc}(E) = \left(\frac{1}{8\pi^3 \hbar^3} \right)^{1/2} E^{-1/4} \sum_i \frac{A_i}{l_i^{1/2}} \cos \left(\frac{l_i}{\hbar} \sqrt{E} + \pi(\alpha_i - \frac{1}{4}) \right). \quad (5.19)$$

We now ‘‘unfold’’ the energy using only first term of N_{av} for the reasons of simplicity (as a trade off between simplicity and accuracy), through mapping $E \rightarrow r_0$:

$$r_0 = \frac{A_R E}{4\pi \hbar^2}. \quad (5.20)$$

This means unfolded levels will not have mean spacing equal to unity exactly but only approximately. In fact from equation (5.1) it is easy to see that mean level spacing after unfolding is less then unity by a factor $(1 - L_D/(\sqrt{4\pi A_R r_0}) + C/r_0)$. Since for semi-classical analysis is valid for large value of r_0 , it is obvious that unfolding levels using just a leading term of $N_{av}(E)$ will not introduce serious error in the analysis for large value of r_0 .

From equation (5.20) we can see that

$$\frac{dr_0}{dE} = \frac{A_R}{4\pi \hbar^2} \simeq d_{av}(E),$$

and hence,

$$d(r_0) = d(E) \left(\frac{dr_0}{dE} \right)^{-1} \simeq 1 + d_{osc}(E) \left(\frac{dr_0}{dE} \right)^{-1} = 1 + d_{osc}(r_0). \quad (5.21)$$

The oscillatory part of the density of states (eq.(5.19)) can then be written in terms of rescaled energies as

$$d_{osc}(r_0) = \left(\frac{r_0^{-1/4}}{\pi^{3/4} A_R^{3/4}} \right) \sum_i \frac{A_i}{l_i^{1/2}} \cos \left(l_i \sqrt{\frac{4\pi r_0}{A_R}} + (\alpha_i - \frac{1}{4})\pi \right). \quad (5.22)$$

As mentioned above when a quantum dynamical system possesses a symmetry, its state space may be decomposed into subspaces of definite symmetry type. The Schrödinger equation can then be restricted to these subspaces resulting in a symmetry- projected spectrum. It is interesting to know how these symmetries influence the fluctuation properties of the whole spectrum.

5.3.1 Symmetry-projected Green's function

Let \hat{H} be a quantum Hamiltonian for a system of f degrees of freedom, invariant under a discrete group G . We will assume that G acts classically as a group of Euclidean point transformations (i.e. combination of translations, rotations, and reflections). The quantum mechanical action of G in the \mathbf{x} representation is given by

$$\hat{U}(g)|\mathbf{x}\rangle = |g \cdot \mathbf{x}\rangle \quad (5.23)$$

where g is an element of G and $g \cdot \mathbf{x}$ denotes its action on \mathbf{x} . By virtue of this symmetry, \hat{H} may be restricted to a subspace which is invariant under the symmetry and whose states transform according to an irreducible representation of G . The projection onto an invariant subspace is given by

$$P_m = \frac{d_m}{|G|} \sum_{g \in G} \chi_m(g) \hat{U}^\top(g), \quad (5.24)$$

where, $\chi_m(g)$ is the character of the m^{th} irreducible representation of dimension d_m , and $|G|$ is the order of group G [5].

A semi-classical approximation for $G_m(E)$, the trace of the symmetry-projected Green's function is defined as

$$G_m(E) = \text{Tr}[P_m(E - \hat{H})^{-1}]. \quad (5.25)$$

The poles of $G_m(E)$ are the energy eigenvalues of symmetry m and the pole strength give the eigenvalue degeneracies. One can now follow steps given in chapter (1) to obtain the periodic orbit sum formula. The symmetry-projected Green's function, $G_m(\mathbf{x}, \mathbf{x}'; E) = \langle \mathbf{x} | P_m(E - \hat{H})^{-1} | \mathbf{x}' \rangle$ can be obtained by restricting to an invariant subspace only which is given by[6]

$$G_m(\mathbf{x}, \mathbf{x}'; E) = \frac{d_m}{|G|} \sum_{g \in G} \chi_m(g) G(g \cdot \mathbf{x}, \mathbf{x}'; E). \quad (5.26)$$

It may be noted that the full semi-classical Green's function involves sum over orbits between \mathbf{x}' and \mathbf{x} , its symmetry projection involves a larger family of orbits. The sum over classical orbits is taken for orbits that begin at \mathbf{x}' and end at $g \cdot \mathbf{x}$, a point related to \mathbf{x} by symmetry. These orbits can be associated in a one-to-one fashion with orbits on a symmetry reduced phase space.

A general form of symmetry (discrete) projected oscillatory part of density of states can be obtained from the corresponding trace formula[6]. In the

case of pseudo-integrable polygonal billiards it reduces to (in an unfolded spectrum)

$$d_{osc}^m(r) = d_m \left(\frac{r^{-1/4}}{\pi^{3/4} A_R^{3/4}} \right) \sum_j \frac{A_j}{l_j^{1/2}} \cos \left(l_j \sqrt{\frac{4\pi r}{A_R}} - \frac{\pi}{4} + \mu_j \pi \right) \chi_m(g_p^m). \quad (5.27)$$

Here, the terms l_p, A_p are length and band area of the periodic orbits in the primitive polygon that tessellate full phase space. The sum over all m , of equation (5.27) reproduces equation (5.22).

The spectrum of the $\pi/3$ -rhombus billiard is composed of superposition of four different modes due to system symmetries [7]. Semi-classically, it is not possible to distinguish all four modes [4] separately. However, it is possible to separate equilateral triangle modes (odd parity classes) where wave function is zero on the shorter diagonal and pure rhombus modes (even parity classes) where gradient of wave function is zero on the shorter diagonal. This can be done by incorporating and exploiting the symmetry of the system in a semi-classical treatment, to obtain symmetry projected spectrum.

We will follow treatment of [6] to study effect of symmetries on the fluctuation properties of the spectrum. We take longer diagonal along y -axis and shorter diagonal along x -axis. $\pi/3$ -rhombus billiard has symmetry group $C_2 \otimes C_2$, consisting of reflections about x and y axes. The elements of the group can be denoted by $x^a y^b$, where x and y represent commuting reflections about a respective axis. The primitive cell V [6] is then half equilateral triangle having sides half of longer (\mathcal{L}_y) and shorter (\mathcal{L}_x) diagonals and one side of the rhombus \mathcal{L} . The group has four one dimensional (d_m in (5.27) is therefore 1) irreducible representations, labeled by numbers (p, q) . These numbers describe parities under reflections about x and y axes respectively. For states, even under x reflection, $p = 0$, and odd under x reflection $p = 1$. Similarly, q takes values 0 or 1 depending on parity under y reflection. The characters of the group can be easily determined in this case and are given as

$$\chi_{p,q}(g_l^n) = \exp\{-\pi n(pa_l + qb_l)\} \quad (5.28)$$

where, a_l, b_l are number of times l^{th} primitive periodic orbit bounces from \mathcal{L}_x and \mathcal{L}_y respectively, n counts repetitions of periodic orbits and g_l^n in group element $x^{a_l} y^{b_l}$. Pure rhombus modes are therefore represented by $p = 0; q = 0$ or 1 and the equilateral triangle modes by $p = 1; q = 0$ or 1.

Recalling the comments about the Maslov indices in the chapter (1), one can see that the character of the group actually play a role of the Maslov

indices μ in this case. Thus, for the pure rhombus modes Neumann boundary condition is applied to the shorter diagonal \mathcal{L}_x and then bounces on the same are not taken into the consideration. For equilateral triangle modes however, since one have Dirichlet boundary condition on \mathcal{L}_x , bounces on it should be counted.

From the polar constructions we have used [8] in chapter (3) to determine and classify the periodic orbits a_l and b_l can be determined easily. It can be seen that b_l is always even, hence qb_l does not play any role here. This is the basic reason that one can not separate these two parity classes (belonging to integrable and pseudo-integrable parts) further into the four different modes. Also it turns out that for all the centre-edge orbits, a_l is even. However, for all the centre-centre orbits there are three bands of periodic orbits each occupying area of $4A_R$ (A_R is area of V). Two of these bands bounces odd number of times on \mathcal{L}_x and one band bounces even number of times (i.e. a_l is odd for two bands and even for one band). The same is true for side \mathcal{L} , since total number of bounces on three sides of V are always even. Using all these facts discussed above, equation (5.27) becomes

$$d_{osc}^m(r) = \left(\frac{r^{-1/4}}{\pi^{3/4} A_R^{3/4}} \right) \sum_j \frac{A_j}{l_j^{1/2}} \cos \left(l_j \sqrt{\frac{4\pi r}{A_R}} - \frac{\pi}{4} + \mu_j \pi - pa_j \pi \right) \quad (5.29)$$

Note, repetition index n is absorbed in a_j here. A_j, l_j and A_R represent respectively the band area of periodic orbits of primitive cell V , length of the periodic orbits and area of half equilateral triangle. The Maslov indices, μ_j here counts bounces only on the side \mathcal{L} of the primitive cell V . Thus for the pure rhombus modes since $p = 0$, μ_j will play important role, while for equilateral triangle modes ($p = 1$), $(\mu_j - a_j)$ is always even for all the periodic orbits. If therefore, μ 's are neglected one will end up in erroneous results.

Using above discussion and following the steps of [6] we write density of states for the pure rhombus modes as

$$d_{osc}^m(r) = \left(\frac{2r^{-1/4}}{\pi^{3/4} A_R^{3/4}} \right) \sum_j \frac{A_j}{l_j^{1/2}} \cos \left(l_j \sqrt{\frac{4\pi r}{A_R}} - \frac{\pi}{4} \right) \quad (5.30)$$

for centre-edge orbits. For all centre-edge points, A_j will be $12A_R$ i.e. same

as phase space area. And for centre-centre orbits we write

$$\begin{aligned}
d_{osc}^m(r) = & \left(\frac{2r^{-1/4}}{\pi^{3/4} A_R^{3/4}} \right) \sum_j^a \frac{A_j}{l_j^{1/2}} \cos \left(l_j \sqrt{\frac{4\pi r}{A_R}} - \frac{\pi}{4} \right) \\
& + \sum_j^e \frac{A_j}{l_j^{1/2}} \cos \left(l_j \sqrt{\frac{4\pi r}{A_R}} - \frac{\pi}{4} \right) - \sum_j^o \frac{A_j}{l_j^{1/2}} \cos \left(l_j \sqrt{\frac{4\pi r}{A_R}} - \frac{\pi}{4} \right)
\end{aligned} \tag{5.31}$$

Here, superscripts a, e, o over summation sign represents all repetitions, even repetitions and odd repetitions of the primitive periodic orbits. This is simple to understand, since centre-edge points do not result in periodic orbits of different lengths in case of the rhombus there contribution will be same as the rhombus or in the half equilateral triangle. However, note that each centre-centre point results in two kinds of bands of the periodic orbits one having the same length as that of the periodic orbits in the half equilateral triangle and other having length twice of the same. These orbits do not belong to the half equilateral triangle. The density of states for equilateral triangle mode has same form as (5.30). It is simple to check that adding these contributions we do get density of states for the complete rhombus. We shall now turn our attention to study of two-level cluster function.

5.4 Two-Level Cluster Function

In this section we shall obtain a closed analytical expression for two level cluster function in pseudo-integrable billiards using semi-classical framework. To do this it is clear from equation (5.17) that we need to evaluate semi-classical product $\langle d_{osc}(y)d_{osc}(y') \rangle$, (i.e. spectral average of density-density correlation function).

5.4.1 Density-density correlation function

As defined above density-density correlation function (oscillatory part) is given by $d_{osc}(y)d_{osc}(y')$. We consider correlation of levels around r_0 i.e. we will put $y = r_0 + r_1$ and $y' = r_0 + r_2$: $r_1, r_2 \ll r_0$ then using equation (5.22) correlation function becomes

$$\begin{aligned}
d_{osc}(r_0 + r_1)d_{osc}(r_0 + r_2) = & \frac{r_0^{-1/2}}{\pi^{3/2} A_R^{3/2}} \sum_{j,k} \frac{A_j A_k}{l_j^{1/2} l_k^{1/2}} \left\{ \cos \left(\sqrt{\frac{4\pi}{A_R}} (l_j \sqrt{r_0 + r_1} + \pi (\alpha_j - \frac{1}{4})) \right) \right. \\
& \left. \times \cos \left(\sqrt{\frac{4\pi}{A_R}} (l_k \sqrt{r_0 + r_2} + \pi (\alpha_k - \frac{1}{4})) \right) \right\}
\end{aligned}$$

or by using simple trigonometrical identities

$$\begin{aligned}
d_{osc}(r_0 + r_1)d_{osc}(r_0 + r_2) &= \frac{r_0^{-1/2}}{2\pi^{3/2}A_R^{3/2}} \sum_{j,k} \frac{A_j A_k}{l_j^{1/2} l_k^{1/2}} \\
&\quad \left\{ \sin \left(\sqrt{\frac{4\pi}{A_R}} (l_j \sqrt{r_0 + r_1} + l_k \sqrt{r_0 + r_2}) + \kappa_+ \right) \right. \\
&\quad \left. + \cos \left(\sqrt{\frac{4\pi}{A_R}} (l_j \sqrt{r_0 + r_1} - l_k \sqrt{r_0 + r_2}) + \kappa_- \right) \right\}
\end{aligned} \tag{5.32}$$

where $\kappa_{\pm} = \pi(\alpha_j \pm \alpha_k)$, terms due to Maslov indices (i.e. number of bounces on the billiard wall). In the case of polygonal billiards it can be seen that the number of bounces of a particle on wall is always even if boundary conditions on the all segments of the boundary are same either Dirichlet or Neumann[9]. Hence, we will drop them from our analysis until we consider an example where they becomes important (these are the cases where boundary conditions are mixed i.e. on some segment it is Dirichlet, on the others it is Neumann).

It is easy to see that due to local averaging the first term in the above equation will be negligibly small even when statistically significant number of levels are considered. The second term also vanishes, unless

$$\left| \sqrt{\frac{4\pi}{A_R}} (l_j \sqrt{r_0 + r_1} - l_k \sqrt{r_0 + r_2}) \right| < 1$$

The reason for this is that in the semi-classical limit this term will oscillates rapidly[10, 11] (it is well known that if argument of cos or sin function is large, any small change in it will result in rapid oscillations). Due to these rapid oscillations, spectral averaging will result in negligibly small contributions unless above condition is satisfied.

Since $r \ll r_0$ we can approximate $\sqrt{r_0 \pm r} \sim \sqrt{r_0} (1 \pm r/2r_0)$ to write above condition as

$$\left| \sqrt{\frac{4\pi r_0}{A_R}} \left(\delta + \frac{r}{2r_0} l \right) \right| < 1 \tag{5.33}$$

where for a simplicity we assume with out loss of any generality $l_j = l + \delta/2$, $l_k = l - \delta/2$, and $r_{1(2)} = +(-)r/2$. Note the presence of correlation range ' $r = |r_1 - r_2|$ ' in the denominator of the second term, which appears because we are dealing with density-density correlation function directly and not with it's Fourier transform as generally done. The equation (5.33) indicates that one can separate the correlation function (5.32) in two parts as

$$d_{osc}(r_0 + r_1)d_{osc}(r_0 + r_2) = \sum_{l_j=l_k} + \sum_{l_j \neq l_k} .$$

The first part is known as diagonal part ($\delta = 0$) and other part is called as off-diagonal part ($\delta \neq 0$).

Now let us take close look at condition (5.33) which can be written as

$$\left| \delta + \frac{r}{2r_0} l \right| < \sqrt{\frac{A_R}{4\pi r_0}}$$

This is equivalent to following conditions

$$\text{for } 0 < \delta : \quad 0 < \delta < \sqrt{\frac{A_R}{4\pi r_0}} - \frac{r}{2r_0} l \quad (5.34)$$

$$\text{for } \delta < 0 \text{ and } |\delta| < \frac{rl}{2r_0} : \quad \frac{r}{2r_0} l - \sqrt{\frac{A_R}{4\pi r_0}} < |\delta| < \frac{r}{2r_0} l$$

$$\text{for } \delta < 0 \text{ and } |\delta| > \frac{rl}{2r_0} : \quad \frac{r}{2r_0} l < |\delta| < \frac{r}{2r_0} l + \sqrt{\frac{A_R}{4\pi r_0}}$$

One can see that in $\lim r_0 \rightarrow \infty$, (or equivalently $\hbar \rightarrow 0$),: $\delta \rightarrow 0$, hence, off-diagonal contributions may not be important in the asymptotic limit and one can safely rely on the diagonal approximation only. Generally, one is interested in the asymptotic properties of spectral fluctuations only.

In practice, however, one always works with finite r_0 , in fact most of the numerical studies deals with at most few thousands of levels. It should be emphasized that in such cases off-diagonal contributions may not be negligible since finite number of levels are considered.

When $\delta = 0$ (i.e. $l_j = l_k$) this condition becomes

$$l < \frac{1}{r} \sqrt{\frac{A_R r_0}{\pi}} = \frac{l_H}{2\pi r} \quad (5.35)$$

where $l_H = \sqrt{4\pi A_R r_0}$ is ‘‘Heisenberg length’’ (which corresponds to well known Heisenberg time $t_H = 2\pi\hbar d_{av}(E)$, via relation $l_H = 2t_H\sqrt{E}$).

The equation (5.35) stipulates a condition for the validity of the diagonal approximation. For any given l_H , it is sufficient to work with diagonal terms for the length of periodic orbits satisfying above condition, since then one can see that in general $\delta \sim 0$ for sufficiently large number of levels. This condition is similar to the one obtained for diagonal approximation for Fourier transform of Y_2 (known as the form factor), except the presence of correlation range r in the denominator. It is obvious from this condition that for any fixed l_H diagonal approximation is strictly valid only at $r \sim 0$. For $0 \ll r$ and $l_H/2r < l$ the contribution of off-diagonal terms may not be insignificant.

Here, in this and next chapter we consider diagonal terms only. Our results will therefore valid for $r \ll 1$.

5.4.2 Diagonal approximation

We can neglect first term of eq. (5.32). Since we are interested in correlations over the number of few mean level spacings, much smaller than total number of levels considered ($r \ll r_0$) we can approximate $\sqrt{r_0 \pm r}$ by $\sqrt{r_0}(1+r/2r_0)$, then density-density correlation function becomes

$$d_{osc}(r_0 + r_1)d_{osc}(r_0 + r_2) = \frac{r_0^{-1/2}}{2\pi^{3/2}A_R^{3/2}} \sum_{j,k} \frac{A_j^2}{l_j} \cos\left(\frac{2\pi l_j r}{l_H}\right), \quad (5.36)$$

where $r = |r_1 - r_2|$ and $l_H = \sqrt{4\pi A_R r_0}$, the Heisenberg length.

We have seen in chapter (3) that the periodic orbits occurring in the pseudo-integrable polygonal billiards can be classified into different families according to the nature of lattice points corresponding to the periodic orbit as well as to the projected phase space area occupied by the bands of periodic orbits. We have seen this via few examples of such billiards. For these billiards density-density correlation function can be written as

$$\begin{aligned} d_{osc}(r_0 + r_1)d_{osc}(r_0 + r_2) = & \frac{r_0^{1/2}}{2\pi^{3/2}A_R^{3/2}} \left\{ \sum_{\alpha} g_{\alpha}^2 A_{\alpha}^2 \sum_j \frac{\cos\left(\frac{2\pi l_{\alpha,j} r}{l_H}\right)}{l_{\alpha,j}} + \right. \\ & \left. \sum_{\alpha, \beta} (1 - \delta_{\alpha, \beta}) g_{\alpha} g_{\beta} A_{\alpha} A_{\beta} \sum_{j, k} \delta_{l_{\alpha, j}, l_{\beta, k}} \frac{\cos\left(\frac{2\pi l_{\alpha, j} r}{l_H}\right)}{l_{\alpha, j}^{1/2} l_{\beta, k}^{1/2}} \right\} \end{aligned} \quad (5.37)$$

Here, subscripts α, β denotes classes of bands of the periodic orbits, $A_{\alpha} A_{\beta}$ are projective phase space area occupied by the periodic orbits in the given class, $g_{\alpha} g_{\beta}$ denotes degeneracy in the lengths of the periodic orbits. Other symbols have their usual meaning. The second term on RHS takes care of systematic length degeneracy occurring in different classes. However, we do not take into account accidental degeneracy here. The summation over j in the above equation can be replaced by integration in the continuum limit, choosing a proper measure. Heuristic arguments to obtain such measure are given below

5.4.3 Summing over all the periodic orbits

Consider a length interval $(l, l + dl)$ such that $dl \ll l$ but sufficiently large enough to contain many events (by events here, we mean occurrence of a

periodic orbit of a length within the above interval). The proliferation law of the periodic orbits, which gives the average number of periodic orbits of length $\leq l$ for a class α , has a form

$$F_\alpha(l) = a_\alpha l^2 + O(l)$$

where a_α is system dependent constant. In our analysis we will neglect $O(l)$ term. Number of periodic orbits having length between (dropping subscript α temporarily), l and $l + dl$, is given as $n=2aldl$. Hence the mean spacing between periodic orbits is $1/2al$. One can divide interval dl in n cells each of the length equal to the mean spacing. The length of the i^{th} periodic orbit, $l_i \varepsilon(l, l + dl)$ can be written as $l_i = l + i/2al + \eta_i$. Here, η_i 's represent local fluctuations in the actual periodic orbit lengths from the average lengths $l + i/2al$. It is therefore, reasonable to assume that η_i 's are distributed symmetrically around zero. Most of the η_i 's will be closely distributed around zero with small fractions extending up to few mean level spacings. The summation of form $\sum \cos(\mathcal{A}l)/l$ over j for $l_j \varepsilon(l, l + dl)$ can be written as

$$\sum_{j=0}^{n-1} \frac{\cos(\mathcal{A}l_j)}{l_j} = \sum_{j=0}^{n-1} \frac{\cos\left(\mathcal{A}\left(l + \frac{j}{2al} + \eta_j\right)\right)}{l} \left(1 - \frac{j}{2al^2} - \frac{\eta_j}{l}\right)$$

In our case $\mathcal{A} = \sqrt{\frac{\pi}{A_R r_0}} r = 2\pi r/l_H \ll 1$, hence $\mathcal{A}\eta_j \sim 0$. One can also notice that 2nd and 3rd terms in the RHS bracket of above equation are $\ll 1$. Using these facts one can write leading order terms of the above summation as

$$\sum_{j=0}^{n-1} \frac{\cos\left(\mathcal{A}\left(l + \frac{j}{2al}\right)\right)}{l_j} \simeq \frac{\cos(\mathcal{A}l)}{l} \sum_{j=0}^{n-1} \cos\left(\frac{j}{2al}\right) - \frac{\sin(\mathcal{A}l)}{l} \sum_{j=0}^{n-1} \sin\left(\frac{j}{2al}\right).$$

Now summations on RHS can be easily performed by substituting, $n = 2a l dl$ and using trigonometric relations (see e.g.[12] page 30)

$$\begin{aligned} \sum_{j=0}^{n-1} \frac{\cos\left(\mathcal{A}\left(l + \frac{j}{2al}\right)\right)}{l_j} &\simeq \frac{\cos(\mathcal{A}l)}{l} \cot\left(\frac{\mathcal{A}}{4al}\right) \frac{Adl}{2} + \frac{\sin(\mathcal{A}l)}{l} \frac{Adl}{2} \\ &\simeq \frac{\cos(\mathcal{A}l)}{l} (2al dl) \sum_{k=0}^{\infty} (-1)^k \frac{2^{2k} B_{2k}}{(2k)!} \frac{\mathcal{A}}{4al} + \frac{\sin(\mathcal{A}l)}{l} \frac{Adl}{2} \\ &\simeq \frac{\cos(\mathcal{A}l)}{l} (2al dl) \left[1 - \frac{\mathcal{A}^2}{64a^2 l^2} + O\left(\frac{\mathcal{A}^3}{l^3}\right)\right] + \frac{\sin(\mathcal{A}l)}{l} \frac{Adl}{2} \end{aligned}$$

Here, B_{2k} 's are Bernoulli's numbers. Neglecting terms of order $O(l^{-1})$ and higher as their contribution to summation is negligibly small, we get

$$\sum_{j=0}^{n-1} \frac{\cos\left(A(l + \frac{j}{2al})\right)}{l_j} \simeq \frac{\cos(Al)}{l} 2al dl \quad (5.38)$$

Same measure can be deduced from following simple relation

$$\begin{aligned} \sum_{j=0}^{n-1} \frac{\cos(Al_j)}{l_j} &= \int \frac{\cos(Al)}{l} \sum_{l_j} \delta(l - l_j) dl \\ &= \int \frac{\cos(Al)}{l} 2al dl + \int \frac{\cos(Al)}{l} d_{osc}(l) dl \end{aligned}$$

However it should be noted that 2nd term will have non-trivial contribution unless $\mathcal{A} \ll 1$ as indicated above. This is the reason for which one can not apply similar treatment to periodic orbit sum in density of states(e.g. eq. (5.22)) or for off-diagonal terms as well.

Thus, returning to discussion on correlation function, using above results the leading term in density- density correlation(5.37) becomes

$$\begin{aligned} d_{osc}(r_0 + r_1)d_{osc}(r_0 + r_2) &= \frac{r_0^{1/2}}{\pi^{3/2} A_R^{3/2}} \left\{ \sum_{\alpha} g_{\alpha}^2 A_{\alpha}^2 a_{\alpha} I_{\alpha\beta} \right. \\ &\quad \left. + \sum_{\alpha, \beta} (1 - \delta_{\alpha, \beta}) g_{\alpha} g_{\beta} A_{\alpha} A_{\beta} \sum_{\mu\nu} \delta_{l_{\mu}, l_{\nu}} I_{\mu\nu} \right\} \end{aligned} \quad (5.39)$$

where

$$I_{\alpha} = \int_{l_{\min, \alpha}}^{l_{\max, \alpha}} dl \cos\left(\frac{2\pi l r}{l_H}\right) \quad (5.40)$$

$I_{\mu\nu}$ can be similarly defined and $a_{\mu\nu}$ is appropriately chosen coefficient. In the subsequent analysis this second term will not be shown explicitly, though it will be included in the calculation of a specific example. The choice of a measure enables us to write two-point density correlation as

$$d_{osc}(r_0 + r_1)d_{osc}(r_0 + r_2) = \sum_{\alpha} \kappa_{\alpha} \left[\frac{\sin\left(\frac{2\pi l_{\max, \alpha} r}{l_H}\right)}{\pi r} - \frac{\sin\left(\frac{2\pi l_{\min, \alpha} r}{l_H}\right)}{\pi r} \right] \quad (5.41)$$

where

$$\kappa_{\alpha} = \frac{a_{\alpha} g_{\alpha}^2 A_{\alpha}^2}{\pi A_R} \quad (5.42)$$

and l_H has usual meaning as above. In limit $l_{\max} \rightarrow \infty$ first term in the bracket represents contribution to the self-correlation term (i.e., $\delta(r_1 - r_2)$) of the levels. In writing the two-level cluster function Y_2 we remove this self-correlation singularity as in eq.(5.19). It may be noted that eq.(5.41) indicates that $Y_2(r_1, r_2)$ is just a function of $r = |r_1 - r_2|$. Hence, we write the cluster function as

$$Y_2(r) = \sum_{\alpha} \kappa_{\alpha} \frac{\langle \sin \left(\frac{2\pi l_{\min, \alpha} r}{l_H} \right) \rangle}{\pi r}. \quad (5.43)$$

Here, $\langle \dots \rangle$ denotes spectral averaging as stated earlier.

5.4.4 Taking spectral average

The spectral average refers to all levels in an energy range that is classically small, i.e. small in comparison with r_0 , but large in comparison with the mean level spacing, which is unity in an unfolded spectrum or to be more precise large in comparison with the energy range defined by outer energy scale defined by Berry [10]. The outer energy scale is given by \hbar/T_{\min} , where T_{\min} is the period of the shortest classical closed orbit. It may be noted that each classical orbit with period T causes deviation(\pm) of a level from the mean position by order \hbar/T . Hence, outer energy scale corresponds to the largest deviation of a level from the mean. In terms of number of mean level spacing it is given by $r_{out} = \hbar d_{av}/T_{\min} \sim l_H/2\pi l_{\min}$. In our case this range (say, σ) then roughly becomes $\sqrt{r_0} \ll \sigma \ll r_0$, since $l_H \sim O(\sqrt{r_0})$.

We now consider spectral average of a function $f \left(\mathcal{A}r / \sqrt{r_0} \right)$

$$\left\langle f \left(\frac{\mathcal{A}r}{\sqrt{r_0}} \right) \right\rangle = \frac{1}{\sigma} \int_{-\sigma/2}^{\sigma/2} d\sigma' f \left(\frac{\mathcal{A}r}{\sqrt{r_0 + \sigma'}} \right).$$

Since $\sigma' \ll r_0$ we can approximate this as

$$\left\langle f \left(\frac{\mathcal{A}r}{\sqrt{r_0}} \right) \right\rangle = \frac{1}{\sigma} \int_{-\sigma/2}^{\sigma/2} d\sigma' f \left(\frac{\mathcal{A}r}{\sqrt{r_0}} \left(1 - \frac{\sigma'}{2r_0} \right) \right).$$

Expanding f in the Taylor series as

$$\begin{aligned} f \left(\frac{\mathcal{A}r}{\sqrt{r_0}} \left(1 - \frac{\sigma'}{2r_0} \right) \right) &= f \left(\frac{\mathcal{A}r}{\sqrt{r_0}} - \frac{\mathcal{A}^2 r^2}{2r_0^2} \right) - \frac{\mathcal{A}r}{2r_0^{3/2}} f' \left(\frac{\mathcal{A}r}{\sqrt{r_0}} - \frac{\mathcal{A}^2 r^2}{2r_0^2} \right) \\ &\quad \left(\sigma' - \frac{\mathcal{A}r}{\sqrt{r_0}} \right) + \dots \end{aligned}$$

If $\mathcal{A}r \ll \sqrt{r_0}$ we can approximate spectral average as

$$\left\langle f\left(\frac{\mathcal{A}r}{\sqrt{r_0}}\right)\right\rangle = \frac{1}{\sigma} \int_{-\sigma/2}^{\sigma/2} d\sigma' \left\{ f\left(\frac{\mathcal{A}r}{\sqrt{r_0}}\right) - f'\left(\frac{\mathcal{A}r}{\sqrt{r_0}}\right) \left(\frac{\mathcal{A}r\sigma'}{2r_0^{3/2}} - \frac{\mathcal{A}^2r^2}{2r_0^2}\right) + \dots \right\}.$$

Which can be easily evaluated and we get

$$\left\langle f\left(\frac{\mathcal{A}r}{\sqrt{r_0}}\right)\right\rangle \sim f\left(\frac{\mathcal{A}r}{\sqrt{r_0}}\right) + f'\left(\frac{\mathcal{A}r}{\sqrt{r_0}}\right) \frac{\mathcal{A}^2r^2}{2r_0^2} + f''\left(\frac{\mathcal{A}r}{\sqrt{r_0}}\right) \frac{\mathcal{A}^2r^2\sigma'^2}{3!2^3r_0^3} + \dots$$

It is thus obvious that second and higher order terms can be neglected (since, $\sigma \ll r_0$) if f' and higher derivatives are also small. We will encounter here trigonometric functions (e.g. sin, cos and sin integrals) only.

Thus after spectral averaging the two-level cluster function becomes

$$Y_2(r) \simeq \sum_{\alpha} \kappa_{\alpha} \frac{\sin\left(\frac{2\pi l_{\min,\alpha} r}{l_H}\right)}{\pi r} \quad (5.44)$$

As per convention negative sign of $Y_2(r)$ represents positive correlation and vice versa. For the finite spectrum occurring between r_{\max} and r_{\min} two-level cluster function is given by[13, 14]

$$Y_2(r) = \delta(r) - \frac{1}{\Delta r} \int_{r_{\min}}^{r_{\max}} dr_0 \langle d_{osc}(r_0 + r_1) d_{osc}(r_0 + r_2) \rangle \quad (5.45)$$

where $\Delta r = r_{\max} - r_{\min}$. Note, that we have used here a simple box function as a window function defined in [14] which takes care of the finite number of levels and should not be misunderstood as double averaging. Using eq.(5.44), $Y_2(r)$ becomes

$$Y_2(r) \simeq \sum_{\alpha} \kappa_{\alpha} \frac{1}{\pi r \Delta r} \int_{r_{\min}}^{r_{\max}} dr_0 \sin\left(\frac{2l_{\min,\alpha} r}{l_H}\right) \quad (5.46)$$

Integration in (5.46) is thus easy to carry out and $Y_2(r)$ can then be

written in simple analytical form as

$$\begin{aligned}
Y_2(r) = & \sum_{\alpha} \frac{\kappa_{\alpha}}{\pi \Delta r} \left\{ r_{\max} \left[\frac{\sin\left(\frac{2\pi l_{\min,\alpha} r}{l_H}\right)}{r} + \frac{2\pi l_{\min,\alpha}}{l_{H,\max}} \cos\left(\frac{2\pi l_{\min,\alpha} r}{l_{H,\max}}\right) + \frac{4\pi^2 l_{\min,\alpha}^2 r}{l_{H,\max}^2} \text{si}\left(\frac{2\pi l_{\min,\alpha} r}{l_{H,\max}}\right) \right] \right. \\
& \left. - r_{\min} \left[\frac{\sin\left(\frac{2\pi l_{\min,\alpha} r}{l_H}\right)}{r} + \frac{2\pi l_{\min,\alpha}}{l_{H,\min}} \cos\left(\frac{2\pi l_{\min,\alpha} r}{l_{H,\min}}\right) + \frac{4\pi^2 l_{\min,\alpha}^2 r}{l_{H,\min}^2} \text{si}\left(\frac{2\pi l_{\min,\alpha} r}{l_{H,\min}}\right) \right] \right\} \quad (5.47)
\end{aligned}$$

where, recall that κ_{α} is $A_{\alpha}^2 g_{\alpha}^2 a_{\alpha} / \pi A_R$, $l_{H,\max(\min)}$ is $\sqrt{4\pi A_R r_{\max(\min)}}$ and $\text{si}(x)$ is sine integral $-\int_x^{\infty} dt \sin(t)/t$.

Apart from dependence on the energy window (r_{\min}, r_{\max}) selected, one can see that $Y_2(r)$ depends on two parameters (1) $l_{\min,\alpha}$, shortest periodic orbits in each class α (we will call it length parameters) and (2) κ_{α} , which is a measure of phase space area occupied by bands of periodic orbits in class α . Without referring to any system, it is interesting to study how these parameters affect the behaviour of $Y_2(r)$. Fig. 5.1 shows effect of variation in length parameters where we have considered three classes of periodic orbits with same value of parameter κ and energy window. The length parameters are, for curve a) 10,20,30, b)10,20,40, c)10,20,50, d)10,20,70. The κ 's are same for all classes and curves: .3333 .3333 .3333. Number of levels considered are 100-1000. Curve (g) is for G.O.E. As one increases highest length parameter one gets more and more level repulsion. This indicates that the presence of relatively longer periodic orbits will result in level repulsion in the quantum spectrum. In Fig. 5.2 we show effect of variation of parameters κ for same values of length parameters. The κ parameters are, for curve a) .6,.2,.2, b).2,.6,.2, c).2,.2,.6, d).1,.1,.8. The "lengths" are same for all classes and curves:10,20,30. Number of levels considered are 100-1000. One can see here that as weightage κ increases for the longer length parameters, $Y_2(r)$ deviates from Poissonian (i.e. $Y_2(r) = 0$) showing more and more negative correlations or level repulsion. As far as the effect of energy window is concerned we can see from above equation that as $r_{\max} \rightarrow \infty$ and $r_{\min} \ll r_{\max}$ so that $\Delta r \sim r_{\max}$, $Y_2(r) \sim \max_{\alpha} (4\pi l_{\min,\alpha} / \sqrt{r_{\max}})$, hence approaches a Poissonian as $r_{\max} \rightarrow \infty$ in the diagonal approximation. Rate of approach is to Poissonian is basically governed by $1/\sqrt{r_{\max}}$. It may be noted that $\max_{\alpha}(l_{\min,\alpha})$ is also important parameter since it will decide when one would expect Poisson like results. For example in the case of $\pi/3$ -rhombus billiard (pure rhombus modes) $\max_{\alpha}(l_{\min,\alpha}) = 2\sqrt{93}\mathcal{L}$, (\mathcal{L} being side length of the

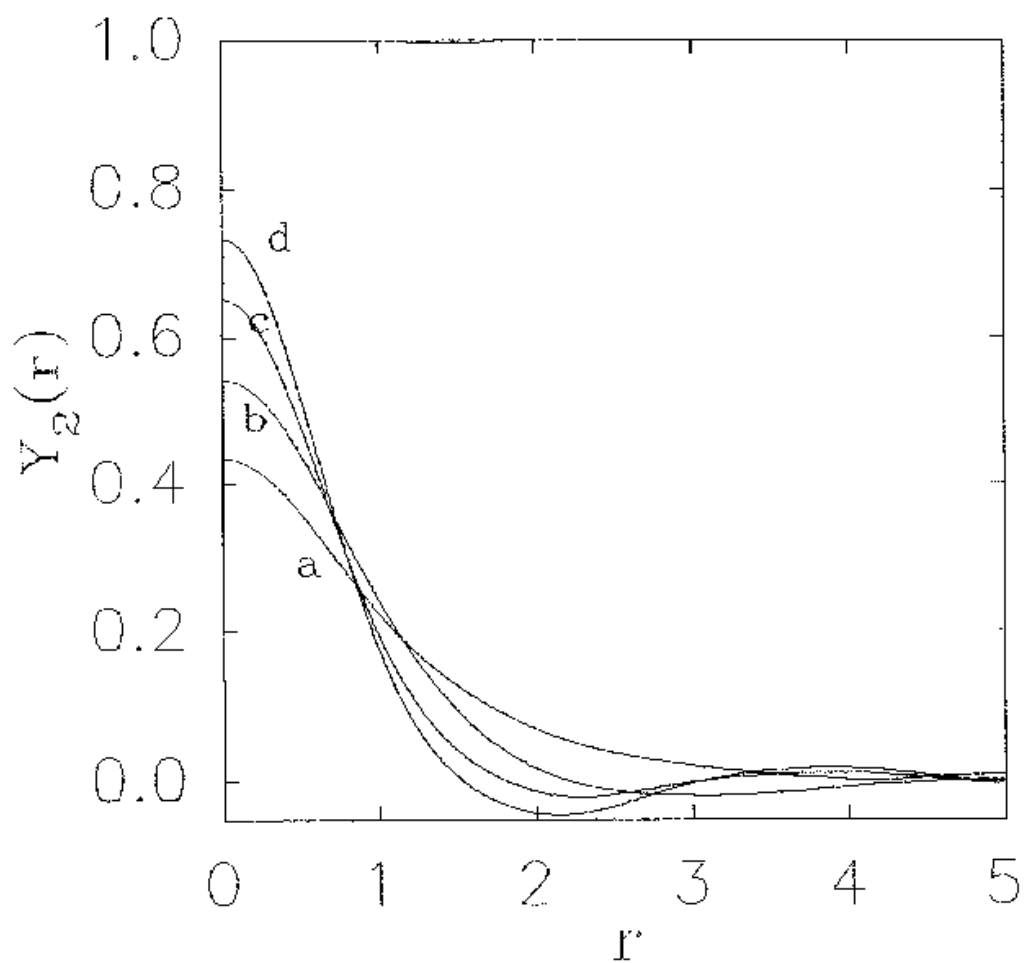


Figure 5.1: Two level cluster function: effect of variation in length parameters (see text)

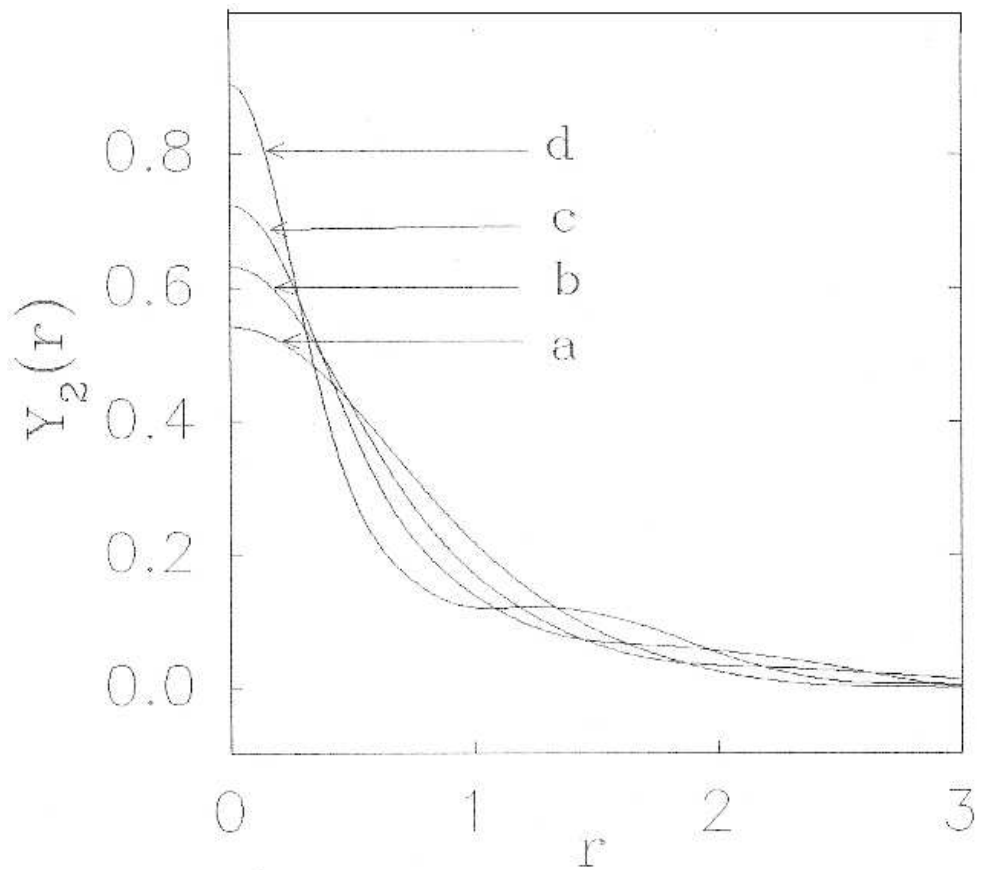


Figure 5.2: Two level cluster function: effect of variation of parameters κ (see text)

billiard), hence to see real asymptotic behaviour one should consider number of levels must be at least a order of magnitude larger than 1600 levels. Unfortunately there exist few numerical results in this range. Most of the numerical experiments can therefore be termed as sub-asymptotic. In such cases as mentioned above off-diagonal contributions may be significant. Any comparison of our results with numerical experiments should be made by keeping this discussion in mind.

We now consider two-point cluster function for $\pi/3$ -rhombus billiard. We reproduce relevant information in table 5.1 and 5.2. In Fig. 5.3 we show Y_2 for complete $\pi/3$ -rhombus billiard, including both even and odd states that corresponds to two pure rhombus modes and two equilateral triangle modes. In Fig 5.4 we consider two pure rhombus modes combinedly (i.e. even states). Effect of number of levels considered is shown via curves a)represents energy window (47, 370) b)(420, 740) c)(47, 743) and d)(1000, 2000). It is evident from these figures that even states are more ‘‘away’’ from the Poissonian than the complete rhombus case. This is obvious due to fact that complete rhombus billiard spectrum is superposition of spectrums of four modes described above. One can also see that as we increase number of levels Y_2 approach Poissonian. Since spectral measures we consider here directly depend on Y_2 we expect similar trend in case of these measures.

5.5 The Form Factor

In this section we will consider one of the interesting quantity, the Fourier transform of two-level cluster function, known as the Form Factor [2]. It is well known that the Fourier transform of the density of states gives important information about classical behaviour of the system, i.e. it generates periodic orbit length spectrum of the classical system. Similarly the form factor yields important information about periodic orbit structure in the classical system. Before we elaborate this point, let us derive a semi-classical expression for the form factor. We will use definition of [13] to derive expression for the form factor

$$b_2(\tau) = -2 \int_0^\infty dr Y_2(r) \cos(2\pi r\tau) \quad (5.48)$$

where τ is a dimensionless time, related to t by

$$\tau = \frac{t}{t_H} \quad t_H = 2\pi\hbar d_{av}.$$

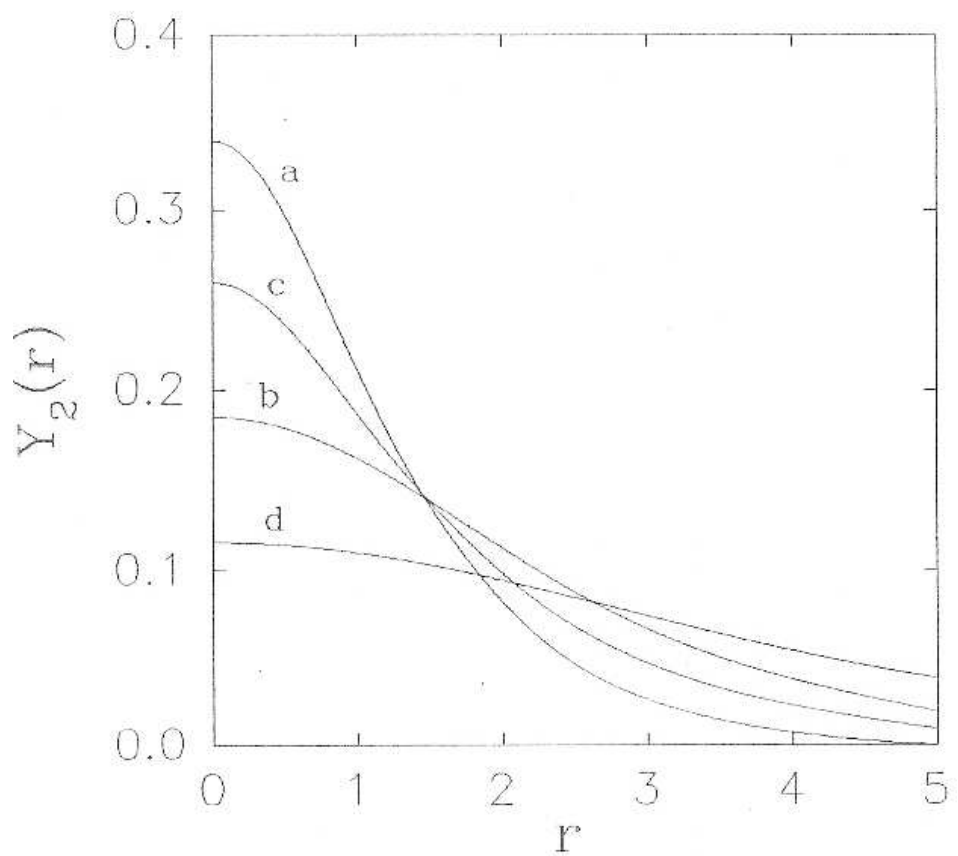


Figure 5.3: Two level cluster function: for complete $\pi/3$ -rhombus billiard (see text)

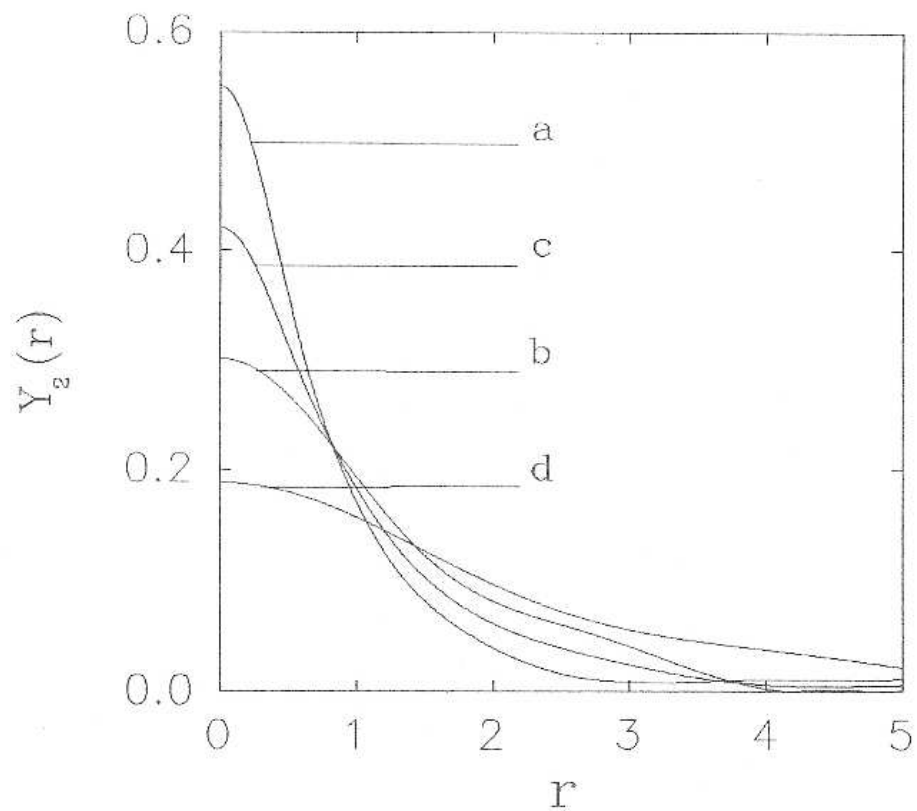


Figure 5.4: Two level cluster function: for $\pi/3$ -rhombus billiard pure rhombus modes(see text)

Using (5.47) the semi-classical expression for the form factor is given by (since only finite numbers of levels are considered, we will integrate above equation from $r = 0$ to $b_\infty = \Delta r/2$, this will not change our results since $Y_2(r) \sim 0$ for large r)

$$\begin{aligned}
b_2(\tau) = & -\sum_{\alpha} \kappa_{\alpha} \left\{ \frac{r_{\max}}{\pi \Delta r} \left[\left(1 - \frac{\gamma_{\alpha, \max}^2}{4\pi^2 \tau^2} \right) [\text{Si}((\gamma_{\alpha, \max} - 2\pi\tau) b_\infty) + \text{Si}((\gamma_{\alpha, \max} + 2\pi\tau) b_\infty)] \right. \right. \\
& + \frac{\gamma_{\alpha, \max}}{\pi\tau} \sin(2\pi\tau b_\infty) \cos(\gamma_{\alpha, \max} b_\infty) \\
& \left. \left. + \frac{\gamma_{\alpha, \max}^2}{\pi\tau} \text{si}(\gamma_{\alpha, \max} b_\infty) \left[b_\infty \sin(2\pi\tau b_\infty) + \frac{\cos(2\pi\tau b_\infty)}{2\pi\tau} \right] + \frac{\gamma_{\alpha, \max}^2}{4\pi\tau^2} \right] \right. \\
& - \frac{r_{\min}}{\pi \Delta r} \left[\left(1 - \frac{\gamma_{\alpha, \min}^2}{4\pi^2 \tau^2} \right) [\text{Si}((\gamma_{\alpha, \min} - 2\pi\tau) b_\infty) + \text{Si}((\gamma_{\alpha, \min} + 2\pi\tau) b_\infty)] \right. \\
& + \frac{\gamma_{\alpha, \min}}{\pi\tau} \sin(2\pi\tau b_\infty) \cos(\gamma_{\alpha, \min} b_\infty) \\
& \left. \left. + \frac{\gamma_{\alpha, \min}^2}{\pi\tau} \text{si}(\gamma_{\alpha, \min} b_\infty) \left[b_\infty \sin(2\pi\tau b_\infty) + \frac{\cos(2\pi\tau b_\infty)}{2\pi\tau} \right] + \frac{\gamma_{\alpha, \min}^2}{4\pi\tau^2} \right] \right\} \quad (5.49)
\end{aligned}$$

where $\gamma_{\alpha, \max(\min)} = 2\pi l_{\alpha, \min}/l_{H, \max(\min)}$. As b_∞ becomes large enough, then we can approximate sine integrals as follows,

$$\text{Si}(\pm x) \simeq \pm \frac{\pi}{2} \mp \frac{\cos(x)}{x}, \quad \text{si}(x) \simeq -\frac{\cos(x)}{x}. \quad (5.50)$$

Substituting above relations in (5.49) we get, for $\tau < \min_{\alpha}(\gamma_{\alpha, \max}/2\pi)$

$$b_2(\tau) = -\sum_{\alpha} \kappa_{\alpha} - \sum_{\alpha} \kappa_{\alpha} \left\{ \frac{r_{\max} \sin(\gamma_{\alpha, \max} b_\infty) - r_{\min} \sin(\gamma_{\alpha, \min} b_\infty)}{\pi \Delta r} \right\} \frac{\sin(2\pi\tau b_\infty)}{\pi\tau b_\infty}. \quad (5.51)$$

And for $\tau \gg \max_{\alpha}(\gamma_{\alpha, \max}/2\pi)$

$$b_2(\tau) = -\sum_{\alpha} \kappa_{\alpha} \left\{ \frac{r_{\max} \cos(\gamma_{\alpha, \max} b_\infty) - r_{\min} \cos(\gamma_{\alpha, \min} b_\infty)}{\pi \Delta r} \right\} \frac{\cos(2\pi\tau b_\infty)}{\pi\tau b_\infty} + O\left(\frac{1}{\tau^2}\right). \quad (5.52)$$

Various important properties of the form factor has been discussed in [13, 14, 15]. We bring out some new (not reported so far) features of the form factor. In general, form factor $b_2(\tau)$ saturates to 0 for $\tau \gg 1$ due to discrete nature of the spectrum. For $\tau \ll 1$, $b_2(\tau) \rightarrow -1$. In case of chaotic systems

diagonal approximation leads to monotonically increasing ($\sim \tau$) form factor. The contribution of the off-diagonal terms however cancels this rise to restore correct asymptotic behaviour of the form factor [15].

From (5.49) one can see that there will be a spike at $\tau = 0$, due to $\sin(2\pi\tau b)/\pi\tau b$ (which is $\sim \delta(\tau)$) factor on RHS. For $0 < \tau < \min_\alpha(\gamma_{\alpha,\min}/2\pi)$, $b_2(\tau)$ will be -1 since contribution of the same factor becomes negligible and $\sum_\alpha \kappa_\alpha = 1$. It should be noted that above expressions for $b_2(\tau)$ have independent contributions from the classes of periodic orbits in the diagonal approximation. The classes of the periodic orbits are characterized by length of shortest periodic orbits ($l_{\min,\alpha}$) that can be arranged in increasing order. For $\tau \sim \min_\alpha(\gamma_{\alpha,\min}/2\pi)$, corresponding contribution from that family will decrease (in absolute sense) and saturating ultimately to 0 as τ becomes greater than $\gamma_{\alpha,\min}/2\pi$, resulting in net increase in the form factor. If lengths of shortest periodic orbits in different classes are well separated then τ may still be less than next ($\gamma_{\alpha,\min}/2\pi$), the form factor will saturate at $-\sum_{\alpha'} \kappa_\alpha > -1$, where summation is now taken over all classes except one (i.e. α). This thus leads to a "step" like structure in the plots of the form factor. If however, lengths of the shortest periodic orbits are not well separated steps may merge into each other. The step structure is thus a hallmark of existence of multiple, distinct "characteristic time scales" (hence also length scales) in these systems.

In fig. 5.5 and 5.6 we study effect of variations in the length parameters and κ 's on the form factor. Again here choice of various parameters is same as that in case of the two-point cluster function. Though general conclusions that can be drawn are similar to that discussed in the previous section, i.e., the existence of larger length parameters or more weightage (via. κ parameters) to higher length parameters shows deviation away from Poissonian behaviour. Most important feature is imprints of classes of periodic orbits. We have considered three classes for all the cases and the form factor rises to zero in the same number of "steps". Existence of steps in the form factor are thus signatures of the classes of bands of marginally stable periodic orbits in the classical system. This feature is apparent in the plots of the form factor in some of the works [13, 14] where systems, not far away from the integrability, like kicked rotor or domino billiards are considered and in the examples that we will consider in this paper. We wish to draw attention of readers to the fact that the form factor saturates at 0 in long τ limit and does not rise monotonically as in case of chaotic system in the diagonal approximation used above. This in turns implies that off-diagonal corrections

may not be considerable as far as the form factor is concerned. As our study indicates the off-diagonal contributions may only affect the form factor in the transition region where it rises from -1 to 0 . Effect of the off-diagonal terms on step like behaviour is difficult to guess. Recent approach([16]) to treat off-diagonal terms in terms of diagonal contribution however, indicates that step like behaviour may be preserved even after consideration of off-diagonal contributions. Secondly, since diagonal form factor saturates at 0 as expected, off-diagonal terms may only change the transition region most likely flattening it.

Our analysis thus brings out a important feature of the form factor that has not been paid attention so far. With increasing energy, rise in these steps become sharper and sharper taking the form factor closer the Poissonian one. Also if differences in the length parameters are small, this step structure may not be easily visible. This is evident from Fig. 5.7 and Fig. 5.8 where we plot form factor for complete rhombus and for even states respectively. Difference between two cases is self evident, rise is sharper in the former case than the later case.

In this chapter we have obtained closed analytical expressions for two interesting quantities that are used to study spectral fluctuation properties using diagonal approximations. This is an important step which should ultimately lead to complete understanding of spectral fluctuations by including other contributions such as off-diagonal terms, diffraction effects etc.

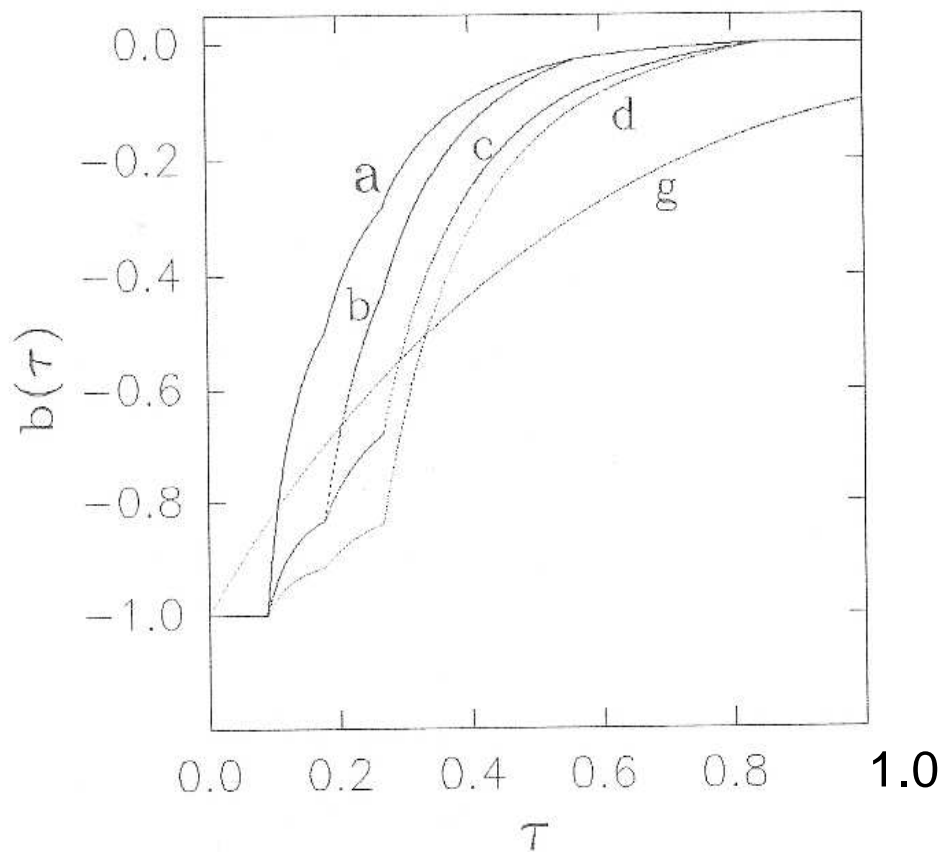


Figure 5.5: The form factor: Effect of variation of the length parameters (see text)

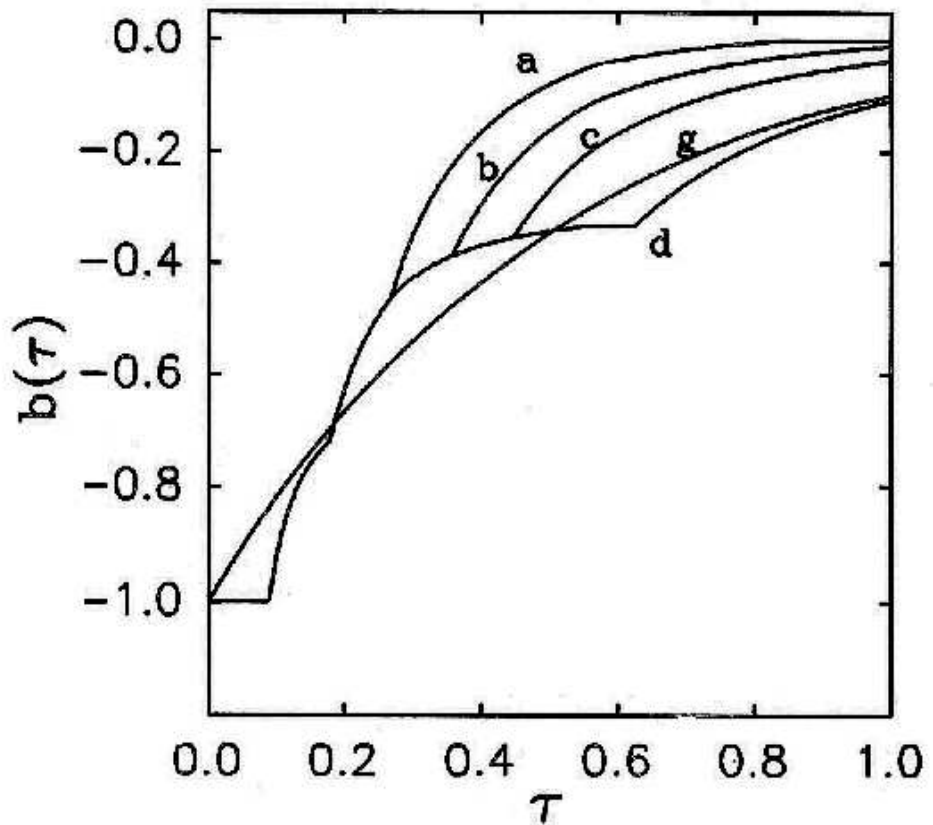


Figure 5.6: The form factor: Effect of variation of the κ parameters (see text)

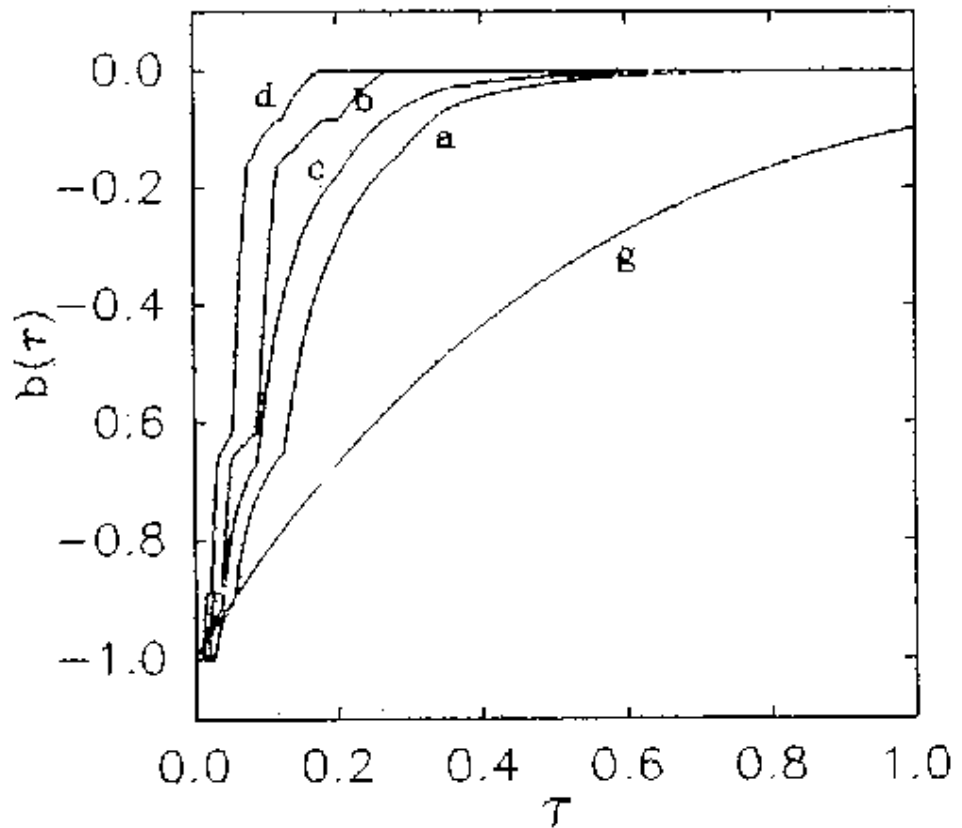


Figure 5.7: The form factor: For complete $\pi/3$ - rhombus billiard (see text)

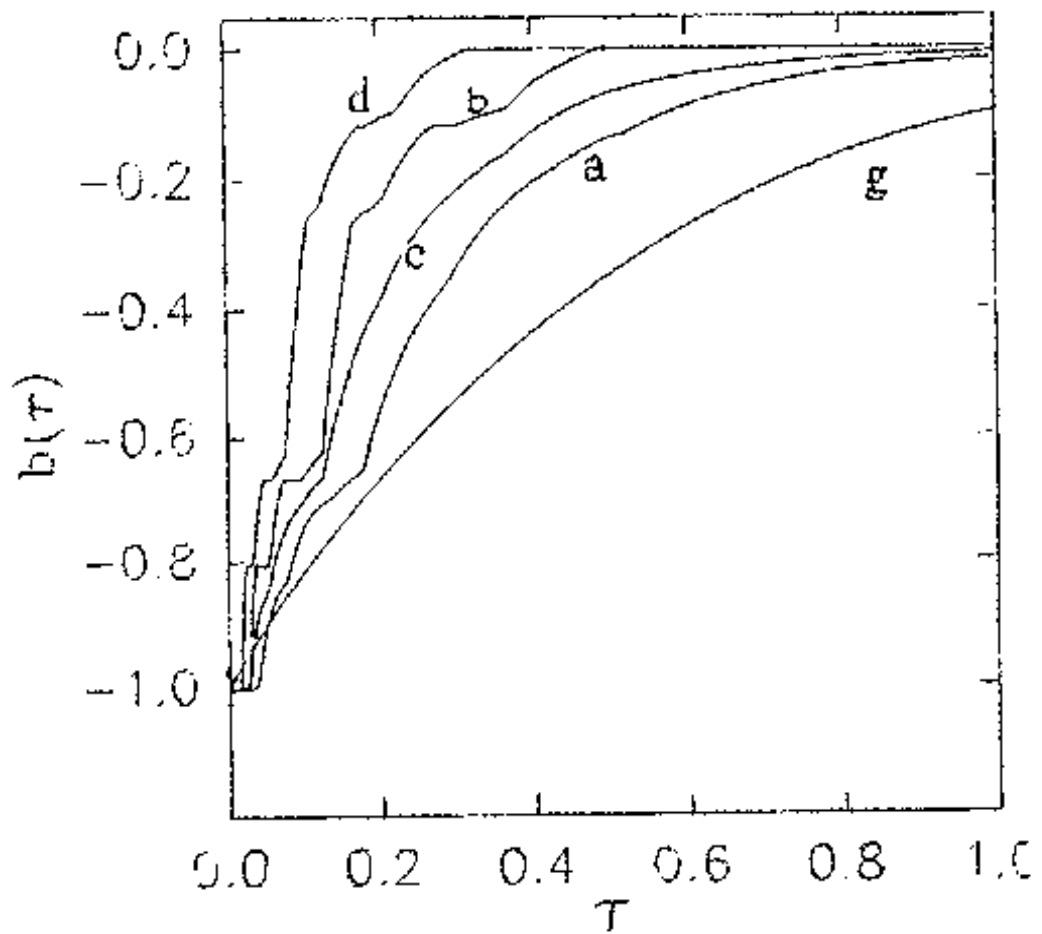


Figure 5.8: The form factor: For pure modes of $\pi/3$ - rhombus billiard (see text)

Type	Class	Closing Point	Band Area	κ_α	l_{min}
centre-centre	odd-odd	$(q/2, p/2)$	A_R	$\frac{1}{9}$	$\sqrt{3}\mathcal{L}$
		(q, p)	$2A_R$	$\frac{2}{9}$	$2\sqrt{3}\mathcal{L}$
	odd-even	(q, p)	A_R	$\frac{1}{36}$	$\sqrt{21}\mathcal{L}$
		$(2q, 2p)$	$2A_R$	$\frac{1}{18}$	$2\sqrt{21}\mathcal{L}$
	even-odd	(q, p)	A_R	$\frac{1}{36}$	$\sqrt{39}\mathcal{L}$
		$(2q, 2p)$	$2A_R$	$\frac{1}{18}$	$2\sqrt{39}\mathcal{L}$
centre-edge	odd-odd	$(3q/2, 3p/2)$	$3A_R$	$\frac{1}{3}$	$3\sqrt{37}\mathcal{L}$
	odd-even	$(3q, 3p)$	$3A_R$	$\frac{1}{12}$	$3\sqrt{7}\mathcal{L}$
	even-odd	$(3q, 3p)$	$3A_R$	$\frac{1}{12}$	$3\sqrt{7}\mathcal{L}$

Table 5.1: Summary of results for complete $\pi/3$ -rhombus billiard.

Type	Class	Closing Point	Band Area	Repetitions	κ_α	l_{min}
centre-centre	odd-odd	$(q/2, p/2)$	$4A_R$	all	$\frac{8}{18}$	$\sqrt{3}\mathcal{L}$
			$8A_R$	even	$\frac{5}{36}$	$2\sqrt{3}\mathcal{L}$
			$8A_R$	odd	$-\frac{1}{4}$	$\sqrt{3}\mathcal{L}$
centre-centre	odd-even	(q, p)	$4A_R$	all	$\frac{2}{18}$	$\sqrt{93}\mathcal{L}$
			$8A_R$	even	$\frac{5}{144}$	$2\sqrt{93}\mathcal{L}$
			$8A_R$	odd	$-\frac{1}{16}$	$\sqrt{93}\mathcal{L}$
centre-centre	odd-even	(q, p)	$4A_R$	all	$\frac{2}{18}$	$\sqrt{39}\mathcal{L}$
			$8A_R$	even	$\frac{5}{144}$	$2\sqrt{39}\mathcal{L}$
			$8A_R$	odd	$-\frac{1}{16}$	$\sqrt{39}\mathcal{L}$
centre-edge	odd-odd	$(3q/2, 3p/2)$	$12A_R$	all	$\frac{1}{3}$	$3\sqrt{37}\mathcal{L}$
	odd-even	$(3q, 3p)$	$12A_R$	all	$\frac{1}{12}$	$3\sqrt{61}\mathcal{L}$
	even-odd	$(3q, 3p)$	$12A_R$	all	$\frac{1}{12}$	$3\sqrt{19}\mathcal{L}$

Table 5.2: Summary of results for $\pi/3$ -rhombus billiard: Only Pure Rhombus Modes. Here A_R is area of V , half equilateral triangle.

Bibliography

- [1] F.J.Dyson, J.Math.Phys., **3**, (1962) 140; 157; 166.
- [2] M. L. Mehta, Random Matrices, Academic, New York (1991).
- [3] F. Haake, Quantum Signatures of Chaos, Springer-Verlag, Berlin (1991).
- [4] P. J. Richens and M. V. Berry, Physica **D2**, 495 (1981).
- [5] M.Tinkham, Group Theory and Quantum Mechanics, McGraw-Hill, New York,1964.
- [6] J. M. Robbins, Phys. Rev. A, **40**, 2128(1989).
- [7] D. Biswas and S. R. Jain, Phys. Rev. **A42**, 3170 (1990).
- [8] S. R. Jain and H. D. Parab, J. Phys. **A25**, 6669 (1992).
- [9] E. Gutkin, Physica **19D** 311(1986)
- [10] M. V. Berry, Proc. Roy. Soc. London **A400**, 229 (1985).
- [11] J. H. Hannay and A. M. Ozorio de Almeida, J. Phys. **A17**, 3429 (1984).
- [12] I.S. Gradshteyn, I.M. Ryzhik, Table of Integrals, Series and products, Academic Press Inc. , New York (1980).
- [13] T. Dittrich, E. Doron, U. Smilansky ,J. Phys. **A27** 79(1994).
- [14] T. Dittrich, Phys. Reports **271** 267(1996).
- [15] D. Cohen, H. Primack, U. Smilansky, Annals of Phys. **264**, 108(1998).
- [16] E.B. Bogomolny, J.P. Keating, Phys. Rev. Lett. **77** 1472(1996).

Chapter 6

Short and Intermediate Range Spectral Fluctuation Measures

6.1 Introduction

We shall obtain expressions for three important and popular spectral fluctuation measures namely spacing distribution, number variance and spectral rigidity using diagonal approximation for pseudo-integrable billiards. Spacing distribution provides information about spectral fluctuations on short energy scale i.e. on the scale of mean level spacing. Other two measures are called as intermediate range spectral measures since they provide information about fluctuations on few mean level spacing. In this chapter

6.2 Nearest Neighbour Spacing Distribution

Nearest neighbour spacing (NNS) distribution is *the probability density $P(S)$ of finding the nearest neighbour of a given level at r , in the range $r + S$ to $r + S + dS$* . As stated above $P(S)$ distribution of any given system enables us to study fine scale texture (i.e., on the scale of mean level spacing) of the spectrum.

For Integrable systems spacing distribution is very well modeled by Poisson distribution ($P(S) = \exp(-S)$) since the energy levels are random due to number theoretic properties. On the other hand in case of chaotic systems with time reversal symmetry (modeled by GOE of random matrix the-

ory(RMT)) spacing distribution is given by the Wigner distribution function.

$$P(S) = \frac{\pi}{2} S \exp\left(-\frac{\pi S^2}{4}\right), \quad (6.1)$$

provided the level sequence has been normalized to unit mean level spacing. RMT is expected to be applicable only on those time scales where the variables associated with the classical dynamics are random enough, to fully randomize the matrices, associated with the corresponding quantum operators. Moreover, due to underlying assumptions on which framework of RMT is build, it is not expected to shed any light on non-universal behaviour of spectral fluctuations which is the characteristic of a given system.

Various formulas have been proposed to analyse $P(S)$ distribution for the systems in the intermediate regime [1, 2, 3]. However, these models are not applicable for the pseudointegrable systems because of basic differences with other mixed systems.

The aim of this section is to develop a model for $P(S)$ distribution in pseudointegrable systems. Once such model is developed it can be extended to more general class of mixed system where almost regular and almost chaotic states coexist. When the spectrum is unfolded to unit mean spacing of neighbouring levels everywhere, one can use probabilistic arguments e.g.[4, 5] to develop expression for $P(S)$ distribution.

The conditional probability $g(S)dS$ of finding a level in the interval $(r + S, r + S + dS)$, given one at r is related to $P(S)$ in the following way. Choose a segment of length λ (integer), and divide it into small intervals, all of the same length ε . We place λ markers at random, independently of one another, with the probability $g(S)dS$, into the small intervals. The first marker above 0 will hit any particular small interval with probability $\varepsilon g(\xi)/\lambda$, and miss any other small interval with probability $1 - \varepsilon g(\xi)/\lambda$, where ξ is some coordinate inside the small interval in question. Now we choose a contiguous interval of length S , and require the probability that none of the markers fall within S , while there is a marker in interval $(r + S, r + S + dS)$. We have to form the product of all the $1 - \varepsilon g(\xi)/\lambda$ for $0 < \xi < S$, and multiply with $\varepsilon g(S)/\lambda$. In the limit of small ε or large λ we find that

$$P(S) = \mathcal{C} g(S) \exp\left(-\int_0^S dS' g(S')\right), \quad (6.2)$$

\mathcal{C} on RHS is used so as to satisfy condition $\int_0^\infty P(S) = 1$. Underlying assumptions in deriving this relation are: 1) Given a level at r , the probability that

another level will be around $r + S$ is proportional to S and does not depend on r . This assumption though applied for all S , is valid only for small S . In other words, this assumption means (1) the two point correlation function $R_2(r_1, r_2)$ is linear in $|r_1 - r_2|$ and (2) the probabilities in various intervals of length S/m obtained by dividing S into m equal parts are mutually independent. In other words three-point and higher correlations are negligibly small. Though both of these the assumptions are inaccurate, above relation gives accurate result for GOE of random matrix in terms of Wigner surmise, which indicates that errors arising due to these assumption almost cancel each other [6]. It is, therefore reasonable to expect that above relation would yield good approximation to $P(S)$ distribution in pseudointegrable billiards as for such systems levels are expected to be less correlated than that in the chaotic systems. Strictly speaking, $P(S)$ depends not only on two-point correlations but on higher correlations too [6, 7].

In case of homogeneous spectrum (i.e. density of states almost independent of energy), unfolded spectrum with unit mean spacing everywhere conditional probability density $g(S)$ is nothing but the two-point correlation function, or $g(S) = 1 - Y_2(S)$ [4, 8]. In terms of this the $P(S)$ distribution can be written as

$$P(S) = \mathcal{C} e^{-S} (1 - Y_2(S)) e^{\int_0^S Y_2(S') dS'} \quad (6.3)$$

In our case $\mathcal{C} = 1$. Using expression for $Y_2(S)$ derived in the last chapter and carrying out necessary algebra one can write NNS distribution for pseudointegrable billiards as

$$P(S) = \mathcal{A}(S) \exp(\mathcal{B}(S) - S) \quad (6.4)$$

where $\mathcal{A}(S) = 1 - Y_2(S)$. And

$$\begin{aligned} \mathcal{B}(S) = & \sum \kappa_\alpha \left\{ \frac{r_{\max}}{\pi \Delta r} \left[\text{Si}(\gamma_{\alpha,\max} S) + \frac{\sin(\gamma_{\alpha,\max} S)}{2} + \frac{\gamma_{\alpha,\max} S}{2} \cos(\gamma_{\alpha,\max} S) \right. \right. \\ & \left. \left. - \frac{\gamma_{\alpha,\max}^2 S^2}{2} \text{si}(\gamma_{\alpha,\max} S) \right] \right. \\ & \left. - \frac{r_{\min}}{\pi \Delta r} \left[\text{Si}(\gamma_{\alpha,\min} S) + \frac{\sin(\gamma_{\alpha,\min} S)}{2} + \frac{\gamma_{\alpha,\min} S}{2} \cos(\gamma_{\alpha,\min} S) \right. \right. \\ & \left. \left. + \frac{\gamma_{\alpha,\min}^2 S^2}{2} \text{si}(\gamma_{\alpha,\min} S) \right] \right\} \end{aligned} \quad (6.5)$$

where $\text{Si}(x) = \pi/2 + \text{si}(x)$ and $\gamma_{\alpha,\min(\max)} = 2\pi l_{\alpha,\min}/l_{H,\min(\max)}$. The expression for $P(S)$ is clearly normalized. For small S , neglecting terms of order $O(S^2)$ and higher, one obtains

$$\begin{aligned}
\mathcal{A}(S) \simeq \mathcal{A}s &= -\sum_{\alpha} \kappa_{\alpha} \frac{2l_{\min,\alpha}}{\sqrt{\pi A_R \Delta r}} \left[\sqrt{r_{\max}} - \sqrt{r_{\min}} \right] \\
\mathcal{B}(S) = \mathcal{B} &= \sum_{\alpha} \kappa_{\alpha} \frac{l_{\min,\alpha}}{\sqrt{\pi A_R \Delta r}} \left[\sqrt{r_{\max}} - \sqrt{r_{\min}} \right] S \\
&= S - \mathcal{A}S \\
&\text{thus} \\
P(S) &\simeq \mathcal{A} \exp[-\mathcal{A}S]
\end{aligned} \tag{6.6}$$

Therefore $dP(S)/dS|_{S=0} = -\mathcal{A}^2 \leq 0$, showing level attraction near $S = 0$, which is weaker than that of a Poissonian distribution for a finite number of levels but approaches the same in the semi-classical limit. For large S again our expression approaches Poissonian distribution. To see this behaviour clearly we study from (6.4), dependence of $P(S)$ on length parameters and parameters κ 's. we will consider only three classes of the periodic orbits. Fig.6.1 shows the effect of variations in the length parameters and Fig.6.2 shows the same for κ_{α} 's, parameters chosen are same as that in case of two-point cluster function. Again conclusions that can be drawn from these figures are similar to that stated in the previous chapter. In the high energy limit, again $P(S)$ distribution converges to a Poissonian distribution. For finite energy levels however, $P(S)$ distribution shows mixed behaviour of weaker level attraction as well as level repulsion with respect to Poissonian and GOE respectively, for different values of S . Note, a closeness of curve (d) in Fig. 6.1 to GOE for $S < 1$, though curve do not rise as much as that of GOE one may easily misunderstood it as showing GOE kind of behaviour.

In Fig. 6.3 and 6.4 we show plots of $P(S)$ distribution for complete rhombus and even states of the rhombus. $P(S)$ for complete rhombus approaches comparatively faster to Poisson distribution reasons are obvious as it is a superposition of four different modes. In Fig. 6.4 for curve (a) we choose levels $r_{\min} = 47$ and $r_{\max} = 370$, to compare our results with that of numerical results of [11] for approximately same number of levels. As stated earlier our results are in good agreement with numerical results for $S < 1$. This can be more clearly seen from Fig. 6.5 where we show cumulative $P(S)$ distribution. The curve (a) in this figure is our results and numerical results are shown

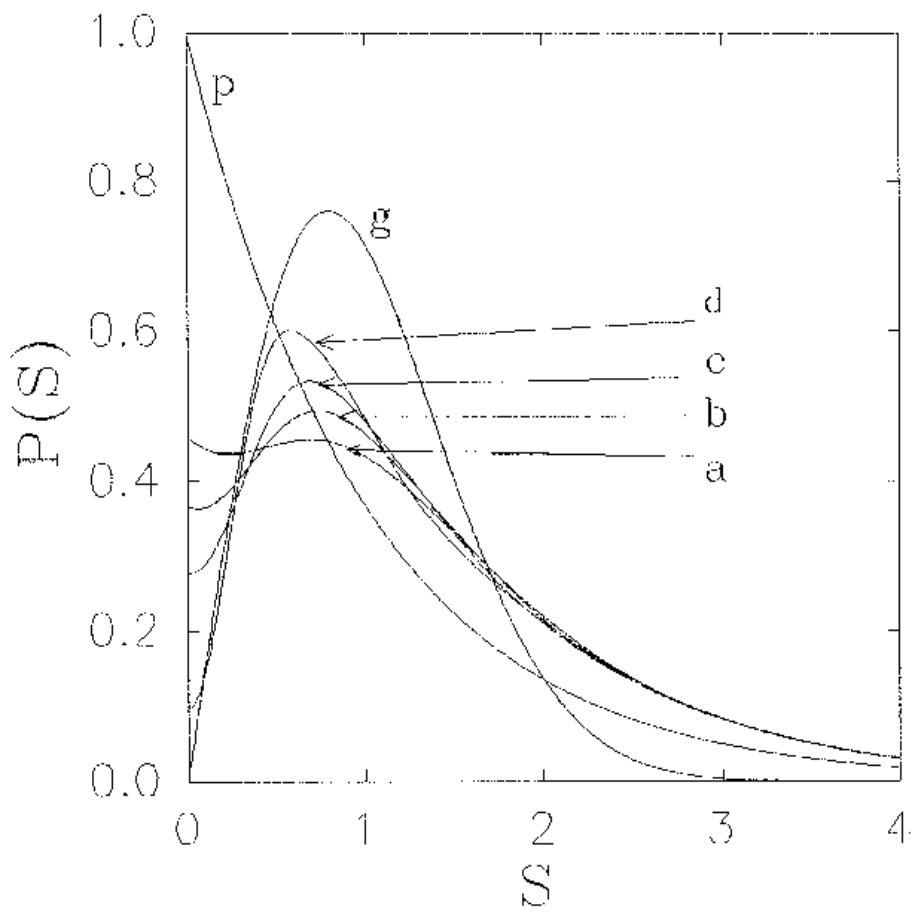


Figure 6.1: Nearest neighbour spacing distribution. Effect of variation of length parameters (see text)

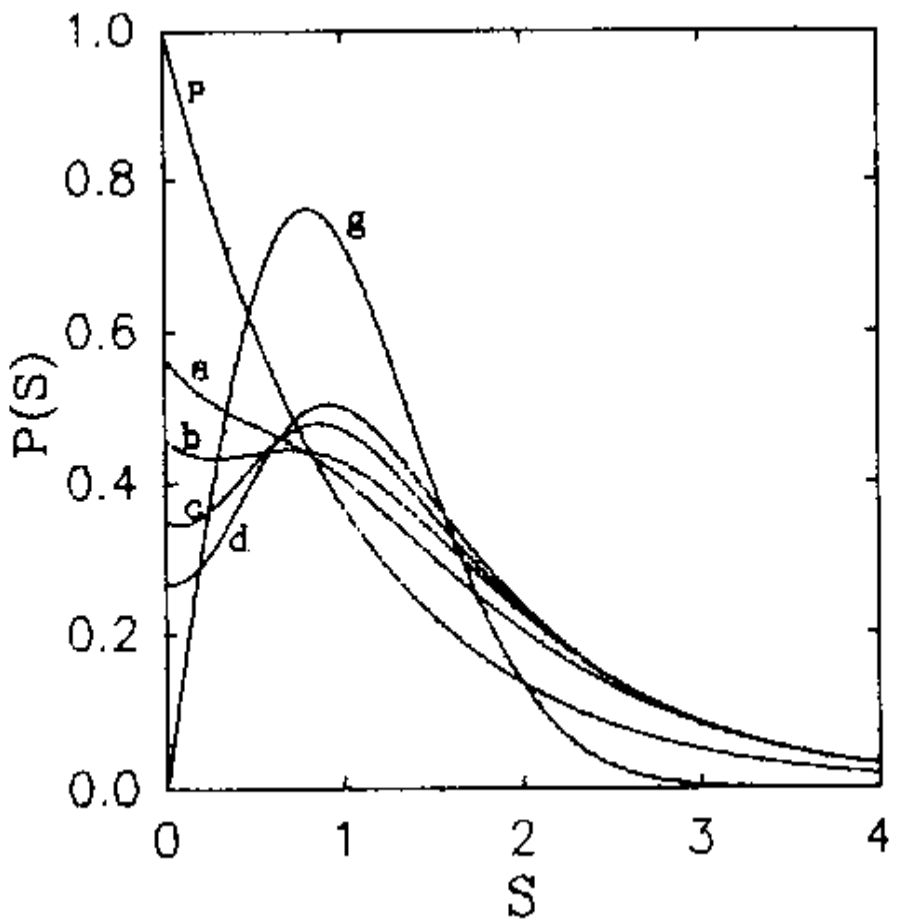


Figure 6.2: Nearest neighbour spacing distribution. Effect of variation of κ parameters (see text)

by triangles and dots (for two different mode of even states). Results are in close agreement for $S < 1$, however for $S > 1$ deviation of our results is too large to be correct. This behaviour of $P(S)$ distribution using diagonal approximation is also in contradiction with recent studies([9, 10]), where one get

$$P(S) = 4S \exp(-2S) \quad (6.7)$$

Again for $S \ll 1$ our results (for finite number of levels) are in agreement with eq. (6.7) but deviates appreciably for $S > 1$. This contradiction may be removed by considering off-diagonal contributions. As the calculation of $P(S)$ involves exponential of integration of $Y_2(S)$, any error in Y_2 will be amplified exponentially and effect of this error will be more for $S > 1$. Further improvements are therefore necessary in (6.4) to take account of off-diagonal contributions.

6.3 The Number Variance

In the preceding section we have discussed one of the important measure for spectral fluctuations on the finer energy scales. On the intermediate scales or on the scale of few mean level spacings, important measures are spectral rigidity and number variance. Both of these statistic provide similar information on spectral correlations. In this section we will discuss number variance for the pseudointegrable billiards. The number variance $\Sigma^2(L; r_0)$ is defined as the variance of the distribution of the number of levels in intervals $[r_0, r_0 + L]$, $n(L; r_0) = N(r_0 + L) - N(r_0)$,

$$\Sigma^2(L; r_0) = \langle [n(L; r_0) - L]^2 \rangle, \quad (6.8)$$

where, $\langle \dots \rangle$ denotes a usual spectral averaging over r_0 . A completely random spectrum that follows Poissonian behaviour shows a linear trend for a number variance, $\Sigma^2(L; r_0) = L$, whereas on the other hand, for the chaotic systems where levels are strongly correlated, a number variance is asymptotically given by $\Sigma^2(L; r_0) \sim (2/\pi^2) \ln(L) + .44$ for $L > 1$. The number variance $\Sigma^2(L; r_0)$ depends on $Y_2(r)$ via relation (e.g., see [12])

$$\Sigma^2(L; r_0) = L - 2 \int_0^L (L - s) Y_2(s) \, ds \quad (6.9)$$

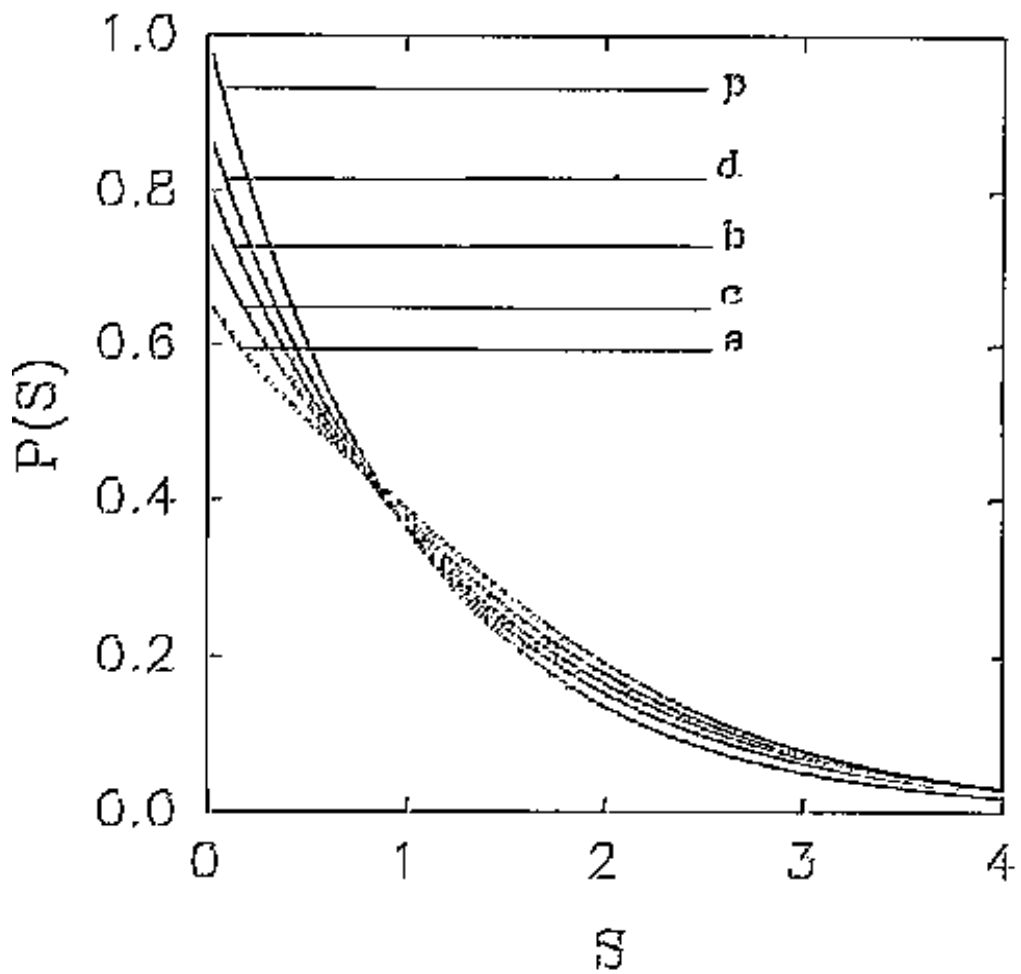


Figure 6.3: Nearest neighbour spacing distribution. complete $\pi/3$ -rhombus billiard (see text)

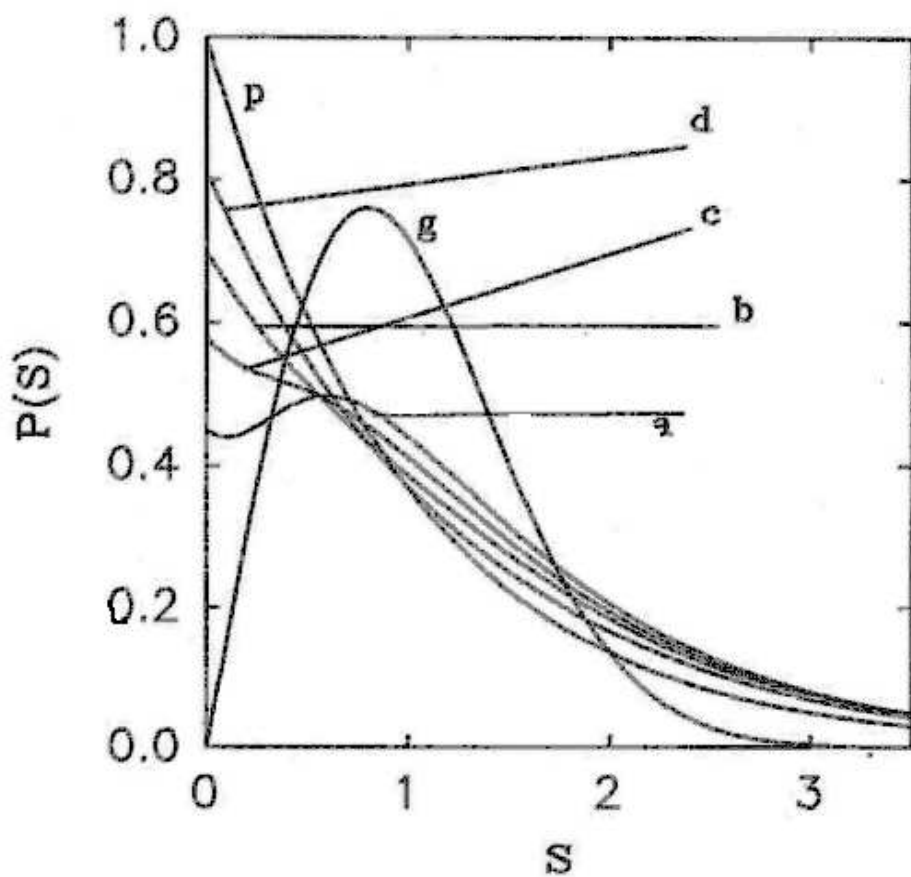


Figure 6.4: Nearest neighbour spacing distribution. pure rhombus modes of $\pi/3$ -rhombus billiard (see text)

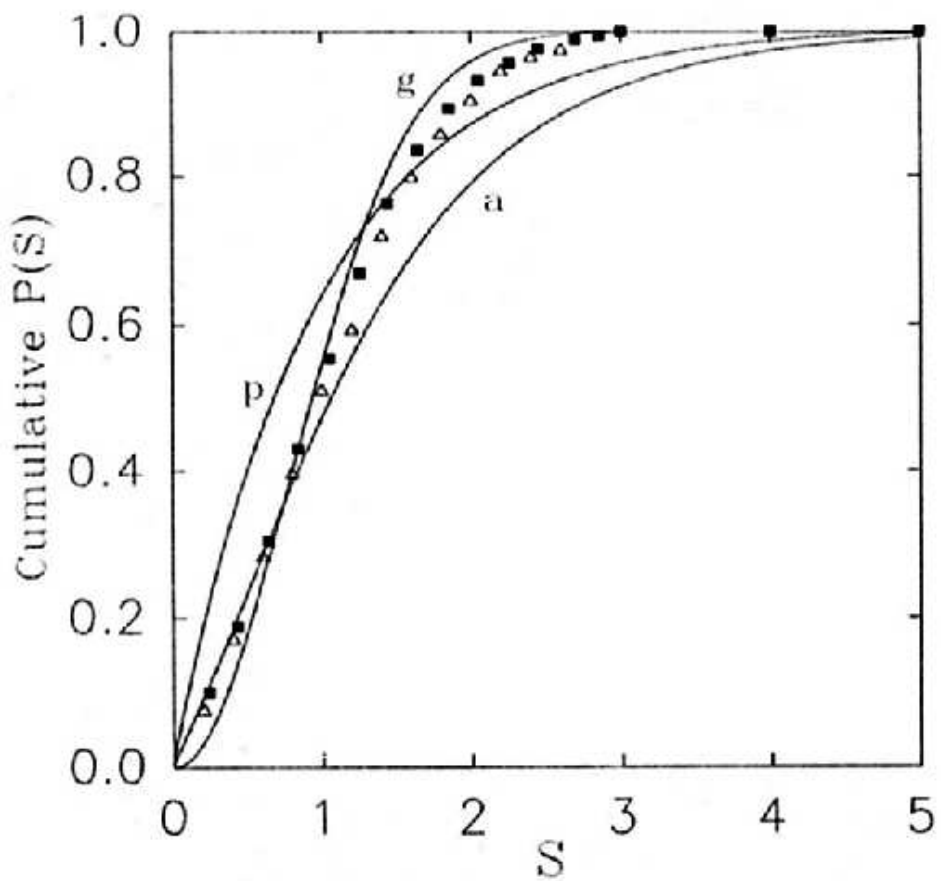


Figure 6.5: Cummulative nearest neighbour spacing distribution. $\pi/3$ -rhombus billiard (only even modes) (see text)

Using results of last chapter, we can exactly integrate above equation to get simple analytical form for $\Sigma^2(L; r_0)$ as,

$$\begin{aligned}
\Sigma^2(L; r_0) = & L - 2 \sum_{\alpha} \kappa_{\alpha} \left\{ \frac{r_{\max}}{\pi \Delta r} \left[L \text{Si}(\gamma_{\alpha, \max} L) + \frac{L \sin(\gamma_{\alpha, \max} L)}{6} \right. \right. \\
& + \frac{\gamma_{\alpha, \max} L^2}{6} \cos(\gamma_{\alpha, \max} L) + \frac{2}{3 \gamma_{\alpha, \max}} \cos(\gamma_{\alpha, \max} L) \\
& \left. \left. + \frac{\gamma_{\alpha, \max}^2 L^3}{6} \text{si}(\gamma_{\alpha, \max} L) - \frac{2}{3 \gamma_{\alpha, \max}} \right] \right. \\
& - \frac{r_{\min}}{\pi \Delta r} \left[L \text{Si}(\gamma_{\alpha, \min} L) + \frac{L \sin(\gamma_{\alpha, \min} L)}{6} + \frac{\gamma_{\alpha, \min} L^2}{6} \cos(\gamma_{\alpha, \min} L) \right. \\
& \left. \left. + \frac{2}{3 \gamma_{\alpha, \min}} \cos(\gamma_{\alpha, \min} L) + \frac{\gamma_{\alpha, \min}^2 L^3}{6} \text{si}(\gamma_{\alpha, \min} L) - \frac{2}{3 \gamma_{\alpha, \min}} \right] \right\} \quad (6.10)
\end{aligned}$$

where again $\gamma_{\alpha, \min(\max)} = 2\pi l_{\alpha, \min}/l_{H, \min(\max)}$. For small L , one can see that $\Sigma^2(L; r_0) \sim L$ i.e. it shows Poissonian behaviour, as L increases, we can approximate $\text{Si}(x) \sim \pi/2 - \cos(x)/x$ and hence $\text{si}(x) \sim \cos(x)/x$, $\Sigma^2(L; r_0)$ starts deviating from the Poissonian and oscillates around a non-universal value as

$$\begin{aligned}
\Sigma^2(L; r_0) = & L - L \sum_{\alpha} \kappa_{\alpha} - 2 \sum_{\alpha} \kappa_{\alpha} \left\{ \frac{r_{\max}}{\pi \Delta r} \left[\frac{L \sin(\gamma_{\alpha, \max} L)}{6} \right. \right. \\
& - \frac{\cos(\gamma_{\alpha, \max} L)}{3 \gamma_{\alpha, \max}} - \frac{2}{3 \gamma_{\alpha, \max}} \left. \right] \\
& \left. - \frac{r_{\min}}{\pi \Delta r} \left[\frac{L \sin(\gamma_{\alpha, \min} L)}{6} - \frac{\cos(\gamma_{\alpha, \min} L)}{3 \gamma_{\alpha, \min}} - \frac{2}{3 \gamma_{\alpha, \min}} \right] \right\}
\end{aligned}$$

Thus the saturation value for very large number of levels (i.e. $\gamma_{\alpha} \gg L$) is given by

$$\Sigma_{\infty}^2(L; r_0) = 2 \sqrt{\frac{A_R}{\pi^3}} \sum_{\alpha} \frac{\kappa_{\alpha}}{l_{\min, \alpha}} \left\{ \frac{r_{\max}^{3/2} - r_{\min}^{3/2}}{\Delta r} \right\}$$

This behaviour is very much akin to that of the spectral rigidity and saturation value is correctly given by $\Sigma_{\infty} \simeq 2\Delta_{3, \infty}$, where $\Delta_{3, \infty}$ is obtain directly (i.e. not from Y_2) in the sext section. In the Fig. 6.6 and 6.7 we show this behaviour as well as effect of variations in the length parameters and κ parameters respectively as done earlier. Trend is same. Hence our conclusions are also similar to the one stated earlier and hardly needs any elaboration. In

Fig. 6.8 and 6.9 we show more realistic cases namely complete rhombus and even states of the rhombus respectively. In Fig. 6.9, one can compare our results for energy level windows (47, 370) (curve (a)) with numerical results of [13]. Discounting oscillations of numerical results agreement is good even for $r > 1$. This is because, number variance involves simple integration over Y_2 and any error due to off-diagonal contributions is not as much amplified as that in the $P(S)$ distribution. In the next section we will confirm this in the case of another spectral measure known as spectral rigidity.

6.4 The Spectral Rigidity

In this section we obtain [14] the Dyson-Mehta Δ_3 -statistic for pseudointegrable billiards and show that it is nonuniversal with a universal trend, also that this trend is similar to the one for integrable billiards. We present a formula, based on exact semiclassical calculations and the proliferation law of periodic orbits, which gives rigidity for the entire range of L . To consolidate our theory, we discuss several examples finding complete agreement with the numerical results , and also the underlying fundamental reasons for the nonuniversality.

In their statistical theory of energy levels of complex systems, Dyson and Mehta [15] proposed the Δ -statistic to study spectral fluctuations on the intermediate energy scale, the most popular being the Δ_3 -statistic defined as *a local average of the mean square deviation of the spectral staircase from the best fitting straight line over an energy range corresponding to L mean level spacings.*

$$\Delta_3(L) = \left\langle \min_{(A,B)} \frac{d_{av}(E)}{L} \int_{-L/2d_{av}}^{L/2d_{av}} d\varepsilon [N(E + \varepsilon) - A - B\varepsilon]^2 \right\rangle \quad (6.11)$$

where $N(E)$ is spectral staircase introduced in chapter(1) (keeping in consonance with existing literature we use symbol L for correlation range in this section, and not to be confused with symbol for side length used earlier). $\langle \dots \rangle$ represents spectral averaging over energy scale much larger than what is called as outer energy scale but much smaller than classical scale[16], which is already discussed in the previous chapter. Though, $\Delta_3(L)$ can also be expressed in terms of the two-point correlation function, we prefer to use above direct definition to obtain an expression for Δ_3 in pseudo-integrable

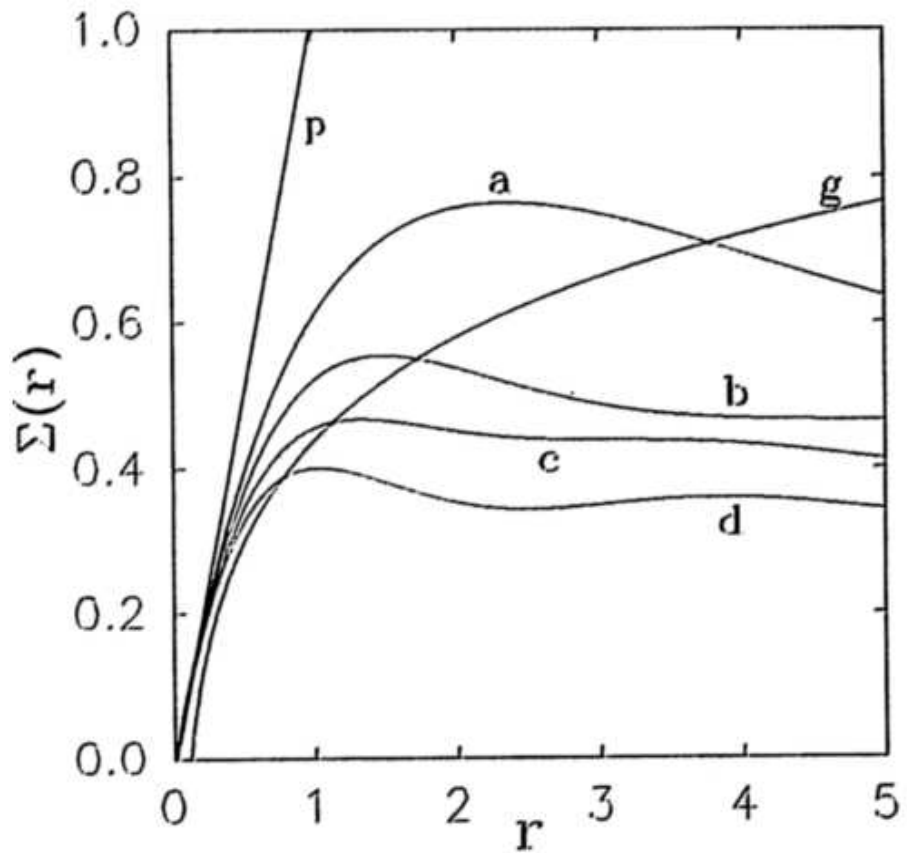


Figure 6.6: The number variance: Efect of variation of length parameters.
(see text)

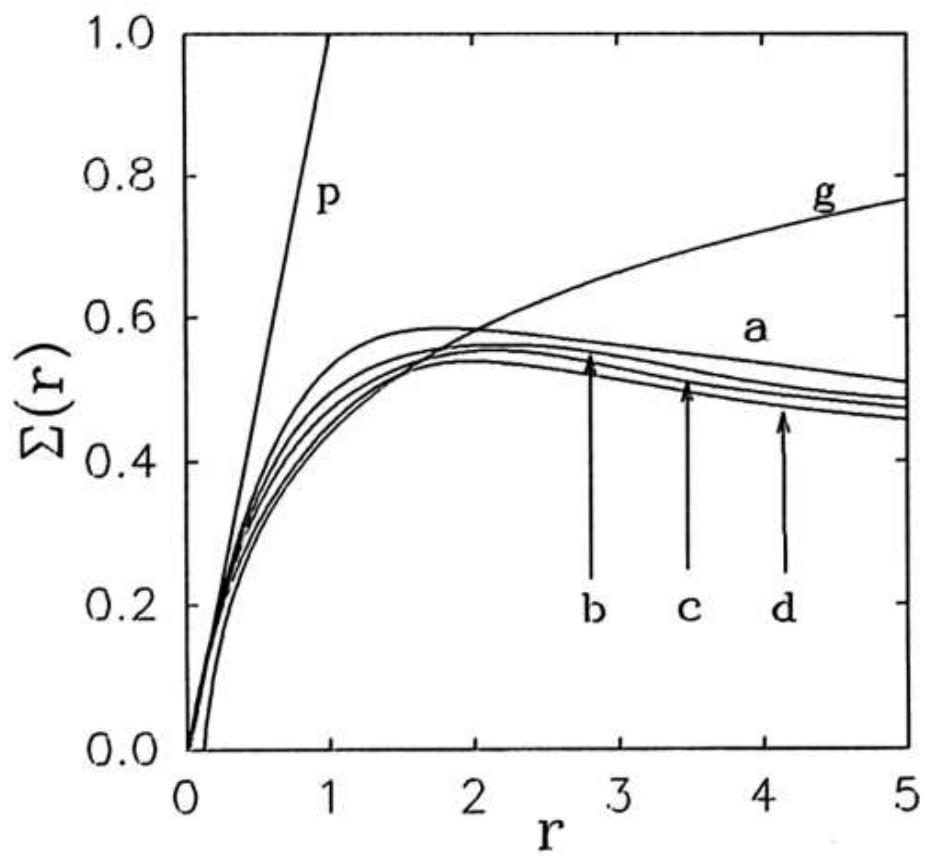


Figure 6.7: The number variance: Efect of variation of κ parameters. (see text)

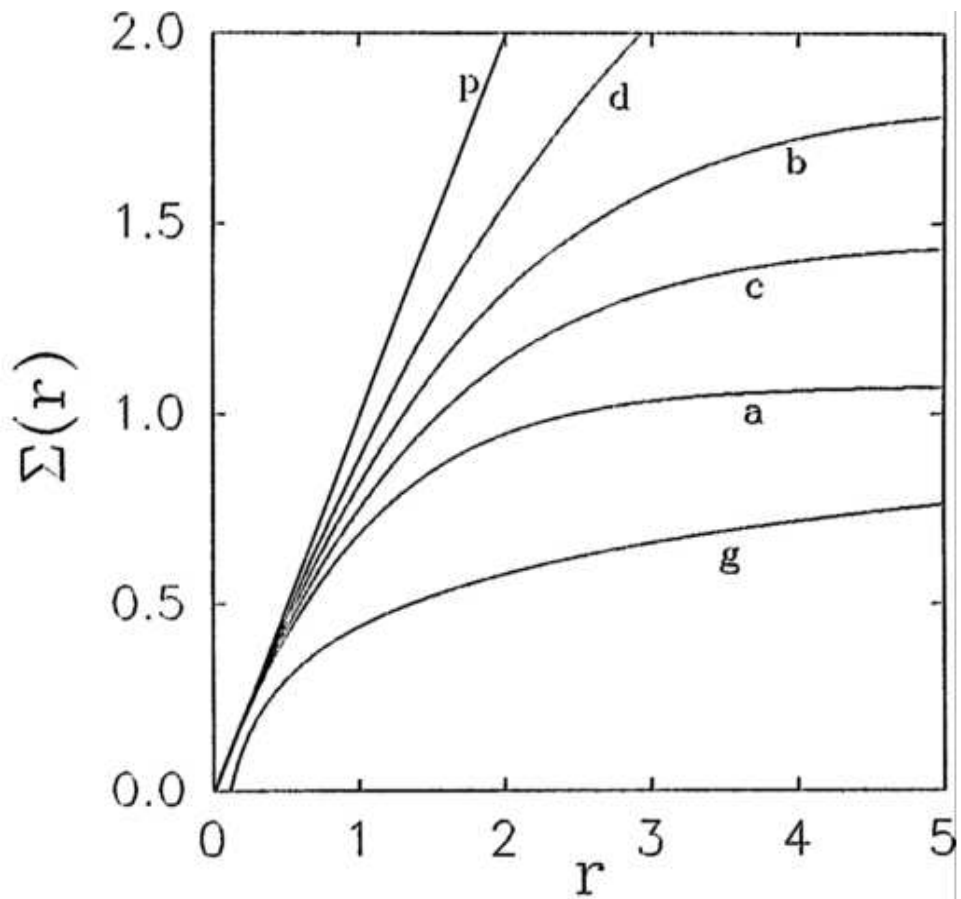


Figure 6.8: The number variance:complete $\pi/3$ -rhombus billiard (see text)

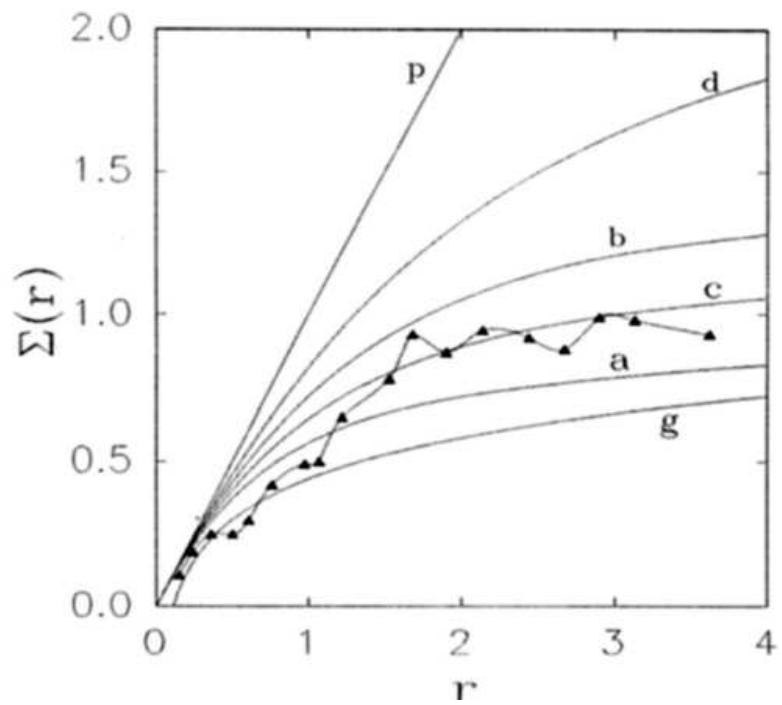


Figure 6.9: The number variance: for even modes of $\pi/3$ -rhombus billiard (see text)

billiards. Minimizing 6.11 over A and B we get

$$\begin{aligned}\Delta_3(L) = & \left\langle \left\{ \frac{d_{av}(E)}{L} \int_{-L/2d_{av}}^{L/2d_{av}} d\varepsilon N^2(E) - \left[\frac{d_{av}(E)}{L} \int_{-L/2d_{av}}^{L/2d_{av}} d\varepsilon N(E + \varepsilon) \right]^2 \right\} \right. \\ & \left. - 12 \left[\left(\frac{d_{av}(E)}{L} \right)^2 \int_{-L/2d_{av}}^{L/2d_{av}} \varepsilon d\varepsilon N(E + \varepsilon) \right]^2 \right\rangle \quad (6.12)\end{aligned}$$

For a Poisson spectrum (by which integrable systems are very well modeled) $\Delta_3(L) = L/15$. Consider another trivial example of a spectrum of the harmonic oscillator in one dimension. Its spectrum is also called picket fence spectrum due to equi-spacing between levels. $N(E)$ for such case is a ideal staircase and obviously mean square deviation of a best fit from this staircase is constant (1/12) independent of L . For the chaotic systems with time reversal symmetry which are modeled by GOE of random matrix theory rigidity is given by $\Delta_3(L) = \ln L/\pi^2 - .007$. It may be noted that for $L \ll 1$, the staircase nature of $N(E)$ leads to the limit $\Delta_3 \rightarrow L/15$, whatever distribution(non-singular) the levels have. We now proceed to obtain expression for spectral rigidity in psedo-integrable billiards.

A asymptotic semiclassical approximation for $N(E) = \int_0^E d(E')dE'$ in case of pseudointegrable billiards is given by

$$N(E) = \frac{E^{1/4}}{\sqrt{2\pi^3\hbar}} \sum_j \frac{A_j}{l_j^{3/2}} \cos \left(\frac{l_j\sqrt{E}}{\hbar} - \frac{3\pi}{4} \right) \quad (6.13)$$

Substituting this in eq. 6.12 we can obtain the rigidity as

$$\Delta_3(L, E) = \frac{E^{1/2}}{4\pi^3\hbar} \sum_j \sum_k \frac{A_j A_k}{l_j^{3/2} l_k^{3/2}} \cos \left\{ \frac{\sqrt{E}(l_j - l_k)}{\hbar} \right\} G(y_j, y_k) \quad (6.14)$$

where

$$G(y_j, y_k) = f(y_j - y_k) - f(y_j)f(y_k) - 3f'(y_j)f'(y_k) \quad (6.15)$$

and $f(y) = \sin y/y$, $y = Ll/(4d_{av}(E)E^{1/2}\hbar) = \pi Ll/l_H$. All other symbols have their usual meaning.

The main questions that ensue from the numerical studies [17, 11, 18, 19] are : a) are the levels of PIB uncorrelated and mimic a Poisson process in a certain range of L , as seen in IB ?; b) is there any saturation of rigidity in

PIB if L exceeds the system dependent range, as seen for the IB ?; c) what is the essential difference between PIB, IB and chaotic billiards in terms of level correlations ?; d) can we obtain a formula for the rigidity such that Poisson and non-Poisson results follow in a natural way for the IB and PIB respectively ? . Here we answers all these questions to a large (sometimes complete) extent. This success holds due to the fact that the rigidity is a direct consequence of the proliferation law with some simple, nontrivial modifications in the known formalism shown below. Recalling discussion in the last chapter, we employ the uniformity principle [20] and retain also, apart from the diagonal, the off-diagonal part corresponding to the systematic degeneracies in the lengths of po's (giving same contribution to the rigidity as the diagonal terms). From the exact results on some of the PIBs obtained in previous chapters, one can classify the bands of the po's in such a way that the projective phase space area occupied by all periodic orbits in a given class (defined by corresponding lattice points where po's closes) (say α) is identical (A_α). With this in mind, we can write $\Delta_3(L, E)$ as

$$\begin{aligned} \Delta_3(L, E) = & \frac{E^{1/2}}{4\pi^3 \hbar} \left[\sum_\alpha g_\alpha^2 A_\alpha^2 \sum_j \frac{G(y_{\alpha,j})}{l_{\alpha,j}^3} \right. \\ & \left. + \sum_\alpha \sum_\beta (1 - \delta_{\alpha,\beta}) g_\alpha g_\beta A_\alpha A_\beta \sum_j \sum_k \delta_{l_{\alpha,j}, l_{\beta,k}} \frac{G(y_{\alpha,j}, y_{\beta,k})}{l_{\alpha,j}^{3/2} l_{\beta,k}^{3/2}} \right] \end{aligned} \quad (6.16)$$

where $G(y) = 1 - f^2(y) - 3(\dot{f}(y))^2$ and Greek subscripts again denote classes of periodic bands. In (6.16), $g_\alpha g_\beta$ denotes the number of po's with the same action belonging to the class $\alpha(\beta)$, and $\delta_{i,j}$ is the usual Kronecker symbol. In the above equation the summation $\sum_j G(y_{\alpha,j})/l_{\alpha,j}^3$ can be written as $\int_{y_{min}}^\infty dF_\alpha G(y_\alpha)/l_\alpha^3$ in the continuum limit due to the mathematical nature of the summand, where dF_α represents number of periodic orbits within length l and $l + dl$. This dF_α can be deduced from the proliferation law (average or asymptotic part) as we have done in the earlier chapters. We then have (after unfolding spectrum via rescaled energies $r_0 = Ed_{av}$)

$$\begin{aligned} \Delta_3(L, r_0) = & \frac{L}{2\pi^2 A_R} [\sum_\alpha g_\alpha^2 A_\alpha^2 a_\alpha I_{1,\alpha} + \sum_\gamma \sum_\eta \delta_{l_\gamma, l_\eta} g_\gamma g_\eta A_\gamma A_\eta a_\eta I_{1,\eta}] \\ & + \frac{L^2}{8\pi^{3/2} A_R^{3/2} r_0^{1/2}} [\sum_\alpha g_\alpha^2 A_\alpha^2 b_\alpha I_{2,\alpha} + \sum_\gamma \sum_\eta \delta_{l_\gamma, l_\eta} g_\gamma g_\eta A_\gamma A_\eta b_\eta I_{2,\eta}] \end{aligned} \quad (6.17)$$

where

$$I_{1,\alpha} = \int_{y_{\min,\alpha}}^{\infty} dy_{\alpha} \ y_{\alpha}^{-2} \ G(y_{\alpha})$$

and

$$I_{2,\alpha} = \int_{y_{\min,\alpha}}^{\infty} dy_{\alpha} \ y_{\alpha}^{-3} \ G(y_{\alpha})$$

both these can be evaluated easily with $y_{\min} = \pi L / L_{\max}$. And

$$L_{\max,\alpha} = \sqrt{4\pi A_R r_0 / l_{\min,\alpha}^2} = \frac{l_H}{l_{\min,\alpha}}$$

where l_H is Heisenberg length already introduced earlier. For small y_{\min} , $I_1 = 2\pi/15$, $I_2 = 1/9$; and for large y_{\min} , $I_{1,\alpha} = L_{\max,\alpha}/\pi L$, $I_{2,\alpha} = L_{\max,\alpha}^2/2\pi^2 L^2$. For $L < \min_{\alpha} L_{\max,\alpha}/\pi$,

$$\begin{aligned} \Delta_3(L, r_0) = & \frac{L}{15\pi A_R} [\sum_{\alpha} g_{\alpha}^2 A_{\alpha}^2 a_{\alpha} + \sum_{\gamma} \sum_{\eta} \delta_{l_{\gamma}, l_{\eta}} g_{\gamma} g_{\eta} A_{\gamma} A_{\eta} a_{\eta}] \\ & + \frac{L^2}{72\pi^{3/2} A_R^{3/2} r_0^{\infty/\infty}} [\sum_{\alpha} g_{\alpha}^2 A_{\alpha}^2 b_{\alpha} + \sum_{\gamma} \sum_{\eta} \delta_{l_{\gamma}, l_{\eta}} g_{\gamma} g_{\eta} A_{\gamma} A_{\eta} b_{\eta}]. \end{aligned} \quad (6.18)$$

For $L \gg \max_{\alpha} L_{\max,\alpha}/\pi$,

$$\begin{aligned} \Delta_3(L, r_0) = & \frac{1}{2\pi^3 A_R} [\sum_{\alpha} g_{\alpha}^2 A_{\alpha}^2 a_{\alpha} L_{\max,\alpha} + \sum_{\gamma} \sum_{\eta} \delta_{l_{\gamma}, l_{\eta}} g_{\gamma} g_{\eta} A_{\gamma} A_{\eta} a_{\eta} L_{\max,\eta}] \\ & + \frac{1}{16\pi^{7/2} A_R^{3/2} \nabla_0^{1/2}} [\sum_{\alpha} g_{\alpha}^2 A_{\alpha}^2 b_{\alpha} L_{\max,\alpha}^2 + \sum_{\gamma} \sum_{\eta} \delta_{l_{\gamma}, l_{\eta}} g_{\gamma} g_{\eta} A_{\gamma} A_{\eta} b_{\eta} L_{\max,\eta}^2]. \end{aligned} \quad (6.19)$$

It is important to note that minimum and maximum (over α) L_{\max} correspond respectively to the longest and shortest (over α) orbits of the set containing shortest periodic orbits of different α 's. It is the consequence of this observation that will lead us to understand the fundamental distinction between the spectral correlations of integrable and pseudointegrable billiards.

Ignoring I_2 for the sake of brevity, the formula valid for the entire range of L is given by (denoting $L_{\max,\alpha}/\pi L = l_H/\pi L l_{\min,\alpha}$ by Λ_{α}),

$$\begin{aligned} \Delta_3(L, \nabla_0) = & \frac{L}{2\pi} \sum_{\alpha} \kappa_{\alpha} [\Lambda_{\alpha} - \frac{2}{3} \Lambda_{\alpha}^3 - \frac{3}{10} \Lambda_{\alpha}^5 \\ & - \frac{2}{15} \Lambda_{\alpha} \cos(2/\Lambda_{\alpha}) - \frac{1}{15} \Lambda_{\alpha}^2 \sin(2/\Lambda_{\alpha}) + \frac{1}{15} \Lambda_{\alpha}^3 \cos(2/\Lambda_{\alpha}) \\ & + \theta \frac{3}{5} \Lambda_{\alpha}^4 \sin(2/\Lambda_{\alpha}) + \frac{3}{10} \Lambda_{\alpha}^5 \cos(2/\Lambda_{\alpha}) - \frac{4}{15} \text{si}(2/\Lambda_{\alpha})] \Lambda \end{aligned} \quad (6.20)$$

where $\text{si}(x) = - \int_x^\infty dt t^{-1} \sin t$ and $\kappa_\alpha = A_\alpha^2 g_\alpha^2 a_\alpha / \pi A_R$. Eq. (6.20) along with the limiting results (6.18), (6.19) ; which clearly establishes relation between Δ_3 and information about the classical periodic orbits such as proliferation law, band areas, degeneracies in lengths etc. This result applies to all integrable and pseudointegrable billiards. To understand the formulae better, we now propose to examine some paradigm systems carefully, and subsequently compare the results with the known numerical results.

In this regard, we consider the specific examples of an Incommensurate Rectangle Billiard (IRB), the Single Slit Rectangle Billiard (SSRB) and the $\pi/3$ -rhombus Billiard (RHB).

Firstly, let us consider the IRB with sides $(\mathcal{L}, \gamma\mathcal{L})$, γ being an irrational number. The all periodic orbits fall in a single class occupying projective phase space area $4A_R$ ($A_R = \gamma\mathcal{L}^2$), except the two shortest periodic orbit bands parallel to either pair of sides of IRB. The area of these two shortest periodic bands is $2A_R$. The proliferation law for the IRB can be easily found by employing the ideas of stacking and replication, we get (counting all the repetitions of the ppo's),

$$F_{IRB}(l) = al^2 + bl = \frac{\pi}{16\mathcal{L}^2}l^2 + \frac{\gamma+1}{4\gamma\mathcal{L}}l. \quad (6.21)$$

Using $a, A (= 4A_R)$ in (9) we get complete quantitative agreement with results obtained earlier [19] for $L < L_{\max}/\pi$. As observed in [19], the oscillations in $\Delta_3(L)$ are rather weak beyond the "crossover regime".

To get the correct saturation values of $\Delta_3(L)$, we have to consider $O(l)$ term in eq. (6.21). Taking account of this, in the region where $L < L_{\max}/\pi$, we get

$$\Delta_3(L, \nabla_0) = \frac{L}{15} + \frac{1}{9\sqrt{2}\pi^{3/2}} \left(\frac{\gamma+1}{\gamma} \frac{L^2}{r_0^{1/2}} \right) \quad (6.22)$$

The second term is quite small as compared to the first one due to $r_0^{-\infty/\epsilon}$ factor. For $L \gg L_{\max}/\pi$, on the other hand, we have

$$\Delta_3(L, r_0) = \frac{r_0^{1/2}}{2\pi^{3/2}} \left(1 + \frac{\sqrt{\gamma}(\gamma+1)}{2\pi} \right), \quad (6.23)$$

which is in very good agreement with the numerical results.

Our next example is the single slit rectangle billiard, which is a simple variation of the barrier billiard already discussed in previous chapters. Recall that this is an example of a PIB whose invariant surface is topologically

equivalent to a sphere with two handles (genus, $g = 3$). The law of proliferation is the same as $a_\alpha^2 l + b_\alpha l$. We can obtain a_α, b_α for different classes of bands in this system in similar manner as in chapter (4).

With these, for $L < \min_\alpha(L_{\max,\alpha}/\pi) = \sqrt{r_0/4\pi}$,

$$\Delta_3(L, r_0) = \frac{L}{15} + \frac{1}{18\sqrt{2\pi^3}} \frac{L^2}{r_0^{1/2}} \quad (6.24)$$

and for $L >> \max_\alpha(L_{\max,\alpha}/\pi) = \sqrt{8r_0/\pi}$,

$$\Delta_3(L, r_0) \sim \left[\frac{\sqrt{2} + 13}{12\pi^{3/2}} + \frac{9}{8\sqrt{2\pi^5}} \right] r_0^{1/2} \quad (6.25)$$

We will discuss these results after we present calculation for yet another well studied system - the $\pi/3$ -rhombus billiard. This is an almost integrable system with an invariant integral surface of genus two. For this system tessellation of the plane is not complete and results in more general barrier structure [21]. Again, recall that each trajectory from origin to a coprime pairs, (q, p) represents ppo ending at $c(q, p)$. We then get for $L < \min_\alpha(L_{\max,\alpha}/\pi) = \sqrt{2r_0/37\sqrt{3}\pi}$,

$$\Delta_3(L, r_0) \sim \frac{L}{15} + \frac{1}{3^{7/4}2^{1/2}\pi^{3/2}} \frac{L^2}{r_0^{1/2}} \quad (6.26)$$

and for $L >> \max_\alpha(L_{\max,\alpha}/\pi) = \sqrt{2\sqrt{3}\pi r_0/3}$

$$\Delta_3(L, r_0) \sim .237 \frac{r_0^{1/2}}{\pi^{3/2}} + \sqrt{\frac{r_0/2}{3^{5/2}\pi^5}} \quad (6.27)$$

From expressions and examples discussed above, one can clearly see that there is an universal trend of $\Delta_3(L)$ with L for integrable and pseudointegrable billiards. More precisely, for $L < \min_\alpha(L_{\max,\alpha}/\pi)$, the rigidity is very well approximated by $L/15$, and for $L >> \max_\alpha(L_{\max,\alpha}/\pi)$ it saturates with a crossover connecting these two limits smoothly. The extent of the crossover region is given by the difference between \min_α and \max_α of $L_{\max,\alpha}$, or in other words, depends on the spectrum of lengths of shortest periodic orbits over α . Nonuniversal aspects, thus, arise due to nontrivial classification depending upon the degree of tessellation of invariant surface in terms

of a system-specific fundamental region. For instance, in IRB, tessellation is complete and there is only one class of bands ($\alpha = 1$); the crossover region is expected to be of lesser extent - a fact fully corroborated by the numerical experiments. In the SSRB, there is a barrier (gap to barrier ratio is unity) in a rectangle which gives rise to a periodic untessellated arabesque in terms of which classification is facilitated - the number of bands here is seven. Similarly for the RHB, the number of bands is eighteen. Importantly, it should be noted that the value of L at which the spectral rigidity deviates from the Poisson value of $L/15$, and the value at which saturation sets in, depends upon the lengths of the shortest periodic orbits distributed over various classes admissible in a given system. Indeed, this is the fundamental source of nonuniversality.

Let us discuss the numerical results on various pseudointegrable billiards. Most of the studies have been on rhombus billiards [11], square torus billiard and its generalizations [17] and singular billiards [22]. The analysis for the singular billiards was carried out and one understands the level spacing statistics [23]. The study of the two-level cluster function (in particular $\Sigma^2(L)$) does not give the GOE result [24] although the level spacing is GOE raising, thereby, a question currently beyond explanation. Therefore, we concentrate to explain the results for non-singular systems.

Perhaps the paradigm pseudointegrable billiard is the RHB [11, 18]. In both these studies, one can observe that the rigidity is intermediate to Poisson and GOE. From our analysis, taking the energy and parameters from these numerical work, it turns out that deviation from $L/15$ would occur at $L \sim 1$ and 2 respectively. We illustrate this in Fig.6.10, where we compare our analytical result with that of the numerical work [11] and the agreement is clearly evident. Here also as in the case of number variance errors due to neglecting off-diagonal contribution do not affect much. The crossover values are also correctly predicted by our analysis. We show behaviour of Δ_3 for small values of L in Fig.6.11, where deviation from $L/15$ is evident. In Fig.6.12 we show Δ_3 for complete range of L , where the crossover region and the saturation can be seen. Since the numerical results are not available for higher energy and for larger range of L , the saturation cannot be clearly seen in the numerical experiments. It is, therefore, desirable to carry out extensive numerical work for higher energy and for larger range of L . The formulae (6.18,6.19) provide the guidelines for choosing appropriate number of levels to bring out all the salient features of the systems discussed above. Our analysis also explains the results of [17] where one gets $L/15$ for very

small values of L and there is a saturation regime. Unfortunately, because of constraints over levels available, the belief of an intermediate behaviour between that of Poisson and GOE has been pursued for quite sometime. Our analysis clearly reveals, that such a behaviour does not exist and the spectral rigidity never becomes GOE.

The occurrence of periodic orbits in the bands is a likely reason for the slow rise of $\Delta_3(L)$ in large L region and overall stronger fluctuations than the GOE result. A recent result on Stadium billiard indicates this possibility too [25] - in this work, $\Delta_3(L)$ is shown to be rising well above the GOE curve if the contribution of the bouncing ball modes is taken into account. In chaotic systems like this (also, e.g. the Sinai billiard) the analysis of bands can be carried out using the above theory and it is expected that there exist a departure from GOE as well as a rise in spectral fluctuations after some L decided by the length of the periodic orbits in the band. Recently, non-genericity of the rigidity arising from banded orbits is discussed for the Stadium billiard [26].

In conclusion, we have obtained good approximation for the Δ_3 -statistic in an close analytical form for systems in which periodic orbits of the marginal stability (in bands) occur, from which Poisson and non-Poisson results follow in a natural way. Answers to the basic questions we have asked above are as follows: a) The levels of PIB are uncorrelated and mimic a Poisson process for $L < \min_\alpha(L_{\max,\alpha})$ which depends on shortest periodic orbit of a given system, hence nonuniversal value. This condition also stipulate minimum number of energy levels that one should be consider in the numerical experiment to observe this effect. b) For $L \gg \max_\alpha(L_{\max,\alpha})$ which depends mainly on the longest of the shortest p.o. among the different classes, the spectral rigidity saturates to a nonuniversal value. c) The fluctuation properties of PIB and IB differ essentially in the extent of transition region. In IB transition region will be of less extent, since there is only one class of p.o., deviation from a Poisson and saturation is determined by same p.o.(i.e. shortest one). In PIB because large number of classes of p.o. are present, all shortest p.o. amongst the different classes play important role in determining shape and extent of crossover region.

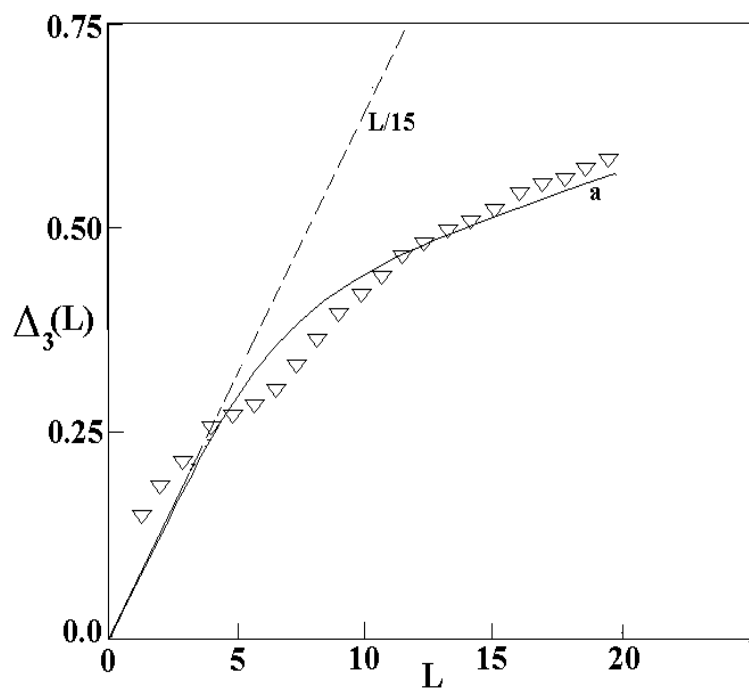


**Fig. 6.10: Spectral rigidity for /3-rhombus billiard.
Curve (a) is our result for no. of levels =350,
triangles represents numerical result and dashed
line is Poissonian L/15.**

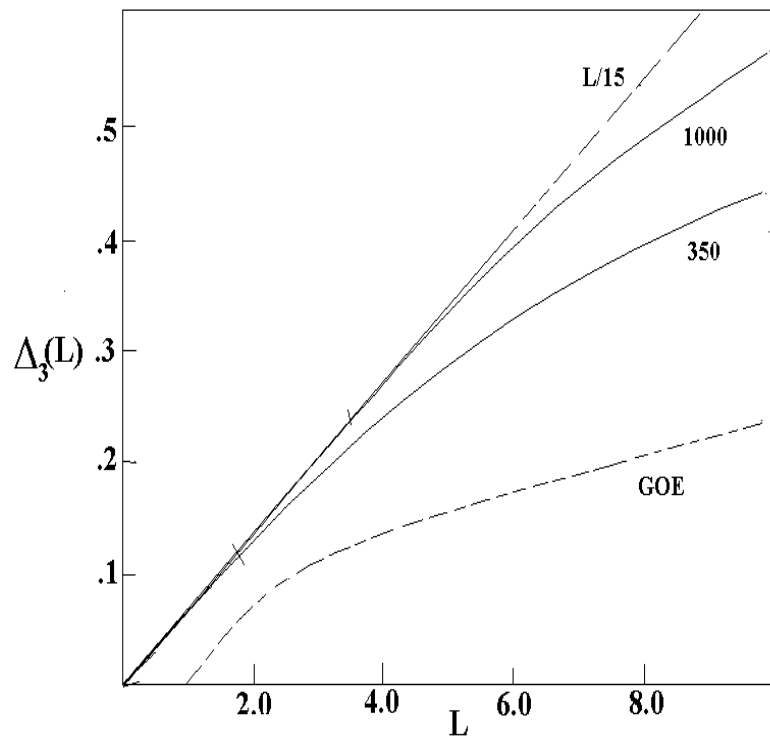


Fig. 6.11: Spectral rigidity for the rhombus. Full curves represents rigidity for 350 and 1000 levels as marked. \ marked on the curve shows point $L = \min_{\alpha} (L_{\max, \alpha})$ where respective curve starts deviating from $L/15$ (Poissonian).

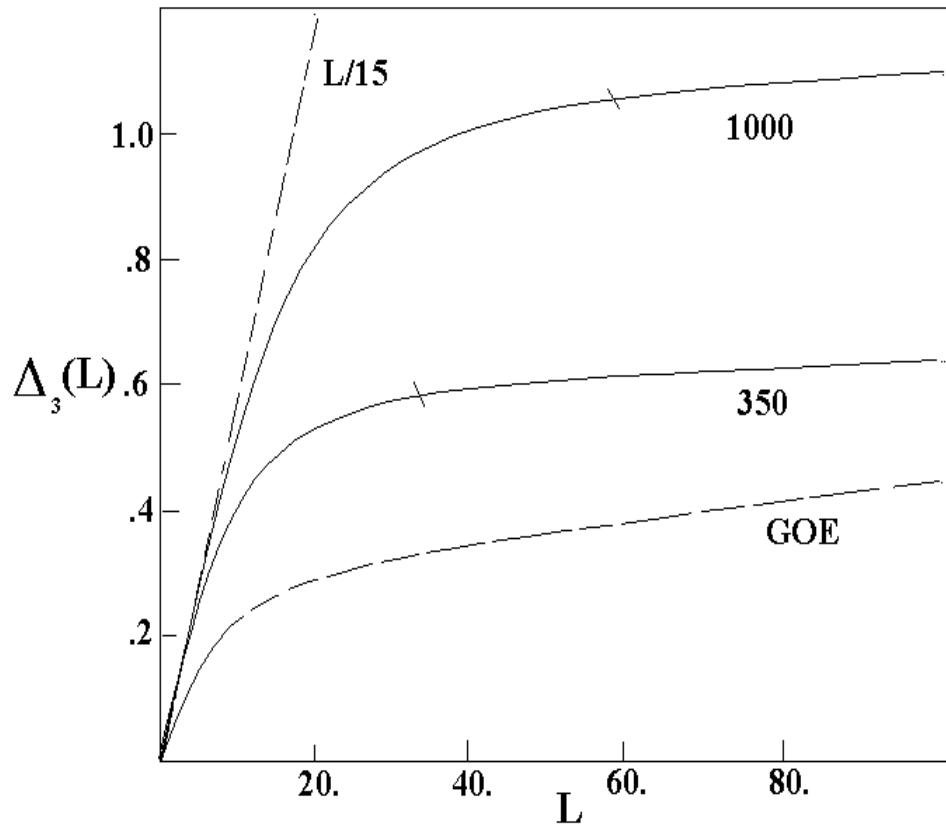


Fig. 6.12: Spectral rigidity for the rhombus as in fig. 6.11. Start of saturation is marked by \n respective curves at $L = \max_{\alpha} (L_{\max, \alpha})$

Bibliography

- [1] T. A. Brody, Lett. Nuovo Cimento **7**, 482(1973).
- [2] M. V. Berry and M. Robnik, J. Phys. **A17**,2413(1984).
- [3] F. M. Izrailev, J. Phys. **A22**, 865(1989).
- [4] F. Haake, Quantum Signatures of Chaos, Springer-Verlag, Berlin (1991).
- [5] M. C. Gutzwiller, Chaos in Classical and Quantum Mechanics, Springer-Verlag, New-York (1990).
- [6] M. L. Mehta, Random Matrices, Academic, New York (1991).
- [7] E. P. Wigner, in Statistical theories of Spectra:Fluctuations, edt. C. E. Porter, Academic, New York, 446(1965).
- [8] O. Bohigas and M. J. Giannoni, Lect. Notes in Phys. **209**, eds. J.S. Dehesa et al , Springer Verlag, Berlin(1084).
- [9] E.B. Bogomolny, U Gerland, C Schmit . priprint, IPN Orsay (1998).
- [10] B. Gremaud, S.R. Jain, J. Phys. A:Math. and gen. **31** L637(1998).
- [11] D. Biswas and S. R. Jain, Phys. Rev. **A42**, 3170 (1990).
- [12] T. Dittrich, E. Doron, U. Smilansky ,J. Phys. **A27** 79(1994).
- [13] D. Biswas, Phys. Rev. A, **44**, 2429(1991).
- [14] H.D.Parab and S.R.Jain, J.phys. A:Math Gen. **29**, (1996)3903.
- [15] F. J. Dyson and M. L. Mehta, J. Math. Phys. **4**, 701 (1963).

- [16] M. V. Berry, Proc. Roy.Soc. London **A400**, 229 (1985).
- [17] T.Cheon and T. D. Cohen, Phys. Rev. Lett. **62**, 2769 (1989).
- [18] A.Shudo, Phys. Rev. **A46**, 809 (1992).
- [19] G. Casati, B. V. Chirikov and I. Guarneri,Phys. Rev. Lett. **54**, 1350 (1985).
- [20] J. H.Hannay and A. M. Ozorio de Almeida, J. Phys. **A17**, 3429 (1984).
- [21] B. Eckhardt, J. Ford and F. Vivaldi, Physica **D13**, 339 (1984).
- [22] P. Seba, Phys. Rev.Lett. **64**, 1855 (1990).
- [23] S.Albeverio and P. Seba, J. Stat. Phys. **64**, 369 (1991).
- [24] P.Seba and K. Zyczkowski, Phys. Rev. **A44**, 3457 (1991).
- [25] H.-D. Graf, H. L. Harney, H. Lengeler, C. H. Lewenkopf, C. Rangacharyulu, A.Richter, P. Schardt and H. A. Weidenmuller, Phys. Rev. Lett. **69**, 1296(1992).
- [26] M. Sieber, U. Smilansky, S. C. Creagh and R. G. Littlejohn, J. Phys. **A26**, 6217 (1993).

Chapter 7

Conclusions

The work presented in this thesis provides first step to attain complete understanding of spectral fluctuation properties in pseudointegrable systems within semiclassical framework. It also supplements our knowledge about underlying reasons for universal and non-universal properties of spectral fluctuations. Furthermore, close analytical forms for various spectral measures are obtained, which in our knowledge were not available before this work (albeit under diagonal approximation only).

Semiclassical framework needs complete information about periodic orbits of a system under consideration. In particular one needs to specify actions of periodic orbits and their stability properties. For example, in the case of pseudointegrable billiards we need to know lengths and band areas of the periodic orbits in a given system. This is a herculean task, and there are very few systems about which complete information regarding this is available. Different methods are developed to gather information about periodic orbits in different kinds of system (e.g. symbolic dynamics). These methods are sometimes system specific and sometimes more general. In chapter three we have developed a methodology to enumerate and classify periodic orbits of some pseudo-integrable billiards. Here we have exploited important geometrical attributes of systems under considerations. To our knowledge these are only pseudointegrable systems about which complete information regarding periodic orbits is available. The same methodology can be used to study large number of rational polygonal billiards in particular one can apply technique to rectangular billiard with many slits(or barriers) or L-shaped billiards or its further generalization. This is one of the open problem in which we will be interested in future. This will also give us opportunity to deal with higher

genus pseudointegrable systems.

As it turns out from our analysis proliferation of periodic orbits (or growth rate) in one of the most important factor in the semiclassical methods. Spectral fluctuation properties indeed depends on the exact asymptotic proliferation of the periodic orbits in the system. We obtained this law in chapter four using probabilistic arguments. We proved that the law of proliferation of periodic orbits in the pseudointegrable billiards under consideration is quadratic in length, in fact , of the form $al^2 + bl + c$. We also obtained coefficients a, b, c explicitly using probabilistic arguments.

A complete knowledge about periodic orbits enabled us to obtain analytical expressions for various spectral measures. Most important of these is two-level cluster function which is studied along with its Fourier transform in chapter five. To obtain two level cluster function one have to evaluate density-density correlation function first. The semiclassical approximation for density correlation function leads us to summation over all periodic orbits. This formulation does not explicitly brings out various factors that affect spectral fluctuations in the system. Using simple but non trivial arguments we convert this form of summation to the integration. It then turns out that proliferation law play important role in this integration and hence, in the spectral fluctuations. This conversion to integration enables us to obtain analytical expressions for various spectral measures. This also enables us to study effect of considering finite number of levels on the spectral fluctuations. In particular spectral properties depends on 1)lengths of shortest periodic orbit occurring in different classes of periodic orbits. 2)phase space areas occupied by classes of periodic orbits along with respective coefficients of proliferation law which forms a factor κ in our analysis. In particular we show importance of factor $l_{\alpha \text{ min}}/l_H$, where $l_H = \sqrt{4\pi A_R r_0}$ is the Heisenberg length. From our analysis it is clear that this ratio for $\max_{\alpha}(l_{\alpha \text{ min}})$ should be $\ll 1$, for one to talk about asymptotic properties ($\hbar \rightarrow 0$) of spectral fluctuations. For $\pi/3$ -rhombus billiard this condition indicates that the number of levels considered should be at orders of magnitude larger than 1600. For other pseudointegrable system this number may still be much higher. Though it is meaningful to study statistically large number of levels in the non-asymptotic regions, this will bring not bring out universal properties of that class of systems as spectral fluctuations are not free of system dependent parameters. This chapter thus we are able to define classical parameters that governs spectral fluctuations and extent of their influence. In the case of form factor even diagonal approximation gives correct asymptotic ($\tau \gg 1$) form unlike

that in chaotic systems where it was found that diagonal approximation leads to linear rise in the form factor in asymptotic region ($\tau \gg 1$), which was compensated by off-diagonal contribution to give correct saturation. This indicates that off-diagonal contribution in pseudointegrable systems can affect only transition region. Further, we have shown that imprints of different classes of periodic orbits can be seen in the behaviour of the form factor. This feature is still gone unnoticed though many numerical experiments do have these imprints.

In chapter six we consider short and intermediate range spectral measures, namely spacing distribution, number variance and spectral rigidity. We also compare our results with numerical experiments available. We found that intermediate range measures are well modeled by our theoretical expressions. The departure from numerical results are not serious and may be attributed to off-diagonal contributions. Spacing distribution however, agree with numerical experiments only for short correlation range this is due to fact that any error due to off-diagonal contributions is exponentially amplified hence rises fast for larger correlation ranges. This can be improved further by considering off-diagonal contributions.

We now enlist some open avenues that our work suggest

1) To obtain complete understanding off-diagonal contributions should be taken into account explicitly. This is however difficult task. Recently developed indirect method by Bogomolny to consider these contributions in terms of diagonal contribution may proved to be fruitful in this regard. Some preliminary study confirms our conclusions above. It also indicate that approach to Poisson like behaviour is further slowed down by these contributions.

2) As mentioned in the thesis trajectories of pseudointegrable billiards resides on foliated surface of genus greater that two. This therefore do not allow trajectories to explore phase available as in the case of chaotic systems. The singular points in the phase space, however, results in diffraction of trajectories that hits it. These diffracted orbits are therefore not confined to one foliated surface but may visit many more via multiple diffractions thus imitating chaotic behaviour. These should be properly accounted for.

3) Yet, another kind of orbits which are on the edges of the band of periodic orbits can give different contribution to periodic orbit sum hence should be studied in detail.

4) Extension of methods developed here to higher genus systems is also a one of the important problem.

- 5) Can one generalise these results on two dimensional polygonal billiard to n-dimensional polyhedra.
- 6) Using semiclassical formalism and complete information about periodic orbits can we develop a method to extract information about the eigenfunctions for these systems.
- 7) One of the important applied field where study about polygonal billiards can be used is semiconductor microstructures where dimensions of a system is much smaller that the mean free paths of electrons (hence electron imitates billiard like dynamics). To design and develop microstructure with desired properties it is important to develop complete semiclassical understanding of such systems.

I hope this is just a beginning of my persuasion of knowledge about dynamical systems in general.